Intelligent Prediction of Air Conditioning System Performance using Artificial Neural Network

機械学習による高精度
空調機性能予測に関する研究

February 2021

Sholahudin

ショーラウディン

Intelligent Prediction of Air Conditioning System Performance using Artificial Neural Network

機械学習による高精度
空調機性能予測に関する研究

February 2021

Waseda University
Graduate School of Fundamental Science and Engineering
Department of Applied Mechanics and Aerospace Engineering,
Research on Dynamics and Control of Mechanical Systems

Sholahudin

ショーラウディン

Abstract

Air conditioning systems consume the largest share of energy in buildings. For this purpose, vapor compression air conditioning systems are widely used. There are billions of installed units of such systems all over the world. However, their operation is still not optimized since their performance during real time operation is mostly unknown. Availability of realistic information about the actual performance of air conditioners could guide the development of energy efficient operation strategies and consequently lead to a substantial reduction of primary energy consumption. Ideally, the system delivers cooling capacity according to load demand with the potentially maximum efficiency. In this study a cost effective and non-intrusive method to predict the actual air conditioning system performance is developed using artificial neural network. Input and output data for prediction are generated from simulation and experimental facility covering a wide range of operating conditions. The method is developed with the motivation that it can be applied to predict the system performance in dynamic operation and different systems using few input parameters that are non-intrusive and inexpensive to measure. The results show that the artificial neural network method with the input of four refrigerant temperatures measured at outdoor unit has successfully predicted the cooling capacity of air conditioning system with relative error and RMSE within 5% and 1.8 kW, respectively.

Keywords: Air conditioning, Prediction, Artificial neural network, Cooling capacity

Acknowledgement

First of all, I say *Alhamdulillah* all praise to Allah the lord of the worlds, who has given all the endless gifts and guidance.

I would like to thank my parents for their prayer and motivation to always guide me in right path of life. Thanks also to my beloved wife Diah Ismawati who always prays and motivates me all the time so that I can complete my doctoral study in Waseda University, my son Khawarizmi Ahmad Musyaffa who always gave an encouraging smile that provides more energy to work.

I would like to express my deepest appreciation to my advisor Prof. Kiyoshi Saito for the valuable advice and support of my Doctoral study and related research. His expertise was invaluable in formulating the research questions and methodology. His insightful feedback pushed me to sharpen my thinking and brought my work to a higher level.

I would also like to extend my deepest gratitude to the rest of my thesis committee: Prof. Hiroaki Yoshimura, Prof. Tomohiro Yanao, and Assoc. Prof. Seiichi Yamaguchi for their constructive comments and suggestions for improving the research study.

Many thanks should go to Mr. Katsuhiko Tanaka, Mr. Hiroto Ogami, and other members of TEPCO research institute for the collaboration and hard work in providing experimental data to accomplish the related research.

I must also thank to Prof. M. Idrus Alhamid and Prof. Nasruddin who always nurtured and motivated me for study. Their valuable advice and support always encourage me to finish the doctoral study.

I had great pleasure of working with my research partner Assoc. Prof. Niccolo Giannetti for his wonderful collaboration. He has extended a great amount of assistance to support the research works particularly in constructing the research road map, methodology, data analysis, and review of papers and thesis.

I gratefully acknowledge the assistance of Dr. Keisuke Ohno for system simulator development. His guidance related to the control development is also very useful for this research.

Special thanks to all members of Saito Laboratory who helped me conducting the research during the Doctoral study: Richard, Mark, Carlo, Arnas, Yulianto and Hifni. I also would like to thank Mr. Miyaoka, Ms. Ohsaki, and Ms. Kochi who helped me in dealing with some related administrative matters.

Nomenclature

Symbol		
A	Area	m^2
a	Activated neuron output	-
b	Bias	-
C	Specific heat capacity	$J \cdot kg^{-1} \cdot K^{-1}$
c	Normalized data	-
c_1, c_2	Regularization parameter	-
c_p	Area per pulse	m^2
c_V	Flow coefficient	-
D	Diameter	m
d	Data	-
E	Energy	W
e	Error	-
E_p	Error of prediction	-
E_w	Error of network weight	-
f	Transfer function	-
f_r	Friction factor	-
G	Mass flow rate	$kg \cdot s^{-1}$
H	System output	-
h	Specific enthalpy	$J \cdot kg^{-1}$
j	Mass flux	$kg \cdot m^{-2} \cdot s^{-1}$
J_{reg}	Objective function of regularization	-
K	Thermal conductance	$W \cdot m^{-2} \cdot K^{-1}$
K_i	Integrative gain	-
K_p	Proportional gain	-
L	Length	m
Lc	Circumference	m
M	Network arcitecture	-
m	Mass of refrigerant	kg
N	Training data sets	-
n	Neuron output	-
n_d	Number of data	-
P	Pressure	Pa
p	ANN input	-

p_v	Valve opening	pulse
Q	Heat flow	W
q	Heat flux	$W \cdot m^{-2}$
Qe	Cooling capacity	W
$Qload$	Cooling load	W
r	Control set point	-
S	Cross sectional area	m^2
s	Specific entropy	$J \cdot kg^{-1} \cdot K^{-1}$
T	Temperature	℃
t	Time	s
t_d	Delay time	s
U	Specific internal energy	$J \cdot kg^{-1}$
u	Control input signal	-
V	Volume	m^3
v	Velocity	$m \cdot s^{-1}$
V_i	Variability index	-
W	Work	W
w	Weight	-
X	Concentration	-
x	Function input	-
y	ANN output	-
y_p	Prediction output	-
y_t	Prediction target	-
Z	Weight and bias vector	-
z	Length of state	-

Greek

ρ	Density	$kg \cdot m^{-3}$
η	Efficiency	-
ω	Compressor speed	rps
α	Heat transfer coefficient	$W \cdot m^{-2} \cdot K^{-1}$
τ	Time constant	s

Subscript

A	Air
ad	Adiabatic
C	Condenser
DB	Dry bulb
E	Evaporator
FC	Fin collar
FIN	FIN
HP	High pressure
I	Inlet
In	Inside
in	Indoor
INV	Inverter
k	Number of input
LP	Low pressure
max	Maximum
min	Minimum
O	Outlet
Out	Outside
out	Outdoor
R	Refrigerant
s	Number of neuron
T	Tube
V	Volume
vap	Vapor
WB	Wet bulb

Table of contents

1. Introduction

1.1 Background

Energy provision and the control of the emissions related to energy consumption have arisen as major global issues in the last decade. The largest share of global energy provision still relies on depletable fossil fuels, such as coal, oil, and gas, which are non-renewable and becoming very limited. The large-scale fossil fuels usage leads to the raising of potential supply difficulties and critical environmental impacts such as greenhouse gas emission, climate change, ozone layer depletion, etc. Energy consumption reduction and environmental safety of energy conversion systems are issues currently targeted by many researchers in the world, especially in building sector. The statistical data show that residential is the second largest energy consumers after industrial sector[1]. Energy consumption in both commercial and residential buildings is steadily increasing. The main reasons contributing to this fact include the population growth, larger demand for building services, more advanced thermal comfort standards, and longer permanence of the occupants inside buildings[2]. These circumstances forewarn the rising of the related energy demand in the future. Effective evaluation approaches can significantly reduce the building energy usage[3]. Accordingly, improving energy efficiency in the building sector has recently become the main concern for policy makers and stakeholders.

Besides the extensive use of cooling systems in the industrial and transportation sectors, today, air conditioning (AC) systems have become a necessity in buildings. The recent change of lifestyle, which has brought many people to spend most of their time inside the building, pushes AC systems to work for long time[4], in different conditions, and different climates. In these modern days, people are estimated to spend approximately 80-90% of their time in conditioned indoor spaces[5]. A comfortable indoor air is directly related to people's health and productivity[6]. The International Energy Agency (IEA) estimates that 1.9 billion units of AC systems are operating all over the world in 2020[7]. This number is projected to experience an increase of as much as 50% by 2030 (Fig. 1.1). A more extensive use of air conditioners is caused by stricter standard requirements of thermal comfort, the established development of this technology (large number of experienced manufactures providing systems at affordable price) and economic welfare in developing countries. Moreover, the AC systems used by consumers are most likely to demonstrate less than half of best available efficiency of this technology[7]. As a result, the growth in energy demand for AC systems tends to increase continuously and, if not operated properly, the related environmental footprint could become a substantial cause for unsustainable greenhouse emissions.

At present, within the building sector, lighting accounts for approximately 15% of the total building energy consumption[2]. However, the global enhancement in light-emitting diodes (LEDs) technology could significantly reduce the lighting energy consumption[8]. Heating ventilating and air conditioning (HVAC) systems are responsible for the largest energy demand in the building sector[3]. The study reported in literature[9] mentioned that as much as almost half of the building

energy consumption in developed countries is dedicated to the operation of HVAC systems. Similarly, in a tropical climate, the HVAC system consumes more than 50% of the total building energy demand[2]. The typical electricity use in Singapore shown in Fig. 1.2 demonstrates that the building sector accounts for a share of approximately 31%, where 60% of this share is used for cooling. This observation indicates that there are large opportunities to reduce energy consumption in the building sector through efficiency improvement of HVAC systems and their operation strategy.

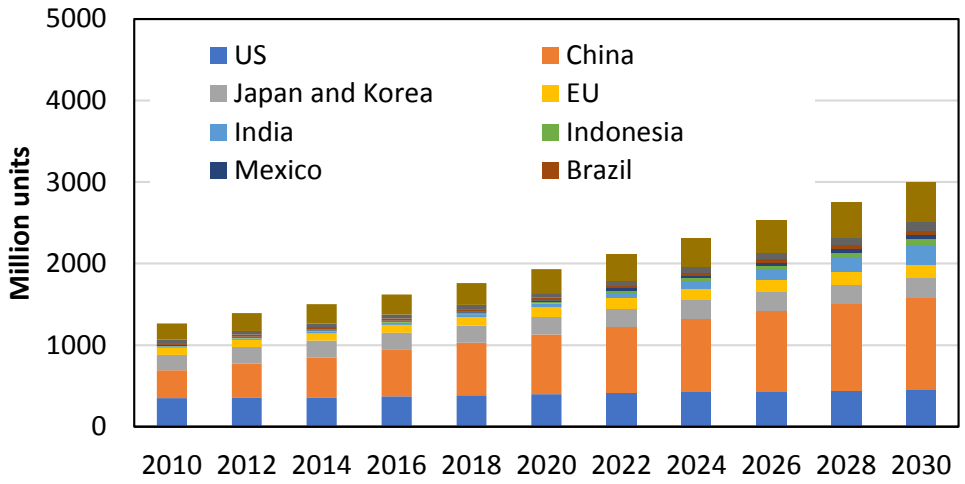

Fig. 1.1 Global air conditioner stock[1]

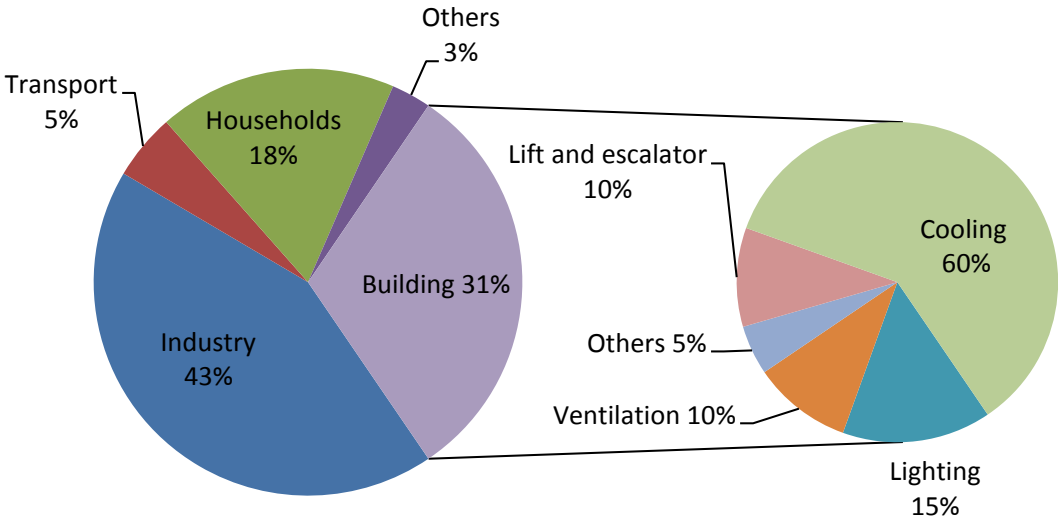

Fig. 1.2 Typical electricity consumption by end use in building sector in Singapore[2]

In recent years, vapor compression technology (see Fig. 1.3) is most commonly applied for AC systems in residential building applications as the system is less bulky, inexpensive, and coefficient of performance (COP) is higher compared to absorption[10], injection[11], and other systems. In order to increase vapor compression system performance, some efforts have been directed to develop advanced control strategies[12, 13], improve component efficiency e.g. compressor[14]; heat exchanger[15]; expansion valve[16]; model system behavior[17], optimize operating condition[18], develop variable refrigerant flow (VRF) for multi indoor units application[19], optimize the system cycles[20], etc. The efficiency of AC system has been successfully increased as the result of variable speed compressor together with the higher efficiency of heat exchanger[21]. Notwithstanding these efforts, their efficiencies have improved only slightly due to the approaching technical limitations. As the above-mentioned progress is generally directed to the technology and not case specific applications, no significant improvement and significant benefit in terms of energy efficiency and environmental impact have been achieved. Accordingly, the users rely on the current, often inefficient, AC systems for a long operation period, where the system will experience performance degradation and run with even lower efficiency.

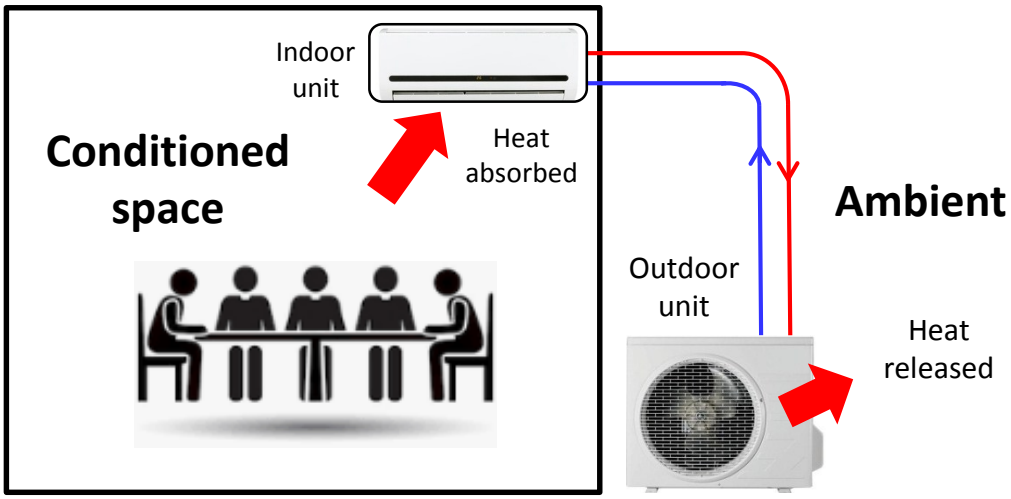

Fig. 1.3 Room air conditioning (AC) system

Optimal operation management can be an effective measure to substantially reduce the energy consumption of AC systems. The system cooling capacity represents the main extensive indicator of the system performance, response to the external disturbances and internal load. This quantity is generally related to the input driving energy to evaluate the system performance in terms of first law thermodynamic efficiency, but also second law efficiency[22]. Ideally the system should be working to deliver appropriate cooling capacity in response to the instantaneous cooling load at the potentially maximum efficiency. According to the investigation presented in literature[23], the

optimal operation of AC systems can be achieved in range of 50-70% of the nominal capacity. To this purpose, a reliable prediction method for actual system performance is necessary to define advanced operation strategies, adapt the available capacity with the load of a facility, and establish system efficiency monitoring techniques. As billions of these systems have already been installed in different types of buildings, capacity sizes, grids, and climates and encountered performance degradation over time due to fouling of the heat exchanger surface[24-26], pipe leakage[27], improper refrigerant mass charge[28], etc., the actual system performance during operation is generally unknown. The efficiency in the reference conditions listed in the product catalogue provided by manufacture represents the system performance in a limited set of steady state conditions only. Therefore, due to the aforementioned factors, actual operating conditions and efficiency encountered by each installation may substantially deviate from those recorded. This suggests the fundamental necessity of a cost-effective, accurate, and non-intrusive method for predicting these systems performance for better system operation management.

1.2 Issue

Recently the appropriate method for performance prediction of AC system is not available. Several issues that should be considered in performance prediction method development include accessibility for input measurement, cost of sensors, reliability and applicability of developed method. All those mentioned issues represent the obstacles when developing model, collecting the input parameters, and implementing the method in field test system. Among the major issues encountered when estimating the actual performance of air conditioners the most challenging points are described as follows:

- Performance of AC system is closely related to the various operating conditions, external disturbances (such as outdoor temperature and solar radiation) and internal building loads including electricity equipment, occupants, lighting, and others (see Fig. 1.4). The heat gain comes from solar radiation, infiltration and conductive heat gains may change frequently and affect the building cooling load pattern[29]. In the other hand, occupant behavior is also commonly recognized as the main source of uncertainty in estimating building energy performance[30-32]. The consequent variability spectrum is extremely broad and featuring dynamic characteristics. Accordingly, the rated performance provided by manufacture in product catalog does not reflect the actual performances. Part load and dynamic operation behavior constitute the main challenge and source of lack of knowledge in estimating the actual system performance. This variability is reflected by the thermophysical behavior of the working fluid (commonly called refrigerant) which is continuously circulating within the system and dynamically experiencing compression, phase change and two-phase lamination. In detail, the effect of weather condition on AC system performances is discussed in literature[33].

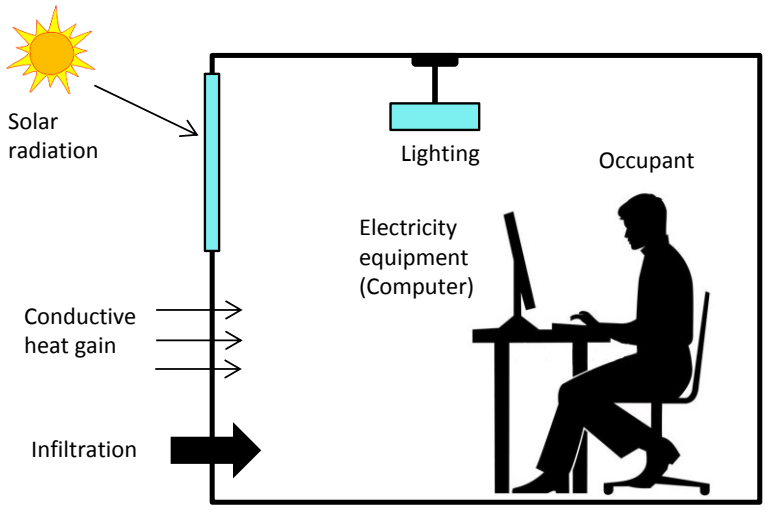

Fig. 1.4 Source of cooling load in buildings

- As explained in previous section, cooling capacity is an important indicator to quantify the performance of AC system. Experimentally, the cooling capacity can be determined by the instantaneous measurement of the refrigerant mass flow rate and the refrigerant enthalpy difference between outlet and inlet of the evaporator[34]. However, measuring pressure and mass flow rate is relatively complex, expensive, and intrusive. The installation of such sensors on an operating system involves the disassemblement to place pressure transmitter and flow meter. It interrupts the system operation and potentially leads to improper refrigerant charge.

- There is a multitude of different systems among those installed all over the world. Every manufactures have different design to achieve the maximum system performance. It is related to the efficiency and specification of system component. As shown in Fig. 1.5, these systems are produced by different manufacturers, with different sizes, types and configurations, which may have different rated capacity and characteristics. In practice, the system installation may have different configuration pertaining to indoor and outdoor unit placement. This affects the accessibility for the input measurement. In the other hand, the package controllers designed in every system are non-identical. As a result, it generates different system dynamic behavior. Various AC system plants in actual application bring the challenge for an effective prediction of air conditioning system performance especially for generalization capability of model.

Fig. 1.5 Types of air conditioning plant[35]

1.3 Possible method for prediction

There are several possible methods that can be applied to predict AC system performance. The options for prediction techniques are described as follows:

- Direct measurement

Cooling capacity of actual system with directly measuring the refrigerant properties has high reliability and quick procedure. It can be determined using refrigerant flow rate and enthalpy difference between inlet and outlet of evaporator[36]. The enthalpy is obtained as a function of pressure and temperature. However as the installation of pressure transmitter and flow meter are intrusive as explained in section 1.2, this method is not applicable for implementation. Moreover, the huge investment cost is required when considering the implementation for a billion units installed in existing buildings since the price for these both sensors are quite expensive.

- Physical model

In the other way, cooling capacity can be predicted using physical model which relies on thermodynamic and heat transfer theory[37]. This technique has been proven to have good approximation and reliability to simulate the system behavior[38]. Unfortunately that method is not appropriate for current application due to many input parameters are required for calculation such as component geometry, refrigerant properties, system specifications, etc.,. While there are only COP

and rated capacity provided by manufacture. All those detail input parameters are difficult to obtain for every system. Additionally there are a lot of equations that should be solved pertaining to the heat transfer and thermodynamic phenomena.

- Statistics

Statistics method is developed based on the available historical data without considering the physical phenomena[39]. The AC systems can be characterized to collect the cooling capacity performances in wide operating conditions. Nonetheless the system performances are very complex and related to physical phenomena which are difficult to estimate using data distribution based. As that method is not related to the physical phenomena, it cannot be generalized to predict the system performance in various condition, different manufacture, and different rated cooling capacity size.

- Machine learning

Machine learning is a black box model that can be used to build the relationship between input and output. It is developed based on learning process on input output data without requiring the complex mathematical functions as involved in physical model. This method has been proven to be able to approximate the input output data accurately when the sufficient training data are available[40]. Regarding to the complexity of AC systems phenomena, this method offers the possibility for simplification of cooling capacity estimation. In physical model, the relationship between the physical phenomena and system performance is established using the complex mathematical functions based on first principle theory[41]. Instead of using the mathematical model, the black box model can be developed to learn the physical phenomena using few input parameters to predict the system performance.

The measurement and estimation of actual AC systems performance is very challenging. By considering the model implementation in actual field test systems, the adopted method should ideally feature the following characteristics:

- be easily implementable to existing systems, with a limited number of reliable input parameters, which can be collected with low-cost sensors placed in measurement points accessible from the outdoor unit without disturbing system installation and operation;

- provide the highest possible prediction accuracy;

- yield generalizable results applicable to different system configurations and climates;

- be able to capture both steady state operation and dynamic responses to external disturbances or internal loads.

1.4 Previous literature

In order to overcome the mentioned issues related to cost of sensors and accessibility during collecting input parameters, a black box model with artificial neural networks (ANN) offers the alternative solution to predict the cooling capacity without requiring many input parameters and equations. This method can be developed using relevant input parameters that are non-intrusive, inexpensive to measure and represent system performance behavior.

The ANN model has been introduced since last two decades to apply for energy analysis in building[42]. This technique is believed to have good approximation in mapping input and output data. The main advantages of ANN method are speed, simplicity, and the ability of solving the complex nonlinear relationship between variables[43]. In some literature, ANN method has been successfully used to predict heating load[44, 45], cooling load[46], absorption system performance[47, 48], and optimize the thermal comfort and energy consumption in building[49].

Furthermore the application of ANN related to air conditioning and refrigeration system application has been reviewed in literature[43]. Kamar et al. (2013)[50] have proposed the ANN method to predict automobile AC system performance. In that work, several parameters, i.e. compressor speed, valve opening, and air temperature at evaporator and condenser inlet have been taken as inputs. The results show that the optimized ANN structure can predict system performance with high accuracy. A similar study has also been conducted by Tian et al. (2015)[51] to predict vehicle AC system performance equipped with scroll compressor and electronic expansion valve (EEV). The results show that high prediction accuracy has been achieved using optimized ANN model with thirteen neurons. Atik et al. (2010)[52] have proposed an ANN model to predict system performance under variation of mass charge and compressor speed. The results have shown that the ANN model using the inputs of compressor speed and amount of refrigerant has successfully predicted mobile air conditioning (MAC) system performance (cooling capacity, compressor power, and COP) with satisfying accuracy. Wu et al. (2017)[53] have developed ANN model to predict split AC system performance and indoor thermal comfort (air temperature and humidity). The training data are collected by directly measuring the input output parameters in existing systems. The prediction is conducted using the inputs of supply air temperature, humidity, and velocity, outdoor temperature and humidity, and input power. The results indicate that the ANN model has successfully predicted energy efficiency ratio (EER) with acceptable accuracy.

1.5 Unresolved issue

According to the aforementioned-works above, the ANN models are mostly developed using the input parameters that are intrusive to measure (refrigerant mass charge, compressor speed, valve opening) or affected by high location variance (air-side temperatures and velocity), which could hinder their actual implementation in operative systems. Moreover, predictions are carried out using the training and testing data generated from the same system, in the same structural condition.

Therefore, the developed ANN model in previous studies cannot be applied in various systems with different rated capacity.

1.6 Objective

The present study aims to develop reliable ANN model that can be used to predict cooling capacity of AC systems using non-intrusive and cost effective input parameters. The research has three main objectives as follows:

- Developing ANN model to capture dynamics systems performances behavior.
- Teaching ANN the physics of air-conditioning cycles via few accessible inputs related to the refrigerant properties to predict actual system performance.
- Developing a generalizable ANN model that can be applied for performance prediction on various systems from different manufacturers and different rated capacity.

1.7 Research hypothesis

The research is conducted with the hypothesis that the system performance can be predicted by properly teaching ANN the physics of air conditioning cycle. Moreover, the ANN model could be applied to predict the performance of different systems with the motivation that all vapor compression systems stand on the same fundamental cycle. The dynamic performance behavior of AC systems could be captured by dynamic ANN model which include previous time step input characteristics for training.

1.8 Originality

This research proposes a new method for cooling capacity prediction that is cost effective, non-intrusive, and applicable for implementation in different systems. The method involves few input parameters representing the refrigerant cycle, resulting in easily measurable in actual operative conditions. In this study, a cost-effective possibility of capturing output cooling capacity considering various operating condition, cooling loads, and different nominal capacity is demonstrated by utilizing an ANN model exclusively based on four refrigerant temperatures that are easily accessible from the outdoor unit.

1.9 Thesis structure

Chapter 1 describes the background, purpose, importance and contribution of the research.

Chapter 2 shows the general vapor compression air conditioning system and simulation tool. In this section the mathematical model based on first principal analysis for each component are

introduced for simulation tool. The description related to the system operation and control development is also presented.

Chapter 3 explains the ANN development as prediction approach. The development includes the analysis on data characteristic, sampling time selection, and data variability. Additionally, the input selection for performance prediction is presented in this chapter.

Chapter 4 describes the experimental facility to generate input output data on actual machine. The operation characteristics such as intermittent, steady and unsteady behavior on actual performance behavior are discussed.

Chapter 5 investigates the ability of ANN model for performance prediction using simulation and experimental data based. In this section the ANN model is trained using the data generated from simulation and applied to predict the system performance on actual system. The difference in data characteristics is analyzed comprehensively.

Chapter 6 introduces the feasibility studies of ANN model for actual implementation. The performance of ANN prediction based on experimental data in various operating condition considering dynamic cooling load, indoor and outdoor temperatures is investigated in this section.

Chapter 7 summarizes the conclusion for the entire works and presents the prospect of related research for future study.

2. System description and simulator development

2.1 System description

The AC system works to maintain indoor temperature by reversing the heat transfer from the conditioned space to the external environment. In general, a vapor compression AC system is composed of four main components i.e. compressor, condenser, expansion valve, and evaporator. Schematic diagram of the system is demonstrated in Fig. 2.1. As the working fluid (refrigerant) circulates, it absorbs the heat Q_e from the conditioned space at low temperature surrounding T_{in} through the evaporator and releases Q_c to the external ambient at outdoor temperature T_{out} through the condenser. When the heat absorbed by the system (cooling capacity) is higher than the heat gained from solar radiation or internal sources (cooling load), the indoor temperature gradually decreases. Conversely, the indoor temperature will increase when the cooling capacity is lower than the cooling load. Different AC systems feature different instantaneous ability to respond to the balance between cooling load and cooling capacity, which is related to the control strategy implemented, the configuration adopted, and the refrigerant used as working fluid. The cooling capacity variations delivered by a certain system can be adjusted by regulating the work of compressor, which adjusts pressures (and saturation temperatures) levels as well as the refrigerant mass flow rate according to the characteristic operation map of the device, and valve opening, which acts on the evaporation pressure and superheat level at the compressor inlet.

As succinctly descripted, the configuration of such vapor compression systems is mirrored by the sequence of thermophysical transfer processes constituting the refrigerant cycle as depicted in Fig. 2.2

- Evaporation (1-2)

In evaporator, the refrigerant temperature is lowered below the level of its surrounding (conditioned space). Therefore, it evaporates by absorbing the heat from the conditioned space. The refrigerant leaves the evaporator in a low-pressure saturated vapor. The superheat occurs when the saturated refrigerant vapor is heated above its boiling point. This parameter is important in AC system to ensure the liquid refrigerant is boiled off when leaving the evaporator, to make the compressor safe[54].

- Compression (2-3)

When the refrigerant enters the compressor, it exhibits a superheated gas phase at low pressure and temperature. During the compression process, its pressure and temperature are increased adiabatically by the mechanical work delivered to the compressor. The increase of gas pressure leads to higher condensing temperature of the refrigerant. A sufficient compression ratio

between inlet and outlet compressor pressures is required to achieve a refrigerant boiling point temperature higher than the outdoor environment.

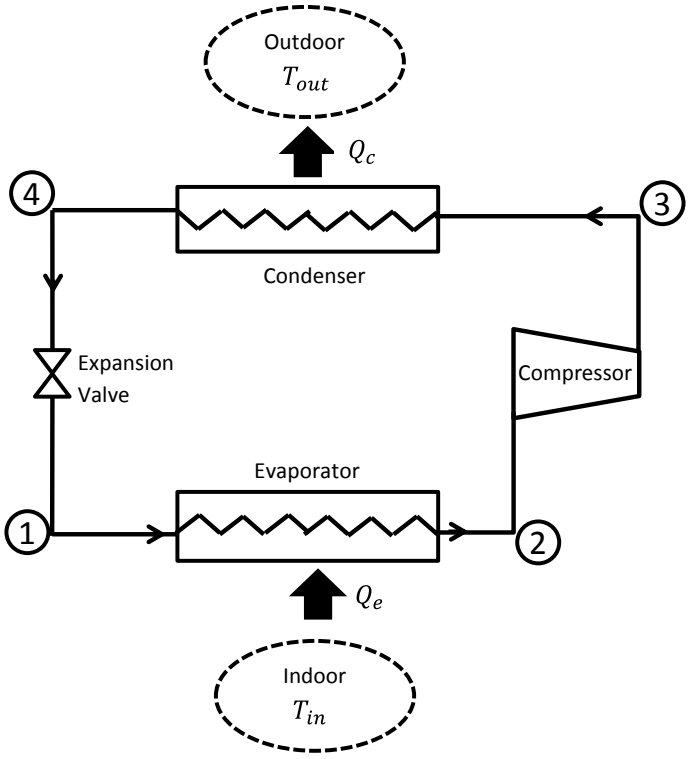

Fig. 2.1 Schematic diagram of general vapor compression air conditioning systems

- Condensation (3-4)

In condensation process, the refrigerant phase is changed from vapor to liquid by extracting the heat. When the refrigerant enters the condenser at high pressure and temperature, it carries the heat energy absorbed in evaporator and work energy transferred by the compressor. As the refrigerant temperature is higher than the outdoor temperature, the related heat transfer condenses the refrigerant from high-pressure vapor to high-pressure saturated liquid. Accordingly, the transfer surface and the control strategy are designed to ensure that the refrigerant leaves the condenser in a liquid phase.

- Expansion (4-1)

When the refrigerant enters the expansion valve, it expands and decreases the pressure. As a result, the temperature drops below the heat source temperature and refrigerant leaves the expansion valve in liquid-vapor mixture. Consequently, the condensed refrigerant is returned to the low

pressure and temperature levels of the evaporator for closing the cycle and operate continuously to the next cycle for uninterruptedly transferring heat from the indoor to the outdoor environment and reaching the desired indoor temperature.

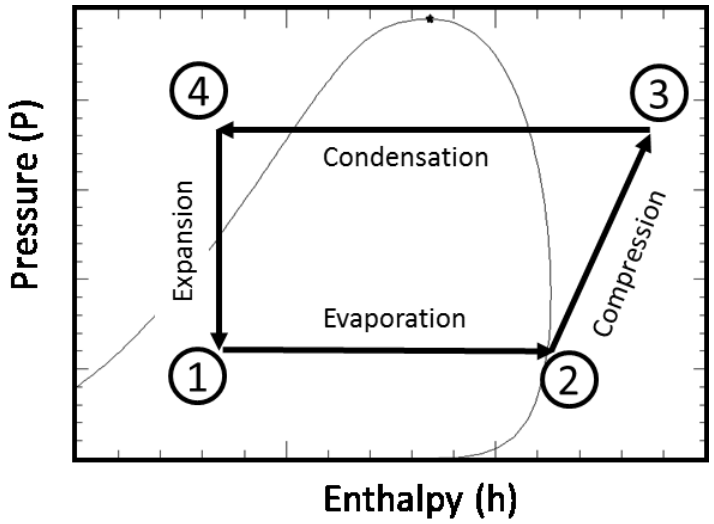

Fig. 2.2 Cycle diagram of vapor compression system

2.2 Simulator development

As previously mentioned, the physical phenomena of refrigerant state in every single component, although very complex in their interdependencies, can be approximated by using the first principle of thermodynamic, mass and momentum balances, and heat and mass transfer theory. Accordingly, such modeling effort can be used to estimate the performance of an air conditioner in various operating conditions, and, if the thermophysical properties of different refrigerants are available for correlating the state to the transfer properties, the operation of the same system can be explored for different working fluids. The implementation of such general principles in a common numerical simulation platform with a modular structure connecting the numerical approximation of the different components in any combination, would enable the user to simulate any possible system configuration on the market and explore others which are not. Finally, a modulation of the transfer properties based on the modeling of possible system faults encountered in real operation expands the simulation scenario to any fault conditions. Such simulator can thus handle the estimation of dynamically variable operating conditions, different climates, different system configurations and size, any working fluid, as well as possible operation faults. This generalizable and broad-spectrum simulation scenario overcomes the limitations related to cost and technology encountered when using in experimental facilities, and constitutes an extremely appealing tool for the generation of a broad and reliable set of training data.

Therefore, in this work, a multi-purpose air conditioning system simulator is designed to be able to simulate any systems with various specifications, nominal capacities, characteristics, configurations, and produced by different manufactures. Practically, the simulator is established by developing mathematical model of each system component, including fin-tube heat exchangers, compressor, expansion valve, accumulator, and reversing valve. The equations for each component used for simulation are briefly described as follows:

2.2.1 Compressor

The compressor can be considered as the heart of vapor compression system. This component plays the utmost important role to circulate the refrigerant within the system. The compressor types used in this system vary including reciprocating compressor, rotary screw compressor, scroll compressor, and others. The mathematical model is developed for scroll compressor type (Fig. 2.3) with considering the volume of compressor, adiabatic efficiency, and volumetric efficiency that can be obtained from the system specification. The compressor is assumed to have inverter so it could provide the part load operating condition. The simulator does not exclude for the other compressor types.

The basic formula of compressor model is developed based on the continuity and energy balance as expressed below.

$$\rho_{R,O}\, v_{R,O}\, S_{R,O} - \rho_{R,I}\, v_{R,I}\, S_{R,I} = 0 \tag{2.1}$$

$$\rho_{R,O}\, v_{R,O}\, h_{R,O}\, S_{R,O} - \rho_{R,I}\, v_{R,I}\, h_{R,I}\, S_{R,I} = W \tag{2.2}$$

$$\rho_{R,I}, s_{R,I} = f(P_{R,I}, h_{R,I}) \tag{2.3}$$

Relationship between adiabatic efficiency and refrigerant properties at the suction and discharge of compressor is modeled using the following equation:

$$\eta_{ad} = \frac{h_{R,O,ad} - h_{R,I}}{h_{R,O} - h_{R,I}} \tag{2.4}$$

When the adiabatic efficiency is neglected, the entropy at the suction and discharge of the compressor does not change as shown in Eq. (2.5).

$$s_{R,O,ad} = s_{R,I} \tag{2.5}$$

Mass flow of refrigerant change in response to the rotational speed modulation is calculated using Eq. (2.6).

$$G_{R,I} = \omega\, \eta_V \rho_{R,I} V \tag{2.6}$$

Energy consumption of the compressor is determined by the following equation:

$$W = \eta_{INV} E \tag{2.7}$$

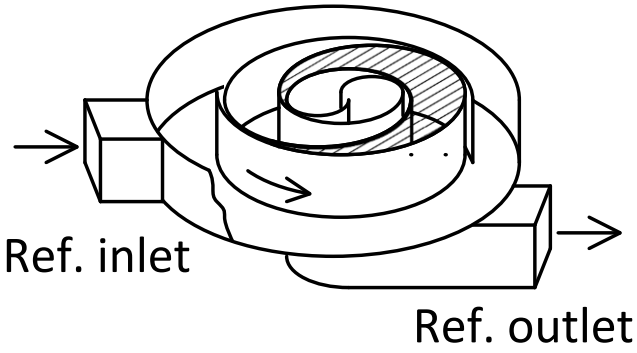

Fig. 2.3 Scroll compressor model[55]

2.2.2 Expansion valve

Expansion valve aims to remove the pressure from liquid refrigerant to allow the refrigerant to change in gas phase when entering the evaporator. There are several expansion valve types used in vapor compression namely capillary tube[56], thermostatic expansion valve (TXV)[57] and electronic expansion valve (EEV)[58, 59]. The capillary tube is not controllable as it has no moving part. The pressure is reduced by passing the refrigerant through this device. Unlike the capillary type, TXV type is equipped with moving part that can control the mass flow of refrigerant. The valve opening is automatically adjusted to regulate the amount of refrigerant liquid injected to the evaporator by sensing the degree of the superheat temperature. The performance of mass flow control by this device is limited to imprecise valve opening regulation, poor accuracy of superheat measurement, and small range of operating condition. An EEV device is more advanced compared to two previous valve types. This technology has a proportional feed-back action control mechanism that can provide variable valve opening to maintain a superheat under various operating condition[60].

The expansion valve control is related to the compressor safety and system efficiency. The proper mass flow of refrigerant should be properly adjusted to provide high cooling capacity and make sure that there is no liquid refrigerant when entering the compressor. In this simulation the expansion valve is modeled with EEV type (see Fig. 2.4). Mass flow of refrigerant can be directly adjusted by assigning the opening of valve.

The basic formula for expansion valve model is written in Eqs. (2.8 and 2.9).

$$\rho_{R,O}\, v_{R,O}\, S_{R,O} - \rho_{R,I}\, v_{R,I}\, S_{R,I} = 0 \tag{2.8}$$

$$\rho_{R,O}\, v_{R,O}\, h_{R,O}\, S_{R,O} - \rho_{R,I}\, v_{R,I}\, h_{R,I}\, S_{R,I} = 0 \tag{2.9}$$

The mass flow rate in expansion valve is modeled using Eq. (2.10).

$$G_{R,I} = c_V S \sqrt{2\, \rho_{R,I}\, \left(P_{R,I} - P_{R,O}\right)} \tag{2.10}$$

During the operation, the pressure and mass flow of refrigerant can be controlled by adjusting the area of valve opening S as shown in Eq. (2.10). The relationship between the area and pulse of valve opening is shown in Eq. (2.11). Notation c_p represents the area per pulse.

$$S = c_p\, p_v \tag{2.11}$$

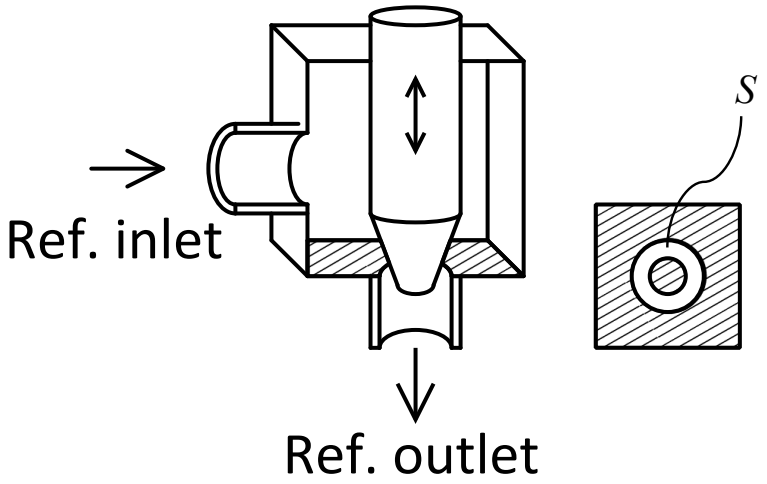

Fig. 2.4 Electronic expansion valve[55]

2.2.3 Heat exchanger

Heat exchangers are intended to interact with the thermal energy sources (external environment) and deliver the useful effect of the cycle (in this case, the cooling capacity Q_e), which is most commonly performed by exchanging heat between the air and refrigerant. There are several heat exchanger types used in vapor compression system that can be developed in simulator such as plate heat exchanger, shell and tube, compact heat exchanger, fin tube and others. Fin-tube heat exchangers are the most common ones for AC system applications[61]. This heat exchanger type is selected for evaporator and condenser in present study. The illustration of fin tube heat exchanger can be seen in Fig. 2.5. Distributed model is employed to describe the phenomena of heat transfer between air and refrigerant in indoor and outdoor unit.

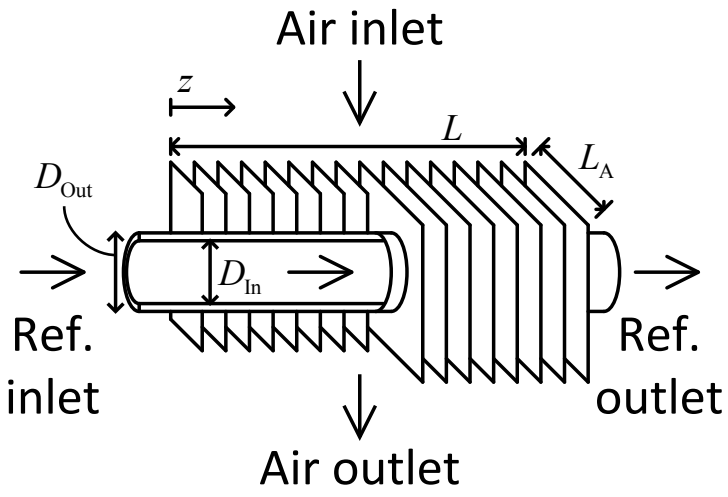

Fig. 2.5 Cut of fin tube heat exchanger[55]

The basic equations representing the continuity, energy balance, and pressure drop for refrigerant at heat exchanger are expressed in Eqs. (2.12 - 2.14). The friction factor f_r is acquired from the equation presented in previous work[62]. The term q_{In} in Eq. (2.14) represents the heat transfer between refrigerant and tube.

$$\frac{\partial \rho_R}{\partial t} + \frac{\partial (\rho_R v_R)}{\partial z} = 0 \tag{2.12}$$

$$\frac{\partial P_R}{dz} = -f_r \frac{1}{D_{In}} 2\, \rho_R\, {v_R}^2 \tag{2.13}$$

$$\frac{\partial (\rho_R U_R)}{\partial t} + \frac{\partial (\rho_R v_R h_R)}{\partial z} = -\frac{Lc_{In}}{S_{In}} q_{In} \tag{2.14}$$

The energy balance of the tube is expressed in Eq. (2.15). The notation q_{Out} shows the heat transfer between air and tube.

$$\rho_T C_T \frac{\partial T_T}{\partial t} = \frac{Lc_{In}}{S_T} q_{In} - \frac{A_{FC} + \eta_{FIN}\, A_{FIN}}{S_T\, L} (q_{Out} + j_{Out}\, h_{vap}) \tag{2.15}$$

The correlation to calculate the air properties including continuity, moisture, pressure drop, and energy balance are described in Eqs. (2.16 - 2.18), respectively.

$$\rho_{A,O}\, v_{A,O}\, L_A - \rho_{A,I}\, v_{A,I}\, L_A = \frac{A_{FC} + \eta_{FIN}\, A_{FIN}}{L} j_{Out} \tag{2.16}$$

$$\rho_{A,O}\, v_{A,O}\, X_{A,O}\, L_A - \rho_{A,I}\, v_{A,I}\, X_{A,I}\, L_A = \frac{A_{FC} + \eta_{FIN}\, A_{FIN}}{L} j_{Out} \tag{2.17}$$

$$P_{A,O} - P_{A,I} = 0 \tag{2.18}$$

The heat transfer between refrigerant and tube q_{In} is calculated using Eq. (2.19), while the heat transfer between the tube and air q_{Out} is determined by Eq. (2.20). The total amount of heat absorbed by evaporator is considered as cooling capacity Q_e and the total heat released to environment in condenser is recognized as condensing capacity Q_c.

$$q_{In} = \alpha_{In}(T_R - T_T) \tag{2.19}$$

$$q_{Out} = \alpha_{Out} \frac{(T_T - T_{A,I}) - (T_T - T_{A,O})}{ln\frac{(T_T - T_{A,I})}{(T_T - T_{A,O})}} \tag{2.20}$$

The amount of refrigerant charge inside the heat exchanger is calculated using Eq. (2.21).

$$m_R = S_{In} \int_0^L \rho_R \, dz \tag{2.21}$$

To calculate the pressure drop in the pipe, the Blasius equation[63] is applied for single phase flow. While the Chisholm[62] and Lockhart-Martinelli[64] equations are applied for two-phase flow. Moreover, the heat transfer coefficient in the pipe is calculated using Dittus-Boelter[65] equation for single-phase flow. Yoshida et al. (1983)[66] and Nozu et al. (1983)[67] equations are for two-phase evaporation and condensation process, respectively. The formula for pressure drop, heat transfer coefficient, and fin efficiency in air side are adopted from Seshita's equation[68].

2.2.4 Room

Mainly, the room model aims to recreate the temperature response in regard to the effect of cooling load, cooling capacity, and the building size (thermal mass). The change of indoor temperature is calculated using the first order differential equation representing the energy balance Eq. (2.22).

$$\rho_A C_A V_A \frac{dT_{in}}{dt} = Q_e - Q_{load} \tag{2.22}$$

The equation for cooling capacity Q_e can be expressed as follows:

$$Q_e = G_{R,I} \, h_{R,I} - G_{R,O} \, h_{R,O} \tag{2.23}$$

2.2.5 Accumulator

A compressor is specifically designed to compress the refrigerant vapor, not liquid. The main function of accumulator is to prevent compressor damage from liquid refrigerant that may enter the compressor from the suction. This device (Fig. 2.6) is a temporary reservoir to ensure that

any liquid exiting from evaporator falls at the bottom of accumulator and give it the time to complete phase change to vapor before entering the compressor suction. The equations of continuity and energy balance for accumulator model are presented in Eqs. (2.24 - 2.25). The pressure at inlet and outlet of accumulator is assumed to be the same.

$$V\frac{d\rho_R}{dt} + \rho_{R,O}v_{R,O}S_{R,O} - \rho_{R,I}v_{R,I}S_{R,I} = 0 \tag{2.24}$$

$$V\frac{d(\rho_R U_R)}{dt} + \rho_{R,O}v_{R,O}S_{R,O}h_{R,O} - \rho_{R,I}v_{R,I}S_{R,I}h_{R,I} = 0 \tag{2.25}$$

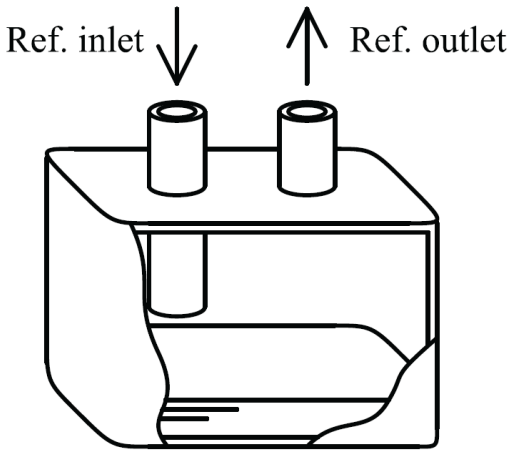

Fig. 2.6 Accumulator[55]

2.2.6 Reversing valve

Reversing valve is modeled to allow the system to function in both heating and cooling modes. When the system is operated in cooling mode, the compressed refrigerant from the compressor goes to the heat exchanger located in the outdoor unit. Otherwise, the refrigerant flows reversely in heating mode and the heat exchanger in conditioned space works as the heating coil. The study presented in this work is focused on cooling mode only, but this does not exclude the application of the method presented to heat pumps and AC systems operating in heating mode. Schematic diagram of the reversing valve is shown in Fig. 2.7. The mathematical equation for this equipment is modeled with assumption that there is no pressure drop in the inlet and outlet. Notation of LP and HP represents low pressure and high pressure of refrigerant.

The correlation for continuity and energy balance is described as in Eqs. (2.26 and 2.27). According to Eq. (2.27), the change of the internal energy of refrigerant is determined as a function of heat transfer between the inlet and outlet of high pressure refrigerant.

$$V_{HP}\frac{d\rho_{R,HP}}{dt}+\rho_{R,HP,O}\,v_{R,HP,O}\,S_{R,HP,O}-\rho_{R,HP,I}\,v_{R,HP,I}\,S_{R,HP,I}=0 \quad (2.26)$$

$$V_{HP}\frac{d(\rho_{R,HP}\,U_{R,HP})}{dt}+\rho_{R,HP,O}\,v_{R,HP,O}\,h_{R,HP,O}\,S_{R,HP,O}-\rho_{R,HP,I}\,v_{R,HP,I}\,h_{R,HP,I}\,S_{R,HP,I}=Q \quad (2.27)$$

The heat transfer between low and high pressure refrigerant is calculated using thermal conductivity as expressed in Eq. (2.28).

$$Q=KA\,(T_{R,HP}-T_{R,LP}) \quad (2.28)$$

The amount of refrigerant in reversing valve is determined using Eq. (2.29).

$$m_R=\rho_{R,HP}V_{HP}+\rho_{R,LP}V_{LP} \quad (2.29)$$

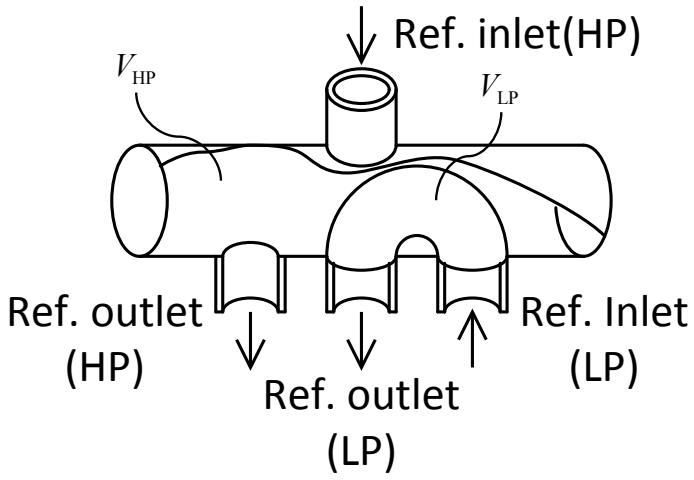

Fig. 2.7 Reversing expansion valve model[55]

2.3 Simulation validation

Validation of simulation results is required to ensure that the mathematical model used for simulation could well represent the actual system behavior including response time, control and thermodynamics phenomena. Simulation results of numerical model have been validated with reference to experimental data[69] collected in intermittent, steady and unsteady operating conditions. When performing the numerical simulations, the dimensions of system components' geometry and the operating scenario are set as precisely as possible as those encountered in the actual experimental facility. The representative validation results are presented in Fig. 2.8. Several parameters including input power, compressor power, cooling capacity, COP, compressor pressure at suction and discharge, and outlet temperature at indoor and outdoor unit show good agreement between simulation and experimental data with relative error of 10%. The validation results suggest

that the simulator is reliable enough to demonstrate the system performance either in steady and unsteady condition, but requires special calibration care of the control method during intermittent operation.

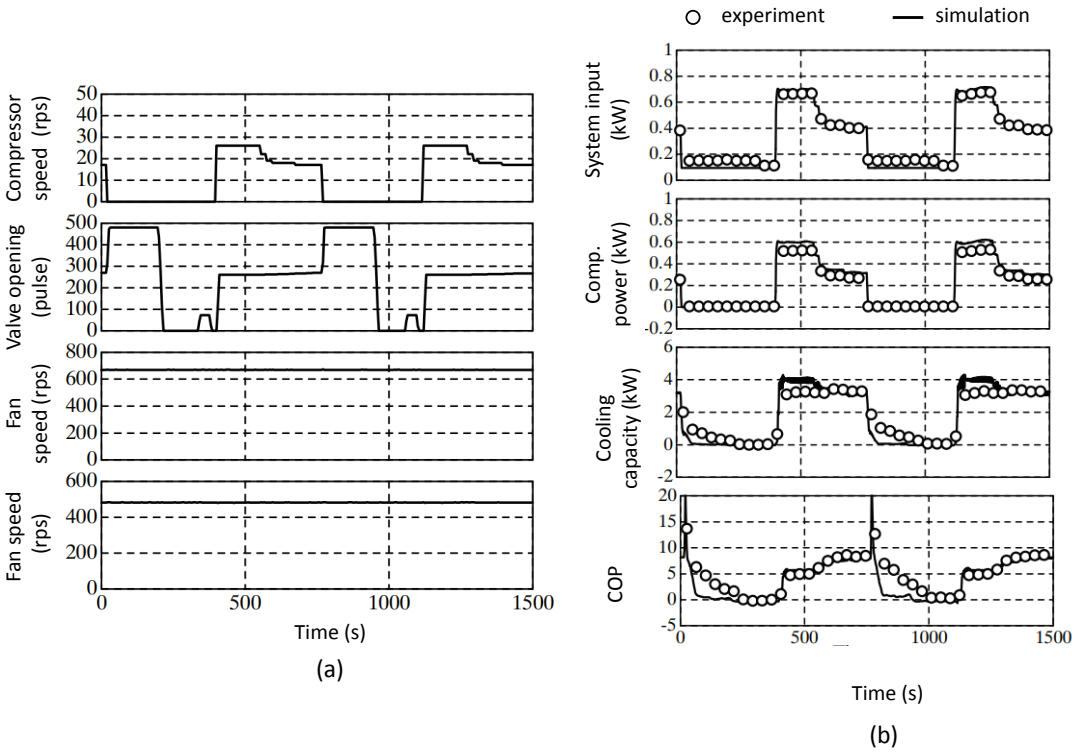

Fig. 2.8 (a) simulation input (b) validation result[69] (line and markers show simulation and experimental data, respectively)

2.4 Controller design

The controller is designed to operate the system in a similar manner to the actual machine and generate reliable simulation results. A proportional integral (PI) controller is developed to control indoor temperature and superheat by regulating compressor speed and valve opening, respectively. The block diagram of PI controller can be seen in Fig. 2.9. The controller calculates the error as the difference between a set point target and a system output. The controllable parameters are adjusted to minimize the error expressed in Eq. (2.30). The optimum signal input is calculated according to the gain values (K_p, K_i) as written in Eq. (2.31).

$$e(t) = r(t) - z(t) \tag{2.30}$$

$$u(t) = K_p e(t) + K_i \int_0^t e(t)\, dt \tag{2.31}$$

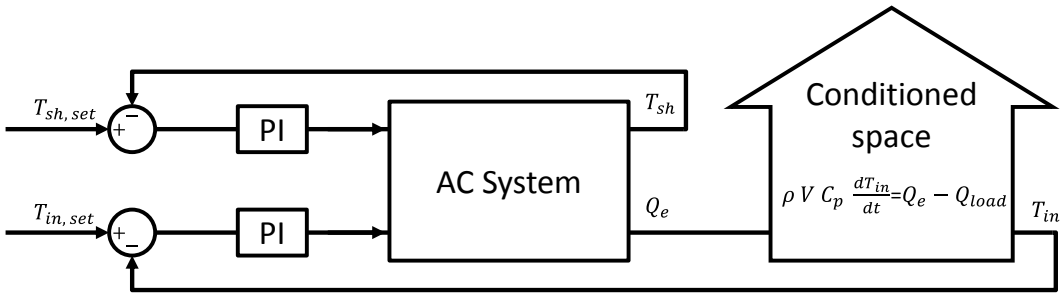

Fig. 2.9 Block diagram of PI controller

The procedure for the tuning of the PI control is described as follows:

2.4.1 Step response test

The development of PI controller begins with the step response test to characterize the system response. As depicted in Fig. 2.10(a), the input unit $u(t)$ is introduced in two different values. Subsequently, the response of plant indicated by $H(t)$ is analyzed since the step change starts until once it approaches the steady state value H (see Fig. 2.10(b)). This output response represents the system characteristics that should be considered while designing the controller.

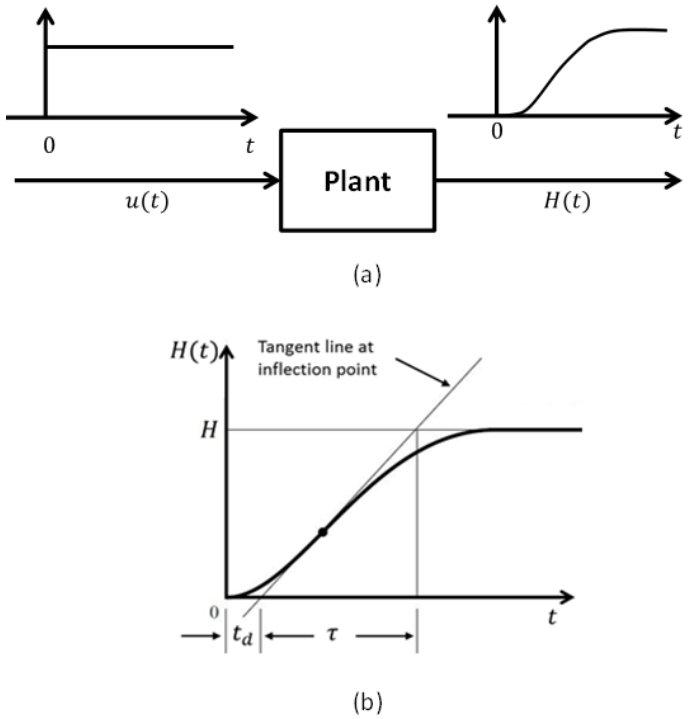

Fig. 2.10 (a) Unit step response and (b) S-shaped response curve

The S-shaped curve shown in Fig. 2.10(b) highlights two important constant parameters of the system response characteristics, namely delay time t_d and time constant τ. These two parameters are determined by the intersection between a tangent line at inflection point of S-shaped curve to the constant value line ($H(t) = 0$) and to the horizontal line of steady state response ($H(t) = H$), respectively. All these parameters are used to tune the gain values of PI controller.

There are two PI controllers designed for compressor and expansion valve. The step response test for compressor and expansion valve is conducted individually. When the step response test for compressor is performed, the other parameters are set constant. Only compressor speed signals are changed. This also applies for the step response test of expansion valve. The signal of expansion valve opening is changed while other parameters are kept constant.

2.4.2 Gain tuning

The gain values of PI controller are tuned by following Ziegler-Nichols rules[70]. The gain values for K_p and K_i are calculated using the delay time and time constant parameters determined in step response test presented above. The equation of K_p and K_i are written in Eqs. (2.32 and 2.33).

$$K_p = 0.9\frac{\tau}{t_d} \tag{2.32}$$

$$K_i = 3.3\, t_d \tag{2.33}$$

2.4.3 Control performance

The performance of designed PI control is evaluated by analyzing the system response while controlling the indoor temperature and superheat. The controller is tested by introducing a sudden step change of cooling load. Initially, the indoor temperature and superheat is controlled at 27 °C and 5 °C, respectively, at nominal capacity (full load) until reaching steady state condition. Then the cooling load is suddenly changed to 90% of the nominal capacity. Based on the results presented in Fig. 2.11, it can be observed that the controller can precisely maintain the desired indoor temperature and superheat. The corresponding control performance test shows the overshoot of cooling capacity, indoor temperature, and superheat are 20% of step change, 0.17 °C, and 1 °C. When the controller works properly, the cooling capacity reaches the proposed load with keeping the indoor temperature as the set point. The cooling capacity response presents a rise time (time spent to reach 90% of the step to the set point) of 81s and settling time (±2% set point) of 493s to reach the cooling load.

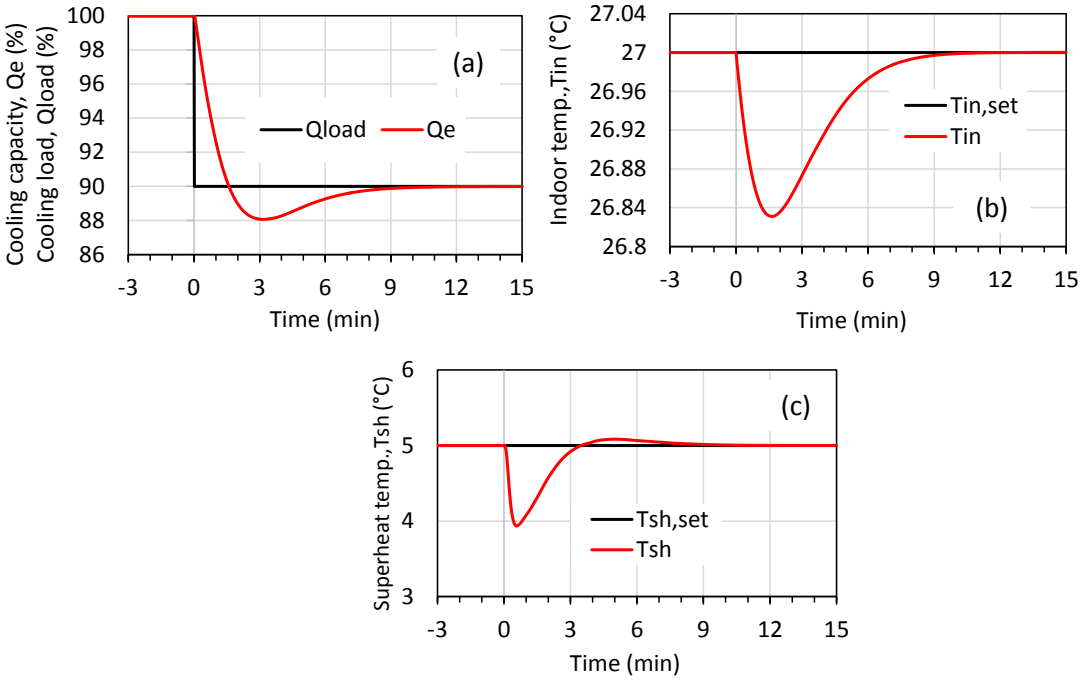

Fig. 2.11 Performance of PI control under load change (a) Cooling capacity (b) Indoor temperature (c) Superheat (T_{in}: 27 °C, T_{out}: 35 °C; Q_{load}: 100 to 90%)

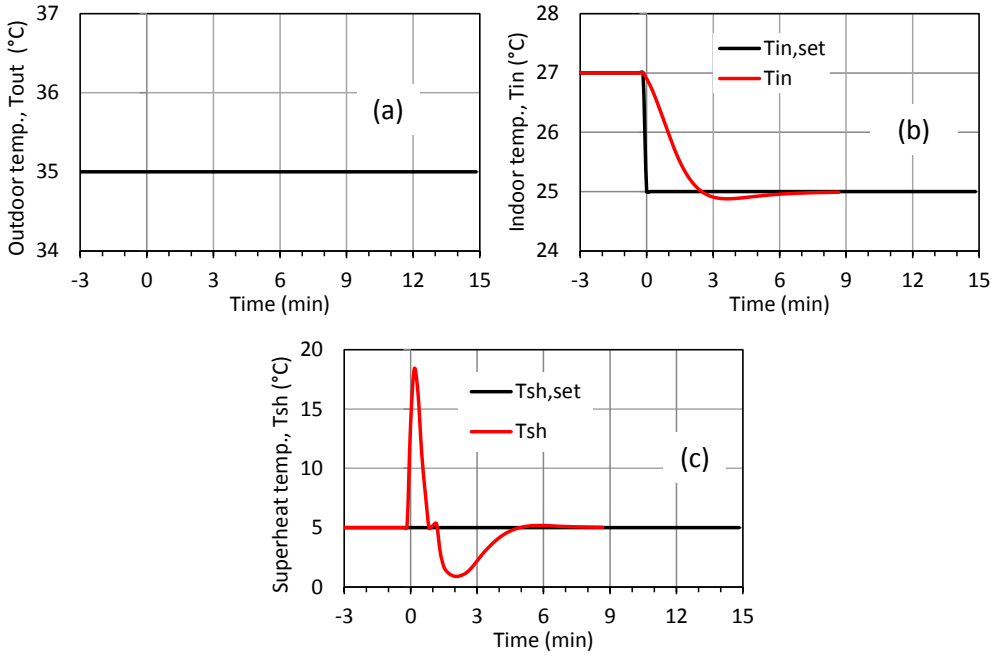

Fig. 2.12 Performance of PI control under indoor temperature change (a) Outdoor temperature (b) Superheat (c) Indoor temperature (T_{in}: 27 to 25 °C, T_{out}: 35 °C; Q_{load}: 50%)

Moreover, the control ability is also tested in response to variations of indoor and outdoor temperature with 50% of the maximum capacity. As presented in Figs. 2.12 and 2.13 the results demonstrate that the indoor temperature and superheat can be controlled accurately with acceptable overshoot and settling time. The satisfying control performance on several testing conditions indicates that the controller could successfully handle the disturbances (different load, indoor and outdoor temperature conditions). Hence such controller calibration method is applied for the characterization of different systems simulated in this study, and for the intelligent prediction of AC system performance presented as follows.

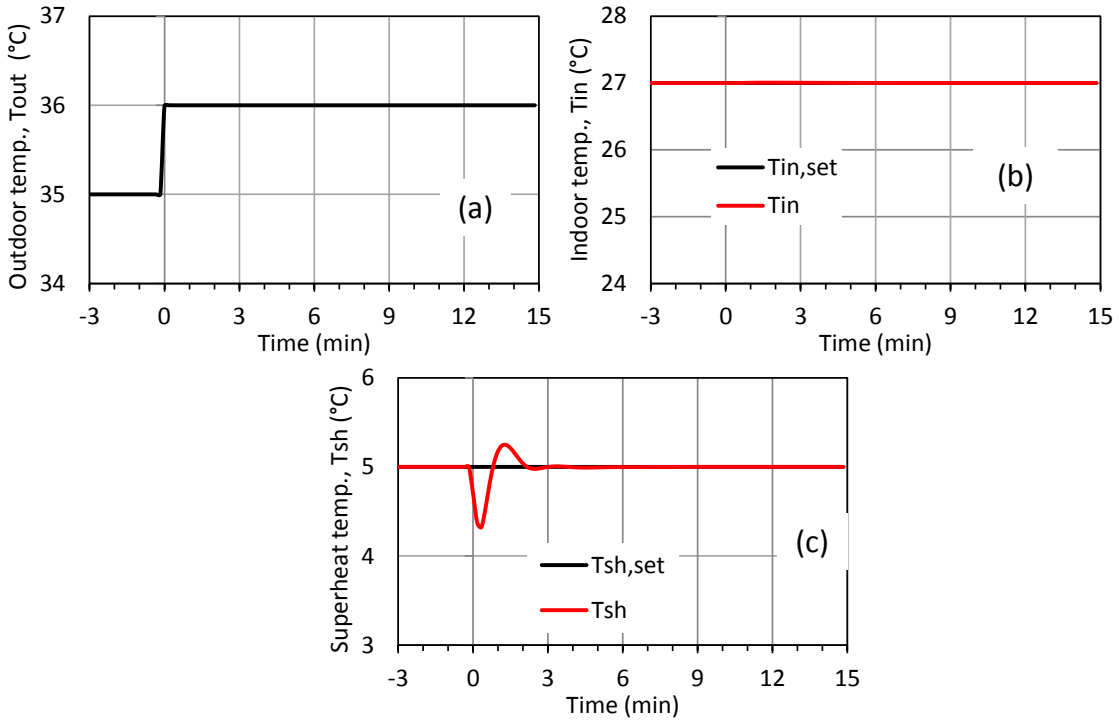

Fig. 2.13 Performance of PI control under indoor temperature change (a) Outdoor temperature (b) Superheat (c) Indoor temperature (T_{in}: 27 °C, T_{out}: 35 to 36 °C; Q_{load}: 50%)

3. Application of artificial neural network to air conditioning system

3.1 ANN theory

Recently everyone perceives the beginning of the overwhelming artificial intelligence (AI) era. There are more and more "intelligent" services, which make use of such technology and have been introduced in many application cases. In the present study, the effective application of artificial neural network (ANN) for an efficient building energy management is proposed.

In short, machine learning can be defined as a part of AI and a modeling technique that involves the development of interrelations between input and output data without requiring the rigorous application of theoretical principles and empirical correlations, while ANN is a kind of machine learning. This approach has been widely applied to solve the engineering problems in various fields[71-73].

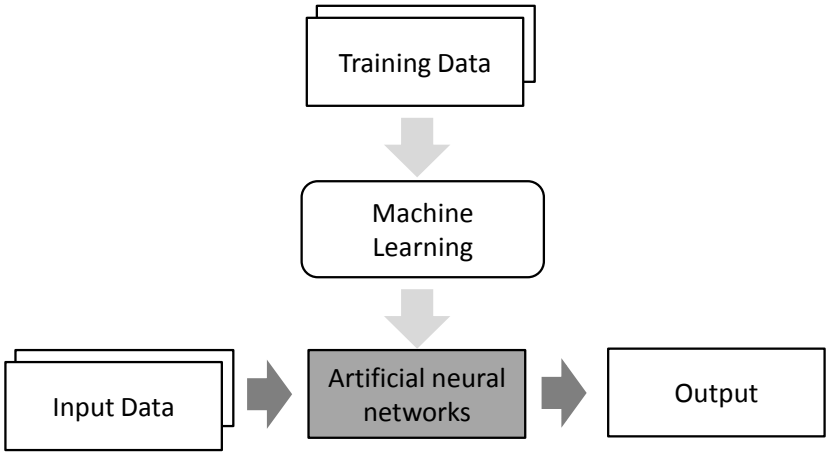

Fig. 3.1 Schematic diagram of machine learning model

The process for developing a model by machine learning relies on a set of data to be used for the training procedure, which outlines the interrelations between input and output quantities as illustrated in Fig. 3.1. The vertical flow describes the learning process where the training data are referred for calibrating the model. The horizontal flow illustrates the application of the model. The model can be reliable when its implementation yields an accurate estimation of the testing data. Therefore, an effective application of the ANN model requires that the data used for the training to comprehensively cover the characteristics of the field occurrence of the actual phenomenon or system operation. The capability of ANN model in data approximation, without requiring complicated mathematical equations, opens up to prediction possibilities in circumstances where there is a lack of theoretical representations due to the over-complexity of the phenomena interrelations. This represents a critical advantage especially for the application to the engineering

field, where a certain system behavior can be characterized without requiring many detailed input parameters which would be necessary for the solution of the mathematical formulation of the model based on physical principles and formulas.

Basically, the ANN technique is inspired by the human brain mechanism[74]. In the same way as the brain is composed of the large number of connected neurons, the ANN is structured around the connections of numerous nodes (neurons). The main role of such nodes is to define the relationship between input and output quantities using mathematical functions. The ANN technique offers an incredible variety of configurations and almost infinite adaptability to physical and technical interrelations. A multi-layer perceptron (MLP) model is one of the most popular structures which has been successfully applied for prediction purposes[75]. This structure is mainly composed of an input layer, hidden layers and an output layer, as demonstrated in Fig. 3.2. The number of hidden layers can be flexibly chosen (one or more). Moreover, the number of nodes in each layer can be arbitrarily set while taking account for the number of input-output variables and the complexity of the network structure.

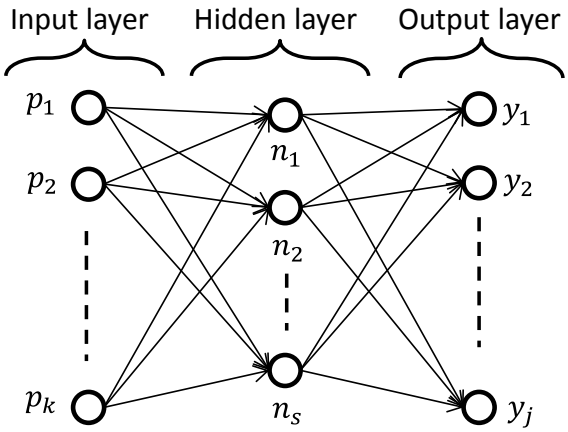

Fig. 3.2 General multi-layer perceptron ANN configuration

A typical MLP structure features connections between every node in a layer and the nodes of the next layer. The mathematical function that builds the relationship between the nodes is described below.

In a single-node form the output of a simple ANN structure with one input (Fig. 3.3) can be calculated as:

$$n = wp + b \tag{3.1}$$

$$a = f(wp + b) \tag{3.2}$$

where p and a represent the input and output quantities of the ANN, respectively. The weight w and bias b are adjustable scalar parameters that can be optimized during the training process to obtain the ANN output as the target values. The ANN output is affected by the selected transfer function f which can be a linear or nonlinear function of n.

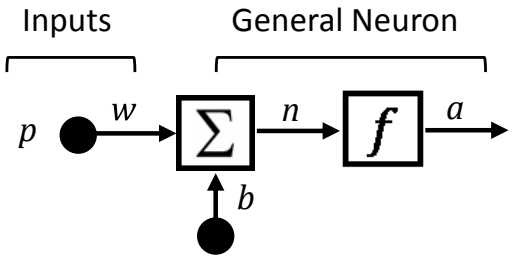

Fig. 3.3 Single input and single neuron

Furthermore the ANN model may have more than one input connected to a neuron. The mathematical representation of ANN structure with k inputs and one neuron is demonstrated in Fig. 3.4. In order to obtain the network output, every input p_1, p_2,…, p_k are multiplied by the corresponding weight coefficients w_1, w_2,…., w_k incorporated inside the matrix [w].

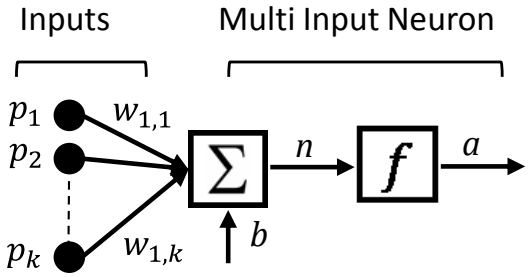

Fig. 3.4 Multi-input and single neuron

The notation n in Fig. 3.4 is determined by the following equation:

$$n = w_{1,1}\, p_1 + w_{1,2}\, p_2 + \cdots + w_{1,k}\, p_k + b \tag{3.3}$$

In matrix form it can be expressed as

$$n = [w]p + b \tag{3.4}$$

Then the network output after applying transfer function can be written as

$$a = f([w]p + b) \tag{3.5}$$

Mathematical functions written in Eqs. (3.4 – 3.5) also apply to the ANN structure with multi input and multi neurons. For several complex cases there can be more neurons in a hidden layer to provide a sufficient number of weight coefficients for representing the target system or phenomenon. A single-layer network of *s* neurons and *k* inputs is shown in Fig. 3.5. In this structure, each neuron is equipped with a bias *b*, a summer, a transfer function *f*, and the output vector *a*. Every input *p* is connected to each neuron via the weight matrix [*w*].

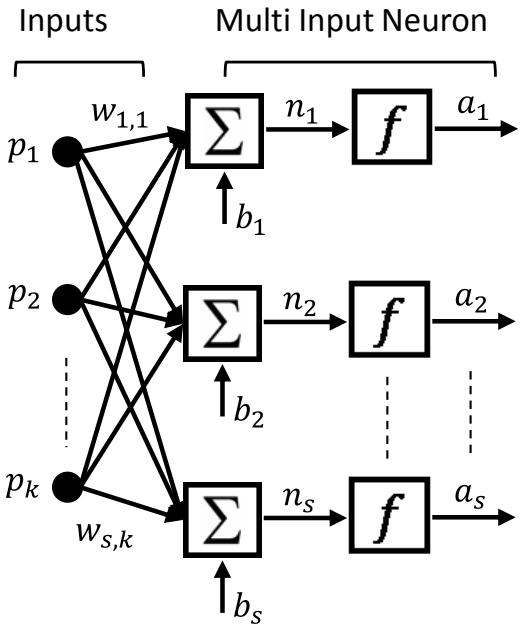

Fig. 3.5 Multi input and multi neuron

The matrix *W* developed in a multi input and multi neurons structure is determined by Eq. (3.6). According to the index in element of matrix weight, the row index indicates the destination neuron associated with that weight. While the column index represents the source of the input for corresponding weight. For instance the index in $w_{2,3}$ represents the weight connection from the second node source to the third node neuron.

$$[w] = \begin{bmatrix} w_{1,1} & w_{1,2} & \dots & w_{1,k} \\ w_{2,1} & w_{2,2} & \dots & w_{2,k} \\ \vdots & \vdots & 1 & \vdots \\ w_{s,1} & w_{s,2} & \dots & w_{s,k} \end{bmatrix} \tag{3.6}$$

It should be noted that the mathematical representation described above can also be used for the additional nodes in the next layer. For general representation, every neuron in hidden layer has a sigma, a bias, and a transfer function. Then every arrow in schematic ANN structures represents a connection associated to a weight coefficient.

Accordingly, the key parameters for the data approximation of performed for developing an ANN model include weights *w*, bias *b*, and transfer function. During the training process the weight and bias parameters are optimized based on the supervised learning rule using Levenberg-marquardt algorithm[76], so that the ANN output meets the target value of the output. A transfer function is particularly selected to satisfy the neurons while solving the problem of data fitting. In this work, Tangen-sigmoid transfer function Eq. (3.7) is applied for the connection of the input layer to the hidden layers, and between hidden layer to hidden layer. While pure linear transfers function written in Eq. (3.8) is applied for the connection between hidden layer and output layer. The notation *n* represents the node output that can be determined based on input, weight and bias.

$$a = \frac{e^{n} - e^{-n}}{e^{n} + e^{-n}} \tag{3.7}$$

$$a = n \tag{3.8}$$

Overfitting may frequently occur when the network fits the training data too rigidly and provides poor prediction accuracy when applied to new data. This phenomenon is directly related to the network complexity, which is defined by the overall magnitude of the weight coefficients. The network complexity is also highly correlated with the generalization capability of the ANN model; a lower network complexity produces a better generalization. The larger the network size, the more complicated the set of calibrated mathematical functions, and thus the network has higher complexity and a poor generalization capability[17]. The Bayesian regularization algorithm is considered as an ideal approach for balancing the learning characteristics of ANN to the network complexity[77]. The main principle of the Bayesian regularization method is the modification of the sum squared error performance index, performed by adding the sum of the squared weight that penalizes the network complexity as written in Eq. (3.9). The importance of adding the sum squared weight is to restrict the weight coefficient to a small number, and accordingly, the network function can generate a smooth interpolation through the training data and overfitting can be avoided.

The regularization term can be expressed as follows:

$$J_{reg} = c_1 E_p + c_2 E_w \tag{3.9}$$

Where J_{reg} is the objective function to be minimized during the training process; E_D is the sum of the squared error of the actual and predicted values; E_w is the sum squared error of the network weight; c_1 and c_2 are the regularization parameters. The network complexity can be reduced by adjusting the ratio of c_1 and c_2. In a Bayesian network, the network weights are assumed to be random variables. The density function of the weights and ratio of c_1 and c_2 are then determined using Bayesian's theorem, which is described by the following equation:

$$P(Z|N, c_1, c_2, M) = \frac{P(N|Z,c_2,M)\, P(Z|c_1,M)}{P(N|c_1,c_2,M)} \tag{3.10}$$

where Z is the vector containing the weight and bias in the network; N represents the datasets for training; and M is the designed network architecture. The details regarding the Bayesian regularization used for improving the generalization is further explained in literature[76].

3.1.1 Static and dynamic ANN approach

The configuration of ANN structures can be classified into static and dynamic models. In previous section, the mathematical representation of an ANN static model has been presented. The ANN output was calculated directly using the input in feed forward neurons connections. For the case of a dynamic ANN model, the output depends not only on the current time input (as in the static one), but also on the inputs from previous steps. Under these circumstances, the network adapts the sequence of time-varying training data pattern and can be trained to capture dynamic system characteristics[78]. The dynamic ANN model can be developed by including the additional information from the previous time steps to input layer. The difference between static and dynamic ANN structure is schematically demonstrated in Fig. 3.6.

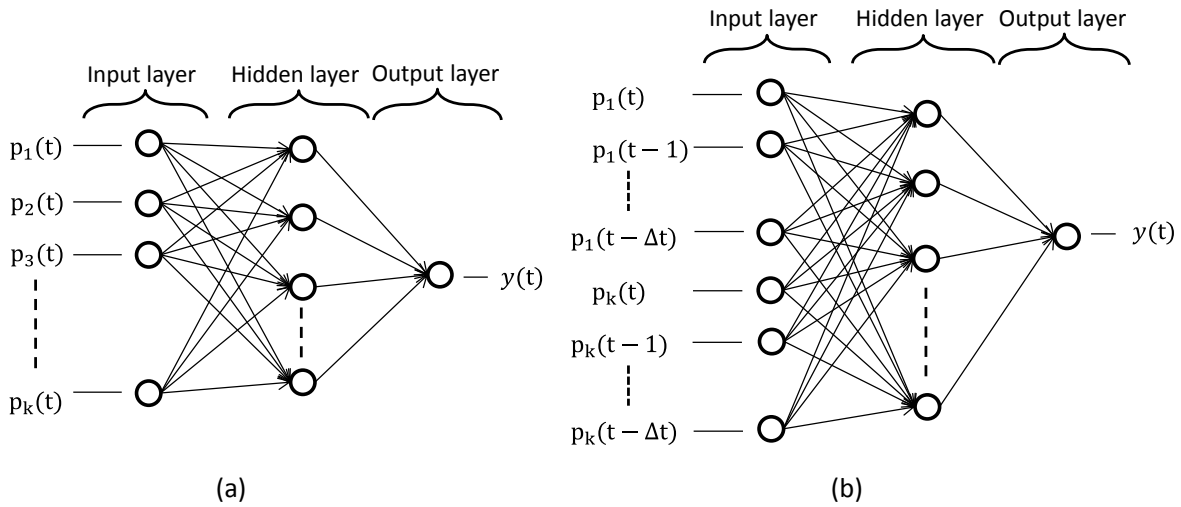

Fig. 3.6 Structure of ANN (a) static (b) dynamic

3.1.2 Training procedure

ANN modeling for input output data prediction is developed using the ANN Toolbox provided in MATLAB. The flow diagram for the training and testing procedures of ANN model is shown in Fig. 3.7. Firstly, the input and output data are collected from simulations and experiments. The data are divided in two groups intended for training and testing to make sure that the testing data are independent from the ones used in training phase. The accuracy of the ANN model is measured according to the error on the testing data. Although significant in the model calibration, it

is not generally recommended to consider the accuracy on the training data approximation as the actual performance of the ANN model. Because the data used during the actual application of the ANN model are different with those used in the training, an extremely low deviation in the training phase may hide overfitting issues yielding large deviations in the testing and application phases.

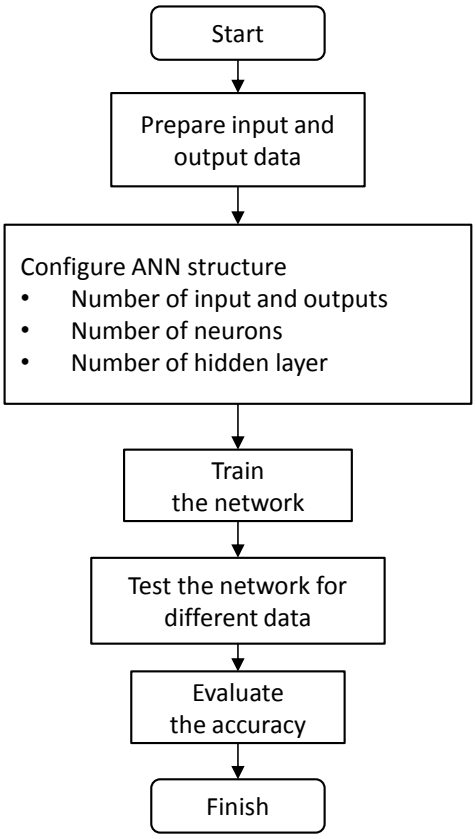

Fig. 3.7 Procedure of ANN training

The ANN structure is developed with considering the optimization of the number of input output nodes, hidden layers, and neurons. The variety of combinations of these parameters ensures the optimal adaptability of the network to the complexity of the problem related to the input output data characteristics. The training of ANN model is established by several trials and error attempts based on the combinations of the above mentioned parameters over a comprehensive range to avoid the local minima. In this study, during the training process, the number of neurons is varied from 1 to 15 with one and two hidden layers. The network with the highest accuracy on the testing data is selected as the optimum. There is no standard procedure reported in literature to determine such optimal ANN structure and the result intrinsically depends on the specific problem complexity and

data characteristics. It is obvious that the increased of number of neuron and hidden layers may increase the training accuracy due to the larger number of weight coefficients, but again, an overly-complex ANN structure may lead overfitting and generate poor accuracy on testing results.

The accuracy of ANN prediction is measured by relative average error (e_{rel}) and root means square error (RMSE). The notation n_d shows the number of data. While $\bar{y}_p$ and $\bar{y}_t$ indicates the predicted and target values.

$$\text{RMSE} = \sqrt{\frac{\sum_{i=1}^{n_d}(y_p - y_t)^2}{n_d}} \tag{3.11}$$

$$e_{rel} = \frac{\bar{y}_p - \bar{y}_t}{\bar{y}_t} x100 \tag{3.12}$$

$$\bar{y} = \frac{1}{\Delta t}\int_0^{\Delta t} y_e \ dt \tag{3.13}$$

3.2 Data sets generation for ANN training

The configuration of AC systems in actual fields may vary depending on the application. The split[79] and VRF[80] system types are the most popular configurations for small to medium size buildings. The systems with VRF configurations can be considered as a multi split AC systems. It connects one outdoor unit to multi-indoor unit, while a split-type system connects one outdoor unit to one indoor unit. One of the advantages of VRF systems is that they can serve multiple rooms delivering different individual capacity and indoor set-temperature conditions.

The numerical simulation of AC systems is based on the model of the simulation platform described in Chapter 2 and has been carried out to characterize the system performance in various operating conditions which reflect those of actual operating systems. Specifically, three different systems, with different nominal capacities and configurations, including the split type systems (2.5 kW and 7.1 kW) manufactured by Daikin, and large VRF system (50 kW) manufactured by Sanyo, have been modeled. The schematic diagram of the split-type and VRF type system configurations are illustrated in Figs. 3.8 and 3.9, respectively. For split-type models, the systems are equipped with a virtual room and do not feature a sub-cooler. Meanwhile, the large VRF system is equipped with an additional heat exchanger to introduce and control the sub-cooling degree of the refrigerant prior entering the expansion device.

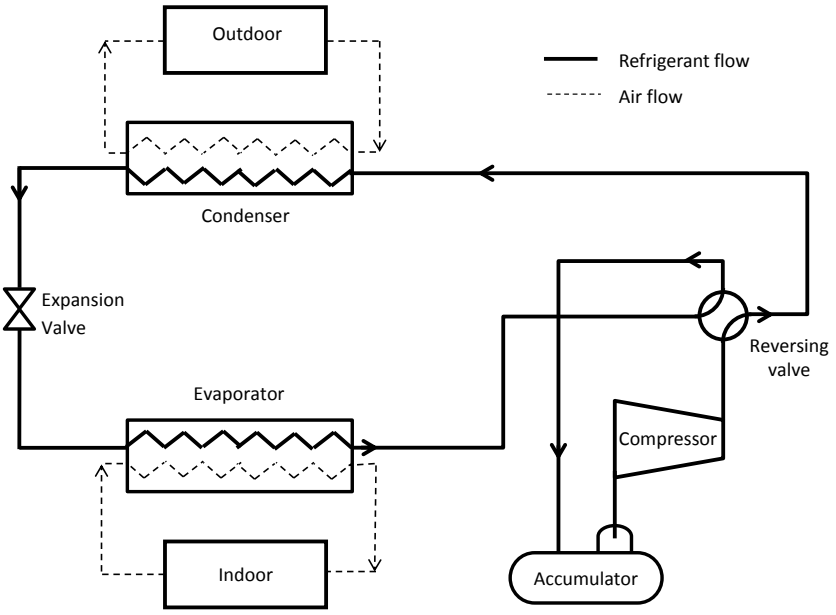

Fig. 3.8 Schematic diagram of split-type air conditioning system

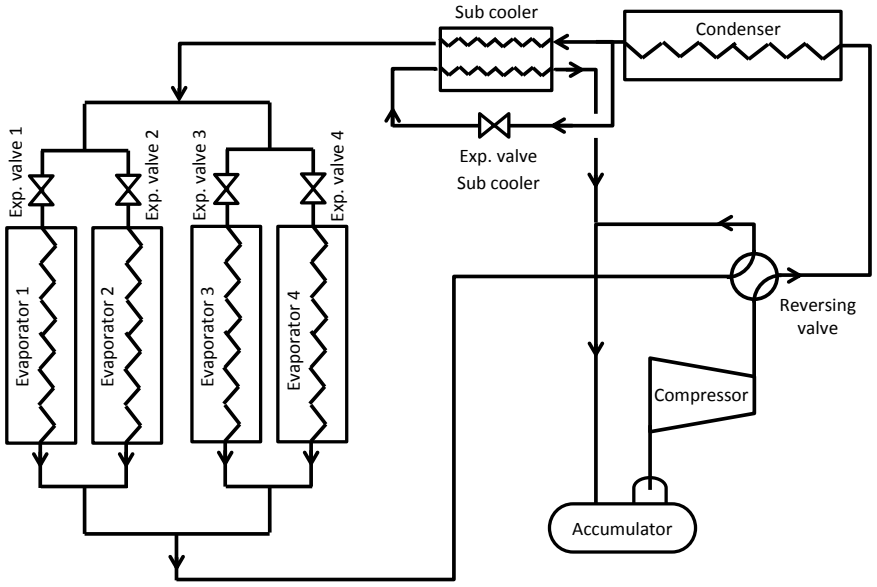

Fig. 3.9 Schematic diagram of VRF air conditioning system with sub cooler

Providing a reliable training data set is an important task to obtain precise and generalizable ANN models. The data must be generated for representing the actual system behavior during real

operation by considering cooling load, outdoor temperature, and indoor temperature set point variations according to the scenarios described in Fig. 3.10. In a real operative condition, outdoor and indoor temperature set point may simultaneously change due to weather and occupant comfort standard. While the cooling load fluctuation is affected by the internal and external heat gain, which is correlated to occupant behavior and weather condition. To cover the variability of real system operation, during the implementation of this method, the scenario depicted in Fig. 3.10 (d), where cooling load, indoor and outdoor temperature are not constant, should also be included in the training data set generation. The other scenarios depicted in Fig. 3.10(a), (b), (c) can be used for investigating the effect of each individual parameter.

In present study, the training data scenario shown in Fig. 3(a) is selected to characterize the system performances on wide range of part load operating conditions. The system is simulated by varying cooling load with step variations of 10% amplitude, from 30% to 100% while fixing outdoor and indoor temperature as constant.

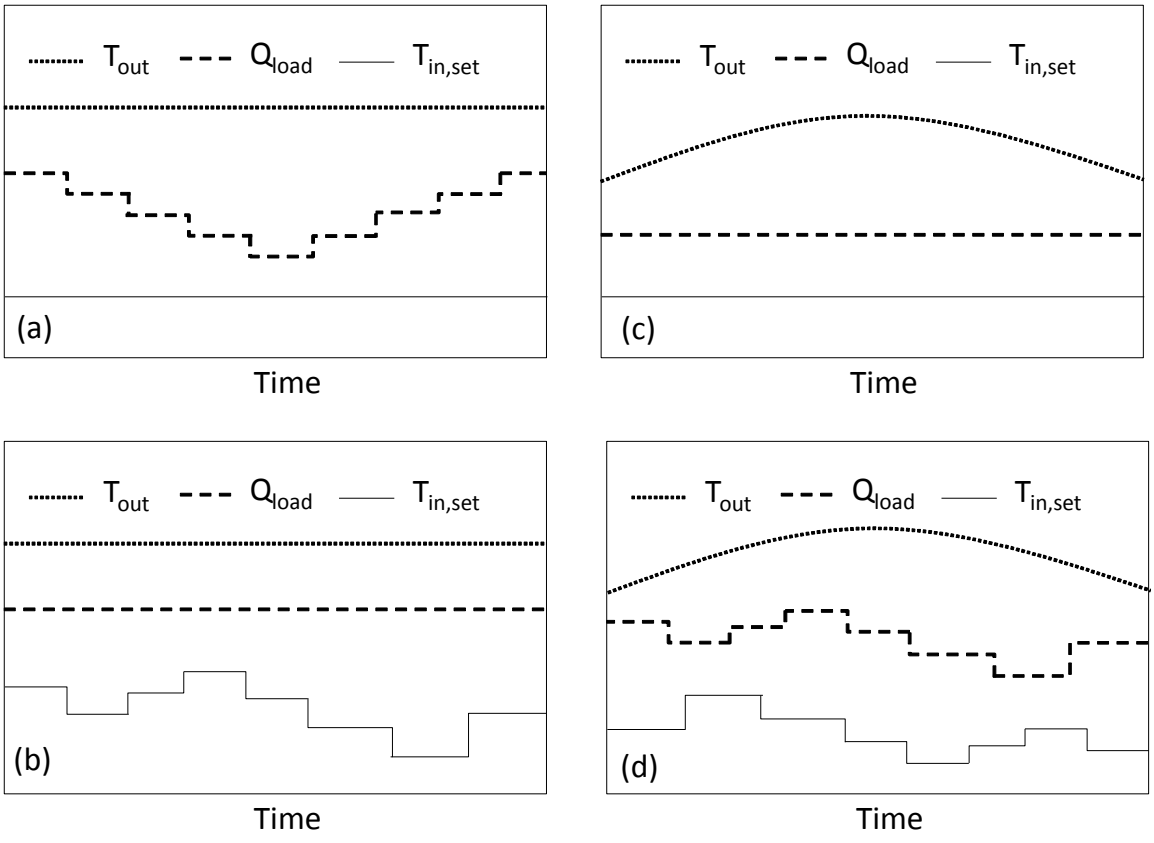

Fig. 3.10 Scenarios of training data generation

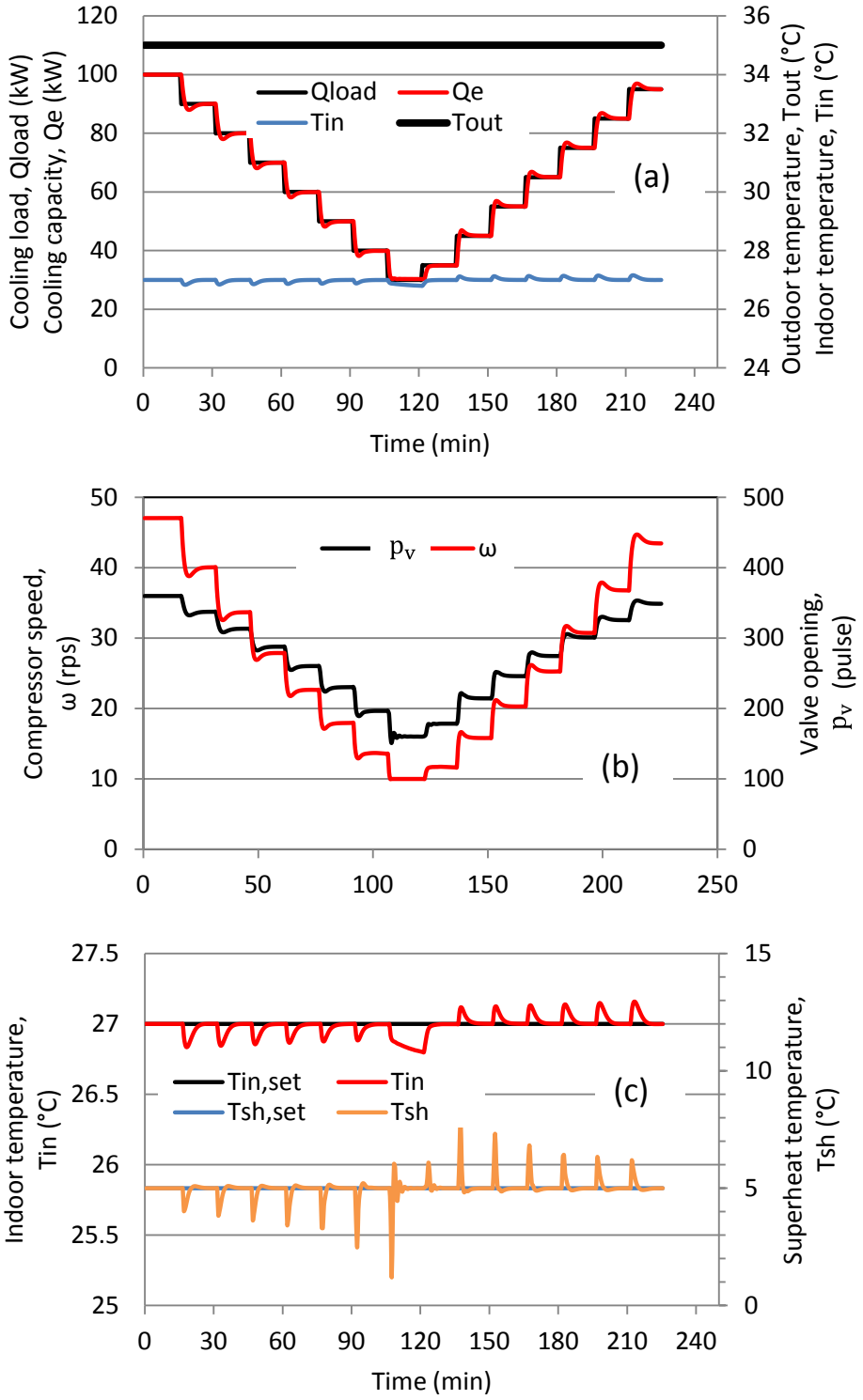

Fig. 3.11 (a) Input output of simulation; (b) Actuator signals; (c) Controlled parameters

The cooling load is changed every 15 minutes to explore realistic circumstances while obtaining balanced combinations of steady and unsteady characteristics. The details of the operation scenario and simulation results are shown in Fig. 3.11. The highest overshoots of superheat and indoor temperature recorded in the training scenario are 4 °C and 0.17 °C, respectively. As in actual machines, the controller exhibits poor accuracy (especially in achieving target room temperature and superheat) when the load is lower than 35% (Fig. 3.11(c)), because the PI controller is designed for meeting the maximum cooling load. This exemplifies the fact that the system cannot work effectively if operated far away from the design point. Further expanding the explored operating range would require an accurate modeling of intermittent operation at critically low cooling loads, but this circumstance is presently overlooked. This corresponding data pattern generated from numerical simulations is considered for the training of the ANN model.

3.3 Selection of input parameters

There are numerous parameters that can be used as inputs to predict the system performance, such as air temperatures, refrigerant temperatures, and controllable parameters. As previously mentioned, several practical factors affect the engineering choice of the inputs required for prediction, which need to be ultimately measured on operating systems for field predictions. Among such factors, non-intrusivity, accessibility, cost, along with the scientific targets of providing accurate and generalizable predictions. As vapor compression AC systems rely on the same fundamental technology, the hypothesis of this study is that parameters able to estimate the refrigerant thermodynamic cycle would be representative of the whole installed units. The illustration of some representative input parameters for the prediction of vapor compression systems performance is presented in Fig. 3.12.

Controllable parameters, such as compressor speed and valve opening are highly correlated with the system performance and the dynamic response to external disturbances. The fluctuation of those parameters is tuned to directly affect the system performance by adjusting the refrigerant cycle and the mass flow rate while controlling the indoor temperature and output cooling capacity. It can be said that the compressor performance map and the expansion valve are the actuators of the "brain" of the systems, namely the control system which run the system operation. Unfortunately, measuring the rotational speed of the compressor or refrigerant flow rate and the opening of the expansion valve could be challenging. In practice some system configurations place the expansion valve in the indoor unit of the system[80]. Additionally, the strictly technological essence of these quantities is not likely to be scalable to different systems having different sizes and configurations. On the other hand, air temperatures are easier to access than controllable parameters, although placing sensors in the indoor space of the end-user could represent a practical challenge. Nonetheless, the high special variability of these parameters and measurement uncertainty require complex and possibly intrusive procedures to obtain precise measurement data. Alternatively, refrigerant temperatures are accessible from the outdoor unit and can be measured non-intrusively

via the placement of inexpensive thermocouples on the outer surface of the refrigerant connecting pipes at strategical locations for capturing the underlying refrigerant operation cycle of a plausibly major number of installed systems in operation.

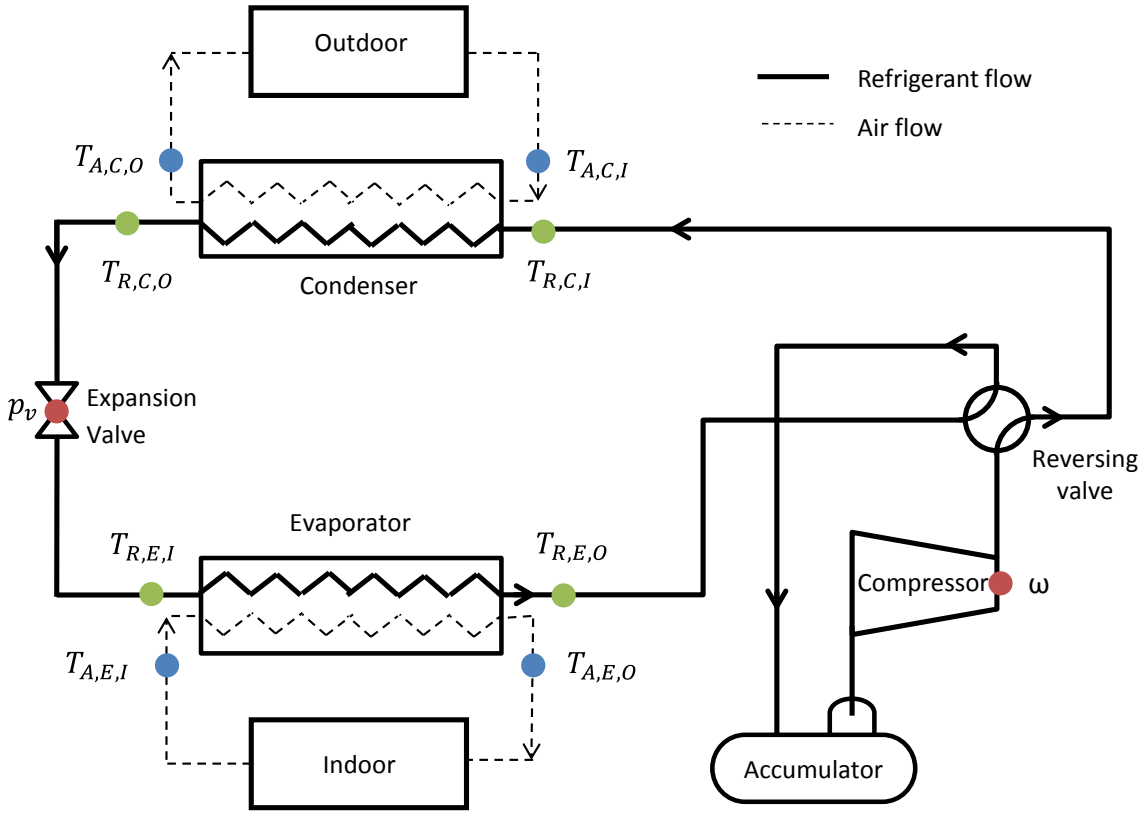

Fig. 3.12 Representation of input parameters on air conditioning systems schematic diagram (Colored markers show different input groups)

In order to explore the suitability of the input parameters for designing an effective intelligent prediction method for broad-spectrum application to AC systems performance prediction using four input groups based on the above discussed categories of parameters (Table 3.1) are investigated and discussed with reference to the above mentioned criteria along with the prediction accuracy.

- The first group includes air temperatures at inlet and outlet of the evaporator and the condenser, which benefit from the response sensitivity to the system performance.

- The second group includes the compressor speed and the expansion valve opening, which are highly correlated to the part load operation conditions.

- The third group includes the refrigerant temperatures at inlet and outlet of evaporator and condenser (or sub-cooler, if installed) which represent the refrigerant cycle of the air conditioner.

- The fourth group consists of the option provided by the combination of all these parameters.

Table 3.1 Input groups for performance prediction

Group	Input parameters		Classification
1	Air temperature	$T_{A,E,I}, T_{A,E,O}, T_{A,C,I}, T_{A,C,O}$	High response sensitivity
2	Controllable parameters	p_v, ω	Representative of external disturbance
3	Refrigerant temperatures	$T_{R,E,I}, T_{R,E,O}, T_{R,C,I}, T_{R,C,O}$	Representative of operative cycles
4	All inputs (Group 1, Group 2, Group 3)		-

The applicability of the selected four input groups including air temperatures, controllable parameters, and refrigerant temperatures and representing different categories of the influent parameters for system performance prediction, is investigated. As a preliminary scenario, the numerical models of two split type AC systems, the first featuring 7.1 kW at the rated condition and the second with 2.5 kW rated capacities are used to characterize the system behavior in various operating condition as listed in Table 3.2.

The investigation is conducted by firstly training the ANN model within a wide range of representative data and consequently testing the developed ANN model in different possible case: on data simulated within the range of training scenarios, on data outside the range of training scenarios, and on data obtained from the simulation of a different system with a different nominal capacity. It should be noted that the data used for testing are not introduced during training phase.

Table 3.2 Training and testing data scenario for input selection

Nominal capacity (kW)	Cooling load (%)	$T_{in,set}$ (℃)	$T_{out,set}$ (℃)	Training	Testing	
7.1	30- 100	Constant	Constant 30 and 35	●	●	Inside range
		23, 25, and 27	Variable 30- 35			
7.1	30- 100	Constant 27	Constant 40		●	Outside range
2.5	30- 100	Constant 27	Constant 35		●	Different system

Figure 3.13 shows the prediction result of different input groups when testing on data inside and outside of the range of external conditions used for the training of the ANN model. The prediction accuracy on the testing data can be interpreted by observing the similarity between the training and testing data in terms of the data range and dynamic characteristics as presented in Fig. 3.14. In general, a commonly accepted conclusion from previous research on ANN modeling is that it is possible to tune the ANN model so that the predicted data will exhibit good agreement with the corresponding real values when the testing data are within the range of the ones used in the training. Otherwise, unless effective pre-processing or post- processing techniques are implemented, ANN will demonstrate a poor accuracy when applied to data characteristics not encountered during the training process.

Accordingly, Fig. 3.13 shows that ANN model has good accuracy for all input groups when applied on the testing data that are inside range of training data. This implies that the trained ANN model has successfully recognized the data as the data behavior of the testing data set is similar to the one used in training, and that the selected ANN structure does not experience overfitting issues. Meanwhile, the accuracy shown by the testing results outside the training data range (specifically, when the system operates under the influence of an outdoor temperature which exceeds the maximum value encountered in the set of training data) indicates that only controllable parameters and all inputs demonstrate acceptable deviations. This demonstrates that the modulation of compressor speed and valve opening are strongly correlated to the cooling capacity fluctuations and could represent a strong choice for reliable predictions. As presented in Fig. 3.14 (a) and (b), there is no significant difference in controllable parameters behavior between the training and testing data. The higher outdoor temperature (outside the training range) at 40 ℃ does not significantly affect the data characteristics of these parameters in relation to corresponding output. Similarly, as the prediction using all inputs include valve opening and compressor rotational speed, the same conclusion applies to the prediction accuracy of this group outside the training range.

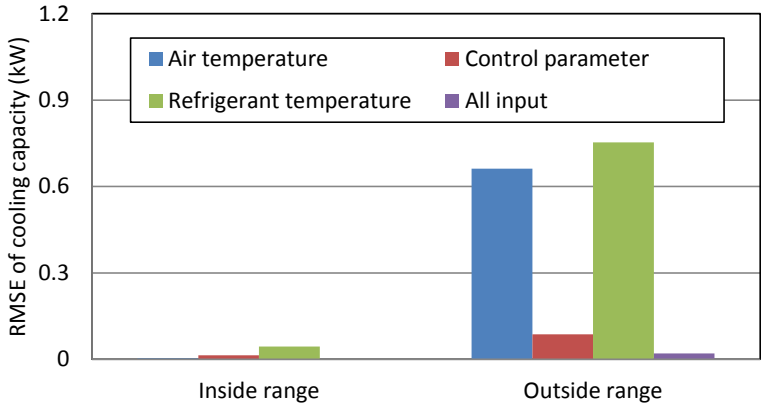

Fig. 3.13 Applicability of different input groups for performance prediction inside and outside the range of data

Conversely, the higher error encountered when air temperature inputs are tested outside the data range is due to the gap of air inlet and outlet temperatures at condenser between training and testing data. As the outdoor unit is exposed to the outdoor environment the air inlet temperature of condenser is directly correlated to the outdoor temperature. This quantity can be considered as an external parameter that affects the system performance, whereas its variation is not related to the modulation of cooling capacity. Accordingly, the prediction based on input of air temperatures does not recognize sufficient input information for capturing the cooling capacity modulation when applied outside the range of the training data. On the other hand, the air inlet and outlet temperature at the evaporator result in similar values since the PI controller maintains the target indoor temperature.

Similar observations can be extracted from the testing results based on refrigerant temperature inputs. It is observed that both the saturation temperature and outlet temperature from the condenser increase as the outdoor temperature increases. The discrepancy of inlet and outlet refrigerant temperatures at the condenser leads the low prediction accuracy when applied outside range of training data. Nonetheless, unlike the results obtained for air temperature inputs, refrigerant temperature inputs are more strongly related to the cooling capacity fluctuations at the evaporator. Although stronger correlations result into higher deviations when the range of training data is insufficient to cover the conditions encountered in the testing data, this suggests that refrigerant temperatures exhibit higher sensitivity to the system response to external and internal disturbances, which is necessary for capturing the complexity of the underlying physical behavior of the system and strongly associating the system performance to the operating conditions.

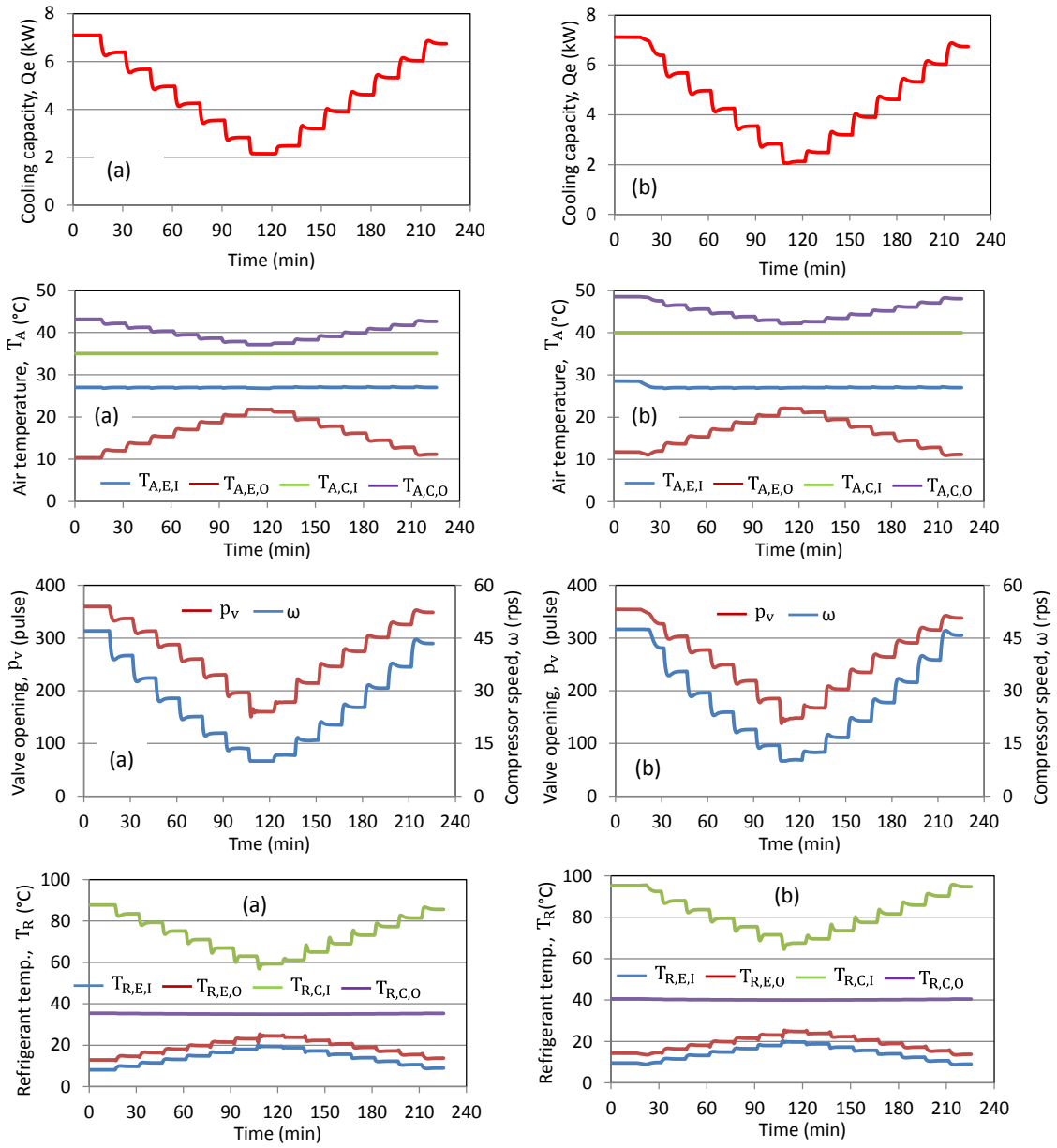

Fig. 3.14 Data characteristics (a) Training; (b) Testing (outside range)

The observations reached at this phase, as in previous literature, are limited to the application of the ANN modeling technique to the single system characterized during the training phase. The applicability of the above conceived input groups for performance prediction is hereby investigated on systems with different sizes (and nominal capacities). The prediction method is based on a scaling process including pre-processing of the input and post-processing of the output data.

The pre-processing data normalization technique is applied before the training process to obtain more manageable data and simplify the convergence to the proper weight and bias coefficients during the training process. Norgaard et al. (2001)[81] previously suggested this technique when input and output parameters have different scales, to avoid the numerical dominance coming from the largest magnitude inputs. Data normalization using the min-max rule[82] expressed in Eq. (3.14) is used to convert all input and output data into the range [-1, 1].

$$c = (d - d_{min}) \frac{(c_{max} - c_{min})}{(d_{max} - d_{min})} + c_{min} \tag{3.14}$$

where, d is the real value, whereas its minimum and maximum values are denoted by d_{min} and d_{max}, respectively. The notation c represents the normalized data ranging from c_{min} to c_{max}. When normalization is applied to training data, the minimum and maximum cooling capacities are obtained from 0 and 100% of rated cooling capacity, whereas the minimum and maximum temperatures refer to the range of the training data.

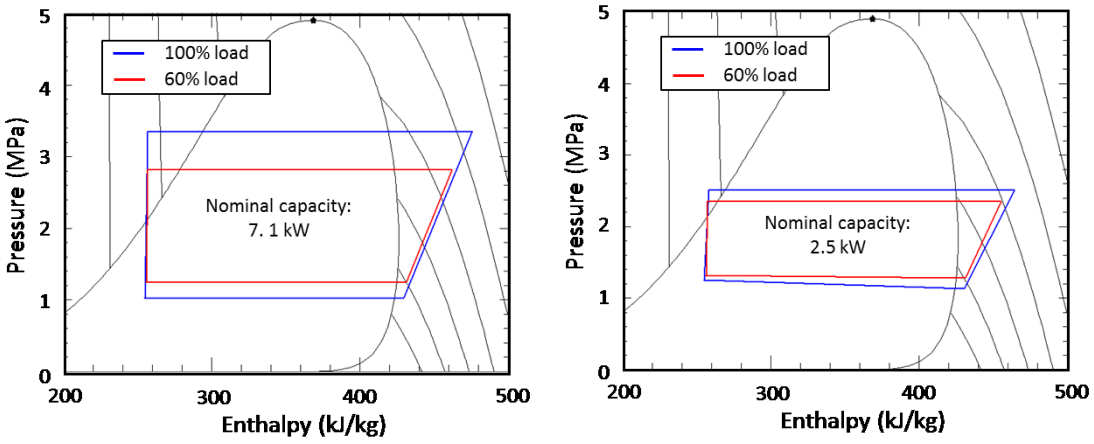

(a) (b)

Fig. 3.15 Air conditioning cycle of different system (a) 7.1 kW and (b) 2.5 kW
(Operating condition: T_{in}: 27 °C, T_{out}: 35 °C)

The consequent post processing of the output data is explored for overcoming one of the main challenges of this field, which limits the validity of ANN predictions to the specific system used in the training process. The technique is based on the observation that the multitude of different air conditioners, although featuring different manufacturers, components, sizes and configurations, all rely on the same underlying thermal machine technology based on vapor compression cycles. Specifically, it is hypothesized that the similarities between the refrigerant cycle of all these systems during their operation (rated or part-load, steady or unsteady) are somehow scalable as presented in Fig. 3.15. Therefore, on the basis of this scaling method the system performance prediction based on ANN models could be extended to different systems.

From this standpoint, the adoption of refrigerant-side properties extracted at strategical locations as input parameters could provide a generalizable representation, which could be expanded to systems other than the one during training phase. That is, while operating between identical heat sources and applications, similar results of the response characteristics and the trend of refrigerant temperatures in two systems with different locations, compressor sizes, heat exchangers and other components, can be obtained.

Figure 3.16 shows the accuracy of the ANN models trained with different input groups on the testing data generated from a different system. It is confirmed that the prediction accuracy obtained for refrigerant temperatures as ANN inputs outperformed the ones predicted by the other input groups when applied on a different system. The details of predicted results comparison by different input groups is shown in Fig. 3.17.

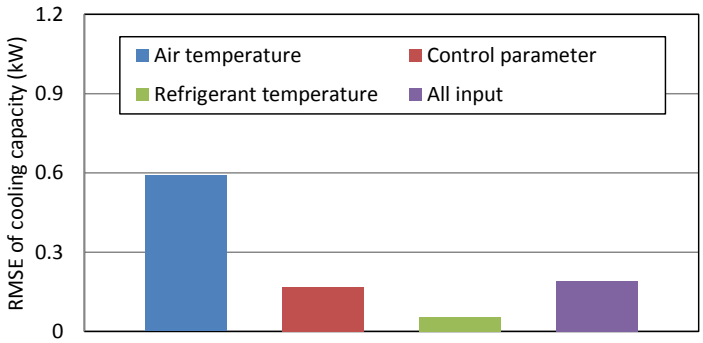

Fig. 3.16 Applicability of different input groups for performance prediction on different system testing

According to data characteristics illustrated in Fig. 3.18, the refrigerant temperatures of the two different systems mostly have similar characteristics when operated at corresponding conditions in terms of indoor temperature, outdoor temperature, and relative cooling load. However, the refrigerant temperature at the outlet of compressor (condenser inlet) exhibits a considerable deviation between the two systems. This could be related to different efficiencies of compressors with different sizes. However, by normalizing the whole input temperatures in the range of [-1, 1], the dominance of the absolute magnitude of this temperature is reduced. Normalization technique distributes equally the importance of each input.

The highest error is recorded when the ANN model is trained by using air temperatures as input parameters. This is due to the limited input information for capturing the dynamics behavior of the cooling capacity and there are two parameters showing the gap between training and testing data. The significant discrepancy on air temperature inputs are indicated by the outlet temperatures at evaporator and condenser ($T_{A,E,O}, T_{A,C,O}$). The parameters changes are related to the amount of cooling capacity and heat exchanger efficiency. In the other hand the refrigerant temperatures have more variables that can recognize the cooling capacity modulation ($T_{R,E,I}, T_{R,E,O}, T_{R,C,I}$). Moreover

the difference between training and testing data on refrigerant temperature is shown by the temperature at condenser inlet only ($T_{R,C,I}$). The higher accuracy of ANN model trained with controllable parameters compared to the one trained with air temperatures is caused by the strong similarity of compressor speed between training and testing data while delivering the various cooling capacity.

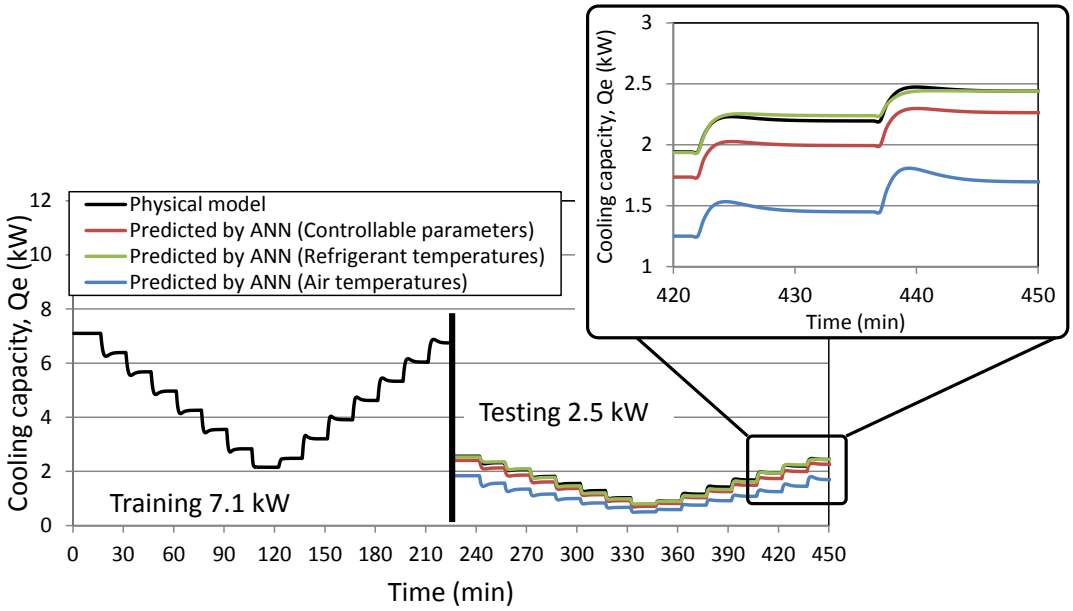

Fig. 3.17 Prediction results on different system using various input parameters

Figure 3.17 shows the comparison of the time distribution of the ANN prediction results with the inputs of controllable parameters, air temperatures and refrigerant temperatures. The enlarged figure clearly shows that the predicted cooling capacity by refrigerant temperature precisely estimates the corresponding data. Even though the controllable parameters are highly correlated with the cooling capacity modulations (Fig. 3.18), response and operating conditions, they are not effectively scalable and strongly related to the specific design of the original system. Accordingly, the related prediction results cannot be expanded to other systems due to the different component characteristics, especially the compressor performance map and the expansion valve design. Therefore, the range of compressor rotational speed and valve opening from one system to the others may be substantially different depending on the component's manufacturer and not related to the fundamental phenomena occurring within the system.

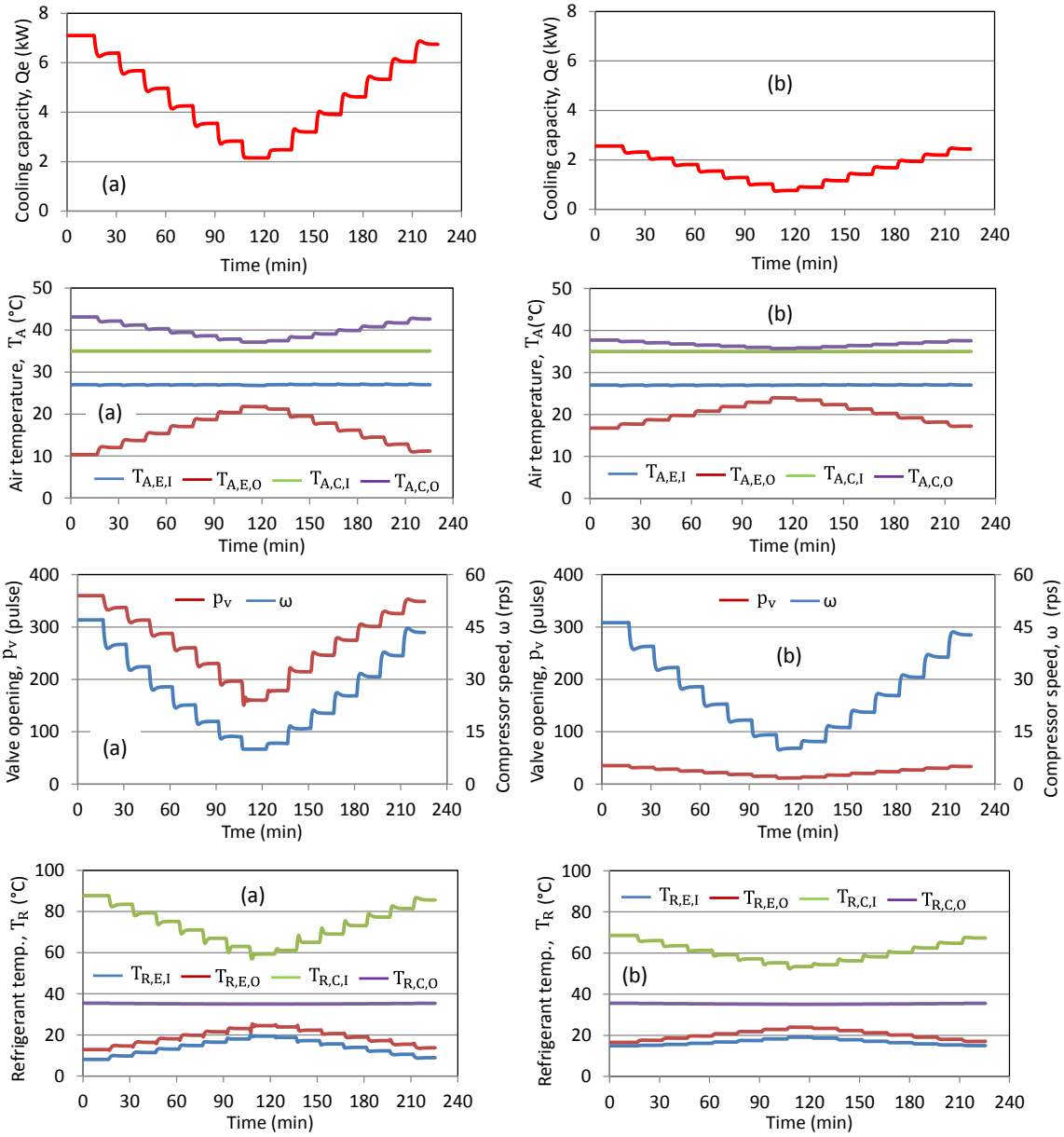

Fig. 3.18 Data characteristics (a) Training; (b) Testing (different system)

The observations extracted from the discussion of the results presented above, indicate that the refrigerant temperatures at the inlet and outlet of evaporator and condenser are selected as the best option for an intelligent prediction method of AC systems on the basis of the following criteria:

- Inexpensive to measure (can be measured using thermocouples installed on the outer surfaces of connecting pipes or heat exchangers).

- Non-intrusive (can be accessed from the outdoor unit).
- Relatively low uncertainty (the placement of the sensor on the refrigerant tube provides an estimation of the refrigerant temperature at that state of the cycle).
- Represent air-conditioning cycle (which is the fundamental basis of this technology, independently from the specific component design or manufacturers).
- Scalable for different systems with different rated capacity and manufacturer.
- Sensitive to cooling capacity and external disturbances (the cycle changes are related to the variation of cooling load, indoor temperature, and outdoor temperature).

3.4 Analysis of data characteristics

3.4.1 Steady and unsteady operation

During the operation the system encounters both steady and steady operating conditions due to the variation of cooling load, outdoor and indoor air temperature over the time. The effect of combination of these different data characteristics on the ANN prediction is investigated for identifying the proper training scenarios to be applied to the ANN model. As illustrated in Fig. 3.19, the steady operation is defined by small amplitude modulations of the data within the range of ± 2% cooling load, data distributions which are not satisfying the previous criterion are considered as part of unsteady operation. A reference representation of steady, unsteady, and continuous data characteristics is demonstrated in Fig. 3.20.

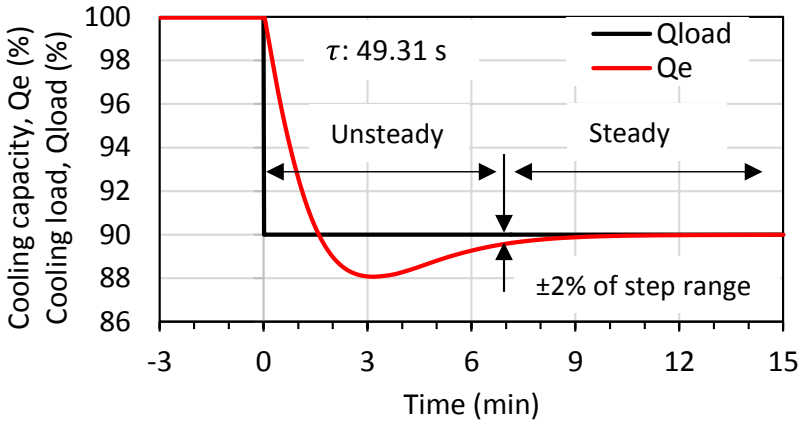

Fig. 3.19 Data division for steady and unsteady operation

A balanced set of training data featuring both steady and unsteady characteristics is necessary for a comprehensive representation of the performance of these systems. The inclusion of an excessive amount of steady state data could lead to redundant information in some specific operation conditions, overfitting in these conditions, and poor representation of the dynamic response of the system. On the other hand, the use of an excessive portion of data captured during unsteady state operation would be likely to yield inaccurate predictions of the steady state operation.

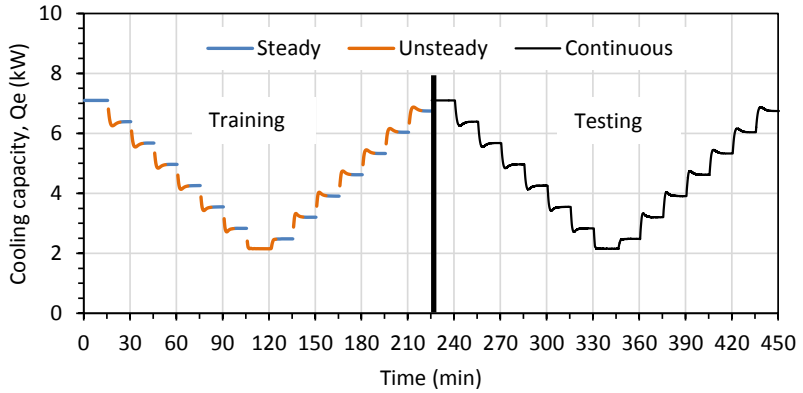

Fig. 3.20 Steady, unsteady, and continuous data

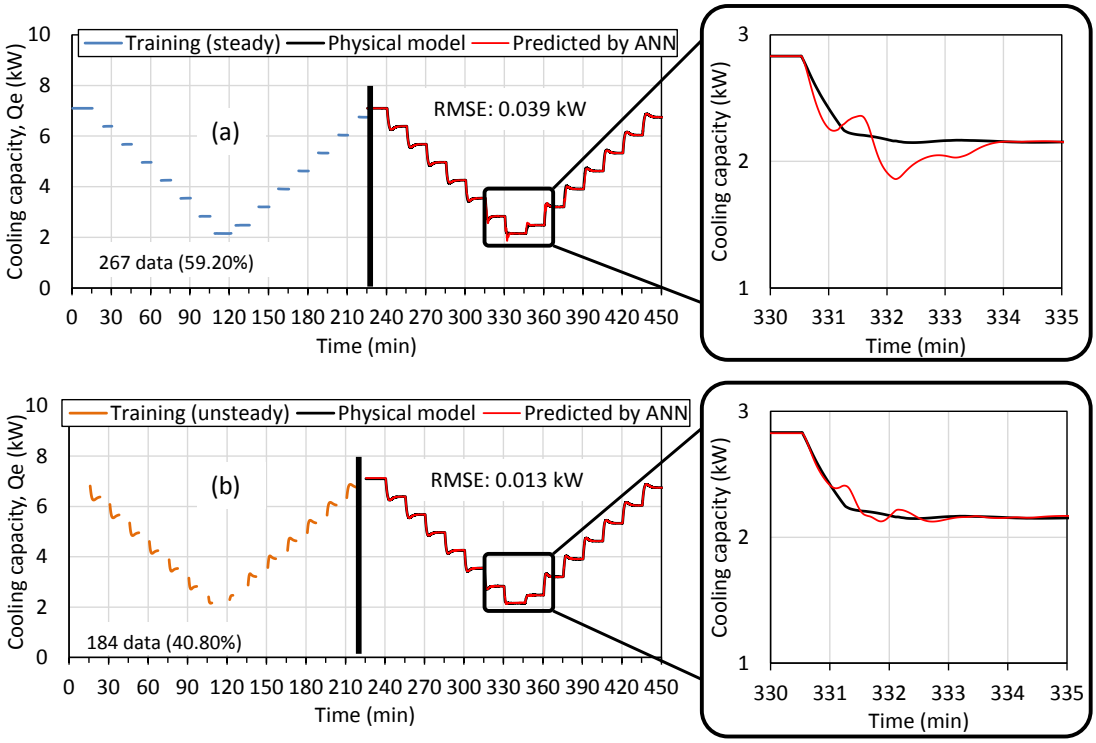

Fig. 3.21 Comparison of steady and unsteady data for ANN training

The investigation on both data characteristic is conducted using 30 s sampling time. Two ANN models with the same structure are trained individually with steady and unsteady training data characteristic. The prediction results shown in Fig. 3.21 indicate that the ANN model trained using unsteady data has higher accuracy than the one trained with steady data. Since the time constant of cooling capacity is not too long, the system operation approaches quasi-static behavior. Unsteady operation represents high data variation, while steady data demonstrates only few conditions and causes high degree of data redundancy. Therefore unsteady data could capture more cooling capacity variation. This comparison reveals that the data variability is very crucial for training to achieve an accurate prediction in wide range of cooling capacity.

3.4.2 Sampling time

The sampling time of prediction data should be selected appropriately for capturing any influent variability of input and output parameters within the limits of experimental tests and simulation capability, while avoiding variations related to noise signals or an excessive number of similar data carrying very little additional information. It is important to note that an excessively short sampling time gives data redundancy in steady-state conditions. Contrarily, an excessively long sampling time will skip important information which is representative of the unsteady operation. Accordingly, the sampling time is selected by considering the time constant of the system. As the data sampling is applied on the same time span, the variation of sampling time affects the number of data point and variability. The smaller the sampling time is the larger the number of data in a given time frames, and vice versa. The variability index (V_i) is calculated to measure data variability for a given sampling time, as expressed in Eq. (3.15).

$$V_i = \frac{\sum_{t=2}^{n_d} |Q_e(t) - Q_e(t-\Delta t)|}{n_d - 1} \tag{3.15}$$

The sampling time selection is performed by considering time constant τ of cooling capacity response. Eight ANN models with different sampling time varying between 0.1τ to 10τ are used for training, and then the pre-trained ANN models are applied to predict the continuous data. The results are analyzed for selecting the sampling time to be applied in the following development of the ANN model and performance prediction method.

Figure 3.22 shows the results of the sampling time investigation. According to Fig. 3.22(a), it can be observed that the highest accuracy is obtained by the training data with the smallest sampling time. Furthermore the error increases as number of data used for training is decreased. This is because the larger number of data, as a consequence of a smaller sampling time, carries more defined information. Even though the data variability at 0.1τ is very small, the large number of data represents almost all conditions. The effect of data variability is demonstrated in Fig. 3.22(b), where it is highlighted that the highest variability of the data with sampling time of 5τ and 10τ lead to a more accurate prediction than the data with sampling time of $2\tau, 3\tau$ and 4τ. As shown in Fig.

3.22(b), a significant change in data variability exists in the range of sampling time between 2τ to 10τ, whereas the number of data is only reduced slightly. In consideration of the accuracy and complexity in data gathering, sampling time in the range of 0.1τ to τ are considered for capturing both steady and unsteady performance. On the other hand, special care should be taken in balancing the permanence of the system in a steady state condition when generating training data, as data redundancy at steady state could lead overfitting and the ANN model might fail in representing unsteady conditions.

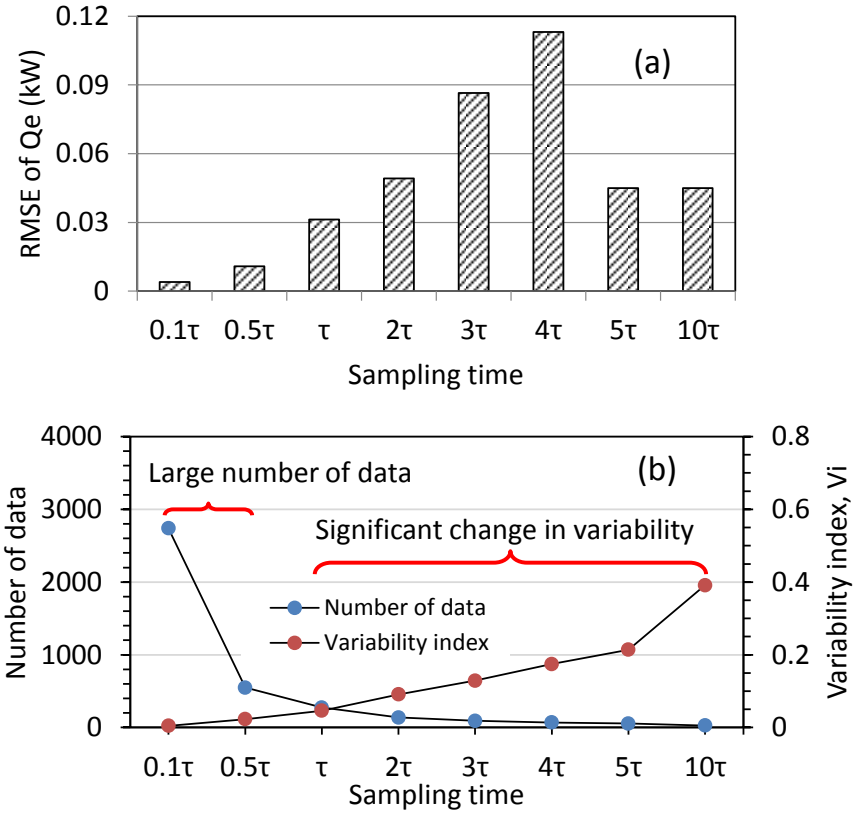

Fig. 3.22 Relationship between sampling time, number of data, and variability

4. Experimental data generation

Up to this chapter, only numerical results have been used as data for training and testing of the ANN model. In this section the experimental facility for actual system performance characterization is presented. The data collected with the experimental equipment hereby described represent a reliable target for demonstrating the prediction ability of the proposed ANN model. Additionally, the analysis of such experimental data provides information regarding the discrepancies between experiment and simulations. Therefore, guiding possible developments of the simulator as well as constituting a possible alternative set for the ANN training. The measuring procedure for collecting input output data for prediction are described.

4.1 Experimental apparatus

The schematic diagram of experimental facility is demonstrated in Fig. 4.1. The experimental facility is used to characterize the performance of two typical variable refrigerant flow (VRF) vapor compression air conditioning systems. These systems are commercial products for multi room air conditioning manufactured by Daikin. It features four evaporators and a single condenser. The first one is a new system with nominal cooling capacity of 33.5 kW, the other one is a system with nominal cooling capacity of 28 kW that has been operated in an existing building for 6 years. The experimental facility serves two conditions-controlled room chambers intended for replacing indoor and outdoor spaces and the related disturbances. The system components are divided in two main parts e.g. indoor unit and outdoor unit. In this specific system configuration, the indoor unit mainly consists of evaporators, expansion valve and evaporator fan. Conversely, the condenser, compressor, accumulator and condenser fan are placed in the outdoor unit. In several different AC system configurations, the expansion valve may be located in outdoor unit[79]. For example, single split AC systems commonly see the placement of the expansion valve in the outdoor unit. Every component is then connected by the refrigerant pipes to circulate the working fluid in a closed loop system realizing the thermodynamic cycle necessary for delivering the useful output effect.

In Fig. 4.1, the blue lines represent the liquid or liquid–vapor mixture refrigerant and the red lines are representing the pipes containing vapor refrigerant. The refrigerant is circulating continuously through the system inside the connection tube to absorb the heat generated in the indoor space via four evaporators, and then release it to the outdoor space via the condenser. As depicted in Fig. 4.2, the four evaporators in the indoor space are centralized in one chamber. This is to specify that the system is operated as a single split unit in this study, thus neglecting the additional operation variability provided by this type of AC system. It should be mentioned that there is no air flow between indoor and outdoor spaces, as the air circulation in each space follows a closed loop. Therefore, the change in air temperature and humidity in indoor space is only affected by the system operation and the condition generator.

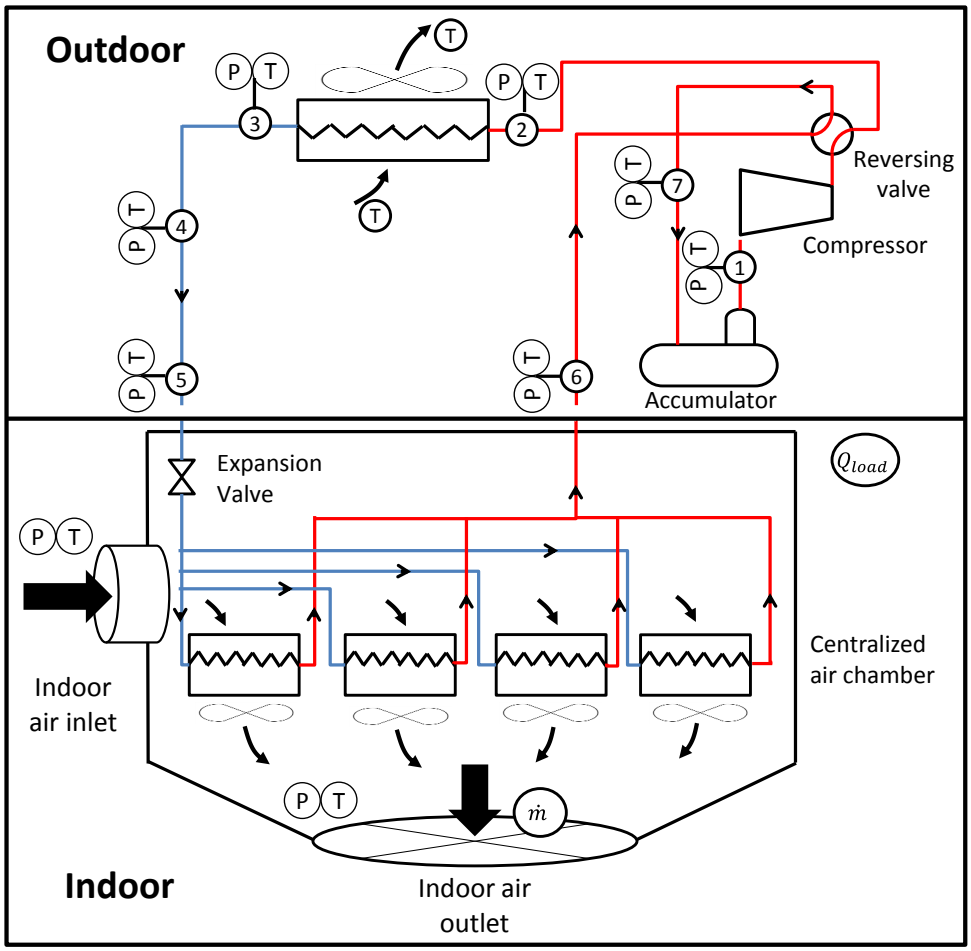

Fig. 4.1 Layout of experimental apparatus

The experimental facility is designed to be able to generate variation of cooling load, outdoor temperature, and indoor temperature as those encountered during actual operation of installed systems. The cooling load is generated by an electric heater and a boiler which are installed in the indoor space. The boiler is operated to adjust the amount of latent heat to a certain sensible heat ratio (SHF). The outdoor environment is conditioned by a dedicated air conditioner featuring a chiller, a heater, and a humidifier to generate the desired outdoor air conditions and control their variations in time. The outdoor temperature and humidity can be manipulated in various conditions for an actual outdoor environment representation. While the system operation is controlled by the package controller, which is already built in the system to respond to a given indoor cooling load and achieve the desired indoor temperature T_{in}. Accordingly, the system performance under a comprehensive range of various working conditions representing the actual system operation can be recreated by manipulating the cooling load Q_{load}, outdoor temperature T_{out} and target indoor temperature $T_{in,set}$.

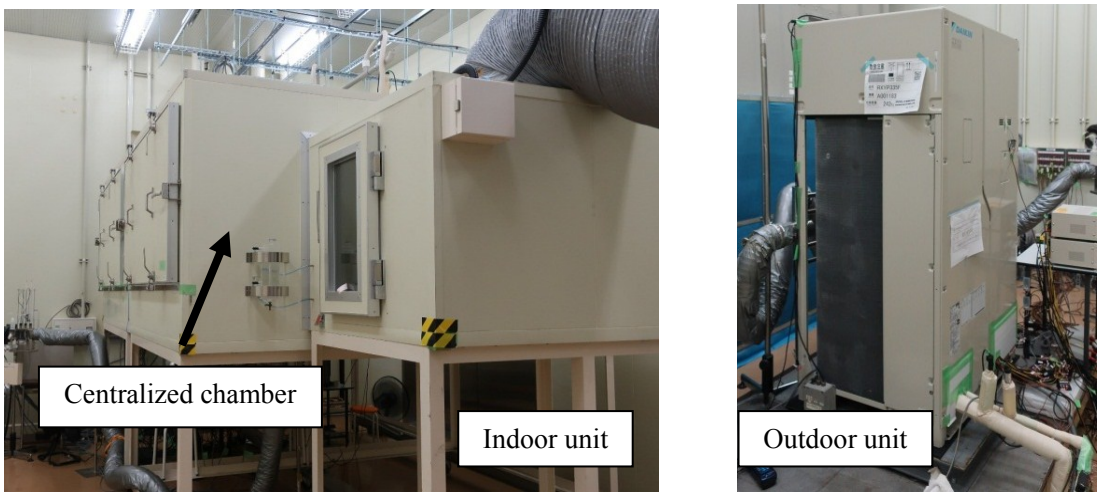

Fig. 4.2 Photograph of experimental system

The outdoor unit is fully instrumented with accurate sensors for measuring input parameters used for the ANN prediction. The thermocouples are placed on the outer pipe surface of the refrigerant tube in the outdoor unit, as illustrated in Fig. 4.3. Other operating quantities, including controllable parameters, air-temperatures and pressures, are measured for a complete monitoring and representation of the system performance. The actual cooling capacity instantaneously delivered by the system, and considered as the output of the ANN prediction, is determined by the mass flow rate of air passing through the centralized chamber $\dot{m}$ multiplied by the enthalpy difference between the inlet and outlet air streams as written in Eq. (4.1). The enthalpy of air (h_A) is a function of air pressure (P), dry bulb and wet bulb temperatures (T_{DB}, T_{WB}).

$$Q_e = G_{A,I}\, h_{A,I} - G_{A,O}\, h_{A,O} \tag{4.1}$$

The experimental procedure, sensor instrumentation and uncertainty evaluation are established to meet the Japan Air Conditioning and Refrigeration Testing Laboratory (JATL) standard[83]. The calibration of the test equipment was outsourced and certified as "testing facility quasi-certification", which qualified an uncertainty of the cooling capacity of ± 3%. Additionally, the uncertainties of the directly measured parameters are presented in Table 4.1.

As represented in Fig. 4.1, the system features a variable speed compressor, expansion valve, one condenser, and four evaporators. In accordance with the engineering criteria, factors such as the limited access for measurement in operative systems, intrusivity of the required measurement procedures, uncertainty, cost of certain parameters, and possibility of generalizable depictions of different operative systems are taken into account[40].

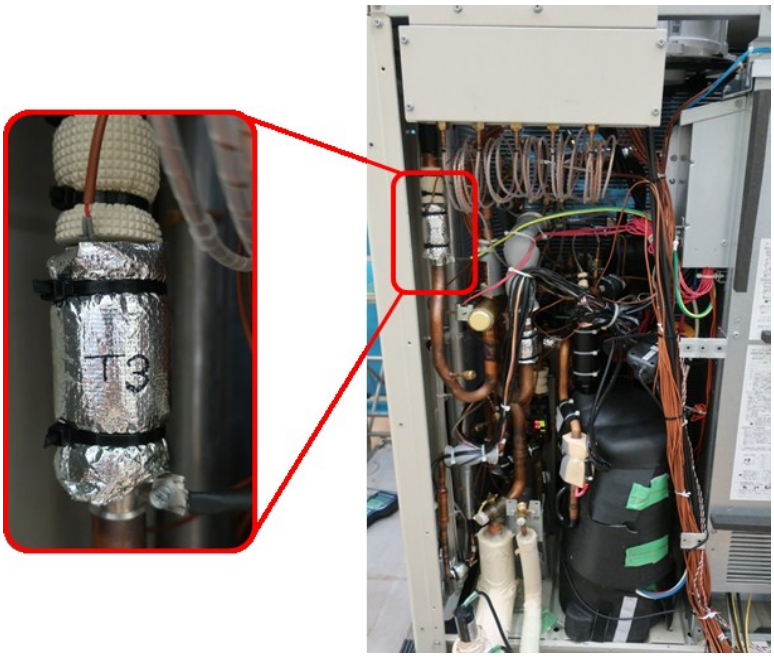

Fig. 4.3 Refrigerant tube measurement by thermocouple

Table 4.1 Sensor uncertainty of measurements

Parameter	Instrument	Model	Uncertainty
Wet bulb air temperature, T_{WB}	Sheath resistance Thermometer	CHINO Pt100 NRHS1 class A	±(0.15 + 0.002|t|) ℃
Dry bulb air temperature, T_{DB}	Sheath resistance Thermometer	CHINO Pt100 NRHS1 class A	±(0.15 + 0.002|t|) ℃
Refrigerant tube temperature, T	Thermocouple	CHINO C060-T JIS class 2	±1.0 ℃
Air pressure, P	Pressure gauge	TP-6001-A1-A-C-A	±1.5 Pa

4.2 Experimental scenario

The performance prediction method presented in chapter 3 relies exclusively on simulation data and demonstrated that the ANN model could predict the testing data that are inside the range of training data. This suggests the importance of a complete set of training data which appropriately

covers the circumstances encountered during actual system operation. Otherwise, the ANN model would not recognize the performance cases of the testing data (if not provided in the training phase) hence resulting into a poor accuracy when training data are not sufficient. The data collected with the experimental equipment hereby described represent a reliable target for demonstrating the prediction ability of the proposed ANN model. Additionally, the analysis of such experimental data provides information regarding the discrepancies between experiment and simulations. Therefore, guiding possible developments of the simulator as well as constituting a possible alternative set for the ANN training.

Table 4.2 Experimental scenarios for input and output data generation (VRF system 33.5 kW)

Case	Load pattern	$T_{in,set}$ (°C)	$T_{out,set}$ (°C)	No. data point
1	Variable rate load	Constant 26	Constant 35	1798
2	Step load; Continuous decline load	Constant 24; 26; 28	Constant 35	43250
3	Step load; Continuous decline load	Constant 24; 26; 28	Constant 40	37238
4	East load	Constant 26	Constant 35	1091
5	Continuous decline	Constant 24; 26; 28	Constant 35; 40	40482
6	East load; West load	Constant 26	Variable 30- 40	4046
7	Step load; Continuous decline load	Constant 26; 28	Constant 30	21950
8	West load	Constant 24; 26; 28	Variable 30- 40	66120
9	East load	Constant 24; 26; 28	Variable 30- 40	23967
10	South load	Constant 24; 26; 28	Variable 30- 40	12232
11	East load; West load	Constant 25; 27	Variable 30- 40	5486

To develop a reliable model, the ANN should be trained using the data with high variability and wide coverage of operative conditions. A broad scenario of training data could improve the reliability and expanding the range of applicability of ANN model. Specifically, in actual application the fluctuation of cooling load and outdoor temperatures cannot be avoided. In addition, indoor temperature is also frequently changed due to the subjectivity of thermal comfort for each occupant. Hence various cooling load patterns together with different indoor and outdoor air temperature settings are introduced to generate a broad-spectrum data set of the input and output

parameters for training and testing. The experimental data generations are conducted using two different machines namely, VRF systems with the nominal capacity of 33.5 and 28 kW.

The experimental scenarios collected in the system of 33.5 kW are presented in Table 4.2. Three constant values of 24, 26, and 28 °C are mainly assigned for the indoor temperature settings. Some cases are set as 25 and 27 °C. This variation is intended to include different individual sensitivities of the thermal comfort of the occupant and show the effect on AC system performance under different indoor set temperature. The outdoor temperature is modulated with constant and variable values representing the actual climate conditions. The representative indoor and outdoor temperature setting combinations are provided in Fig. 4.4.

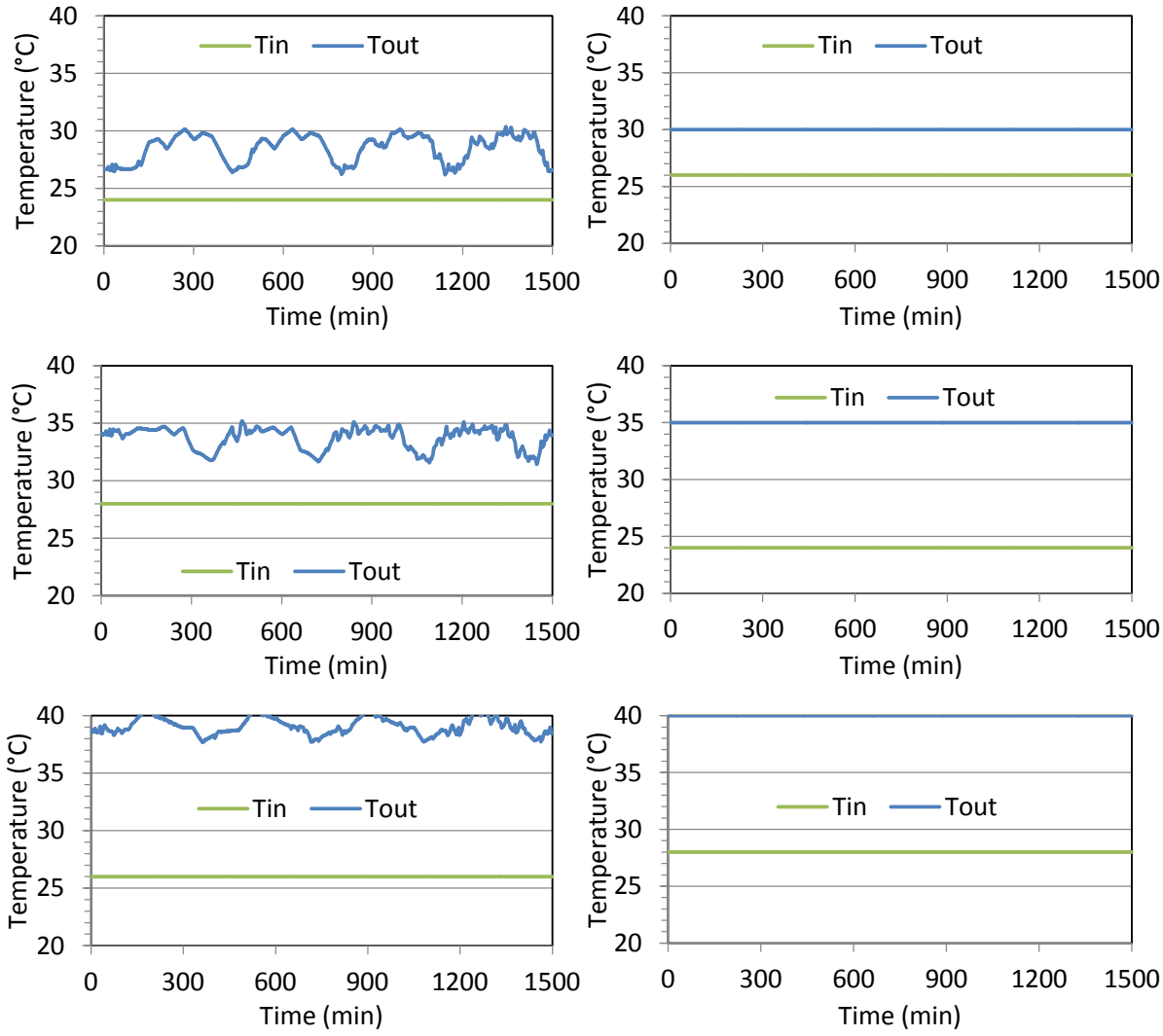

Fig. 4.4 Representative indoor and outdoor temperature settings

Variation of cooling load patterns is depicted in Fig. 4.5. It covers variable rate modulation, step variation, continuous decline pattern, and load behavior on the west, east, and south zones. The variable rate modulation is applied to demonstrate high variability in the cooling load in consequence of the occupant behavior and activity or the operation of other devices such as computers, kitchen stoves, and built in refrigerator units. The step variation aims to represent small variations of the cooling load and the related adjustment of the cooling capacity as a response of the system guided by its integrated control. The continuous decline pattern could represent the gradually decreasing cooling load due to continuous reduction of the load coming from solar radiation in the afternoon; finally, the west, east, and south zone loads illustrate the cooling load behavior related to the window and building orientation.

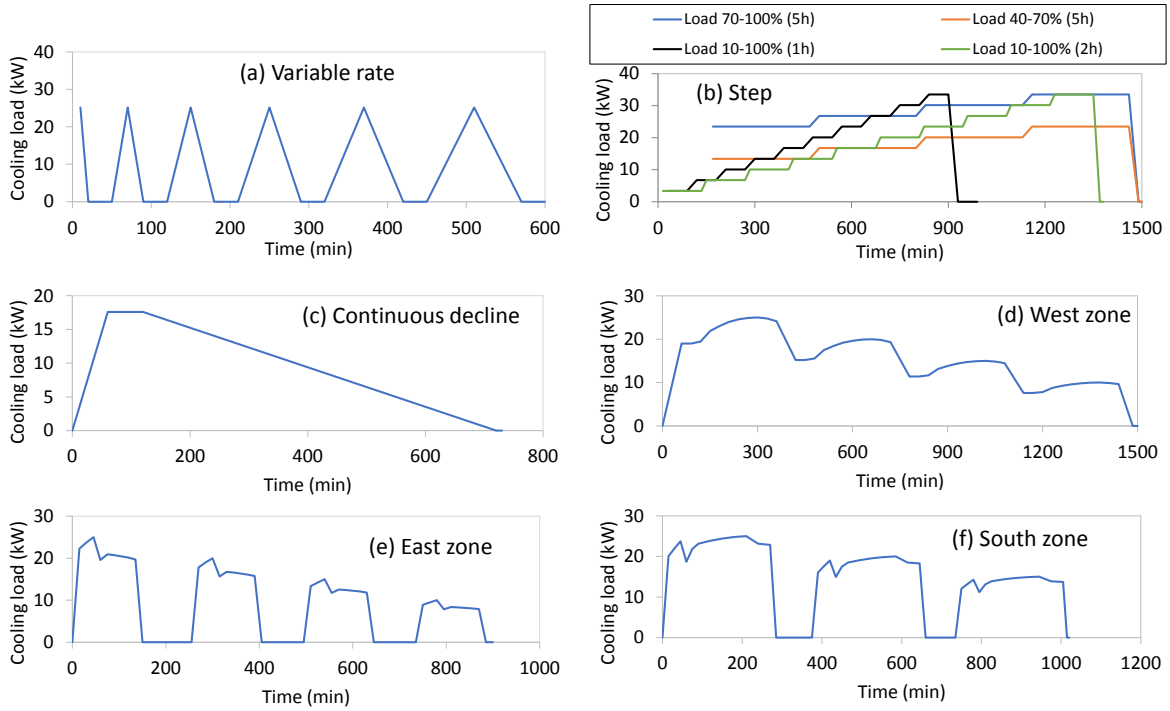

Fig. 4.5 Main categories of cooling load pattern (a) Variable rate; (b) Step; (c) Continuous decline; (d) West zone; (e) East zone; (f) South zone;

In total there are more than 250,000 data points generated by the system of 33.5 kW in various operating conditions. The representative data characteristics covering all six load patterns are presented in Figs. 4.6 to 4.11. According to the graphs, the indoor temperatures do not stand in the constant value as the desired value. It indicates that the package controller designed on actual system is not as good as the one in simulator. However it helps ANN to learn more data variation as the experimental data provide more variability in indoor temperature variation.

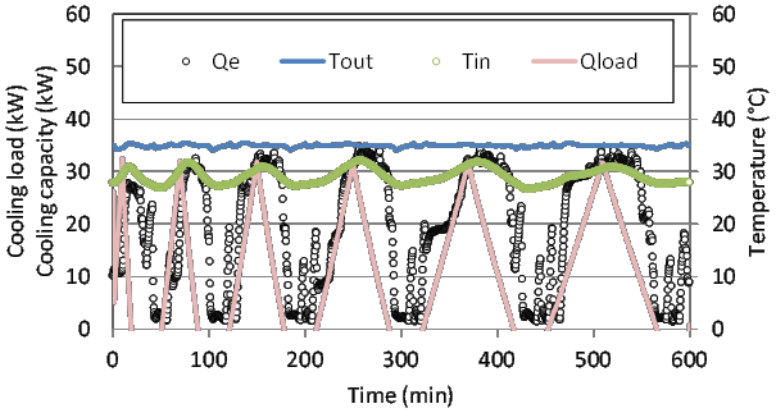

Fig. 4.6 Experimental data (Rated capacity: 33.5 kW; Variable rate load; T_{out}: constant 35 °C)

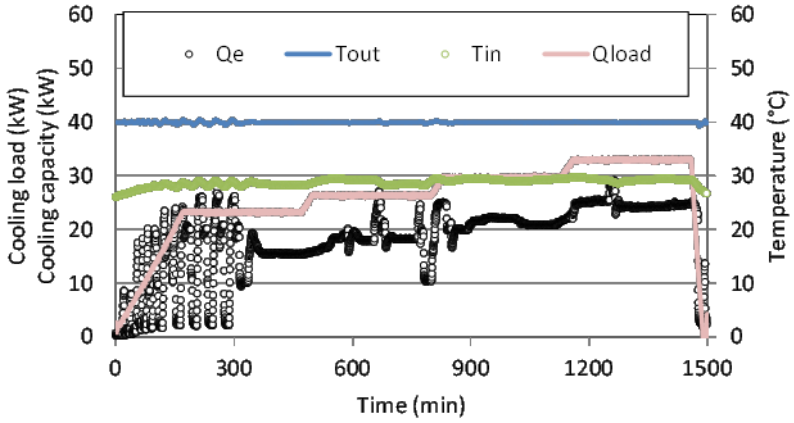

Fig. 4.7 Experimental data (Rated capacity: 33.5 kW; Step load; T_{out}: constant 40 °C)

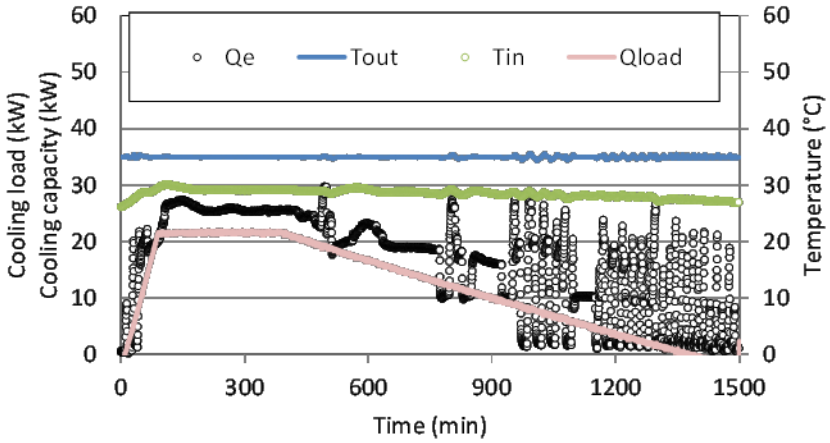

Fig. 4.8 Experimental data (Rated capacity: 33.5 kW; Con. decline load; T_{out}: constant 35 °C)

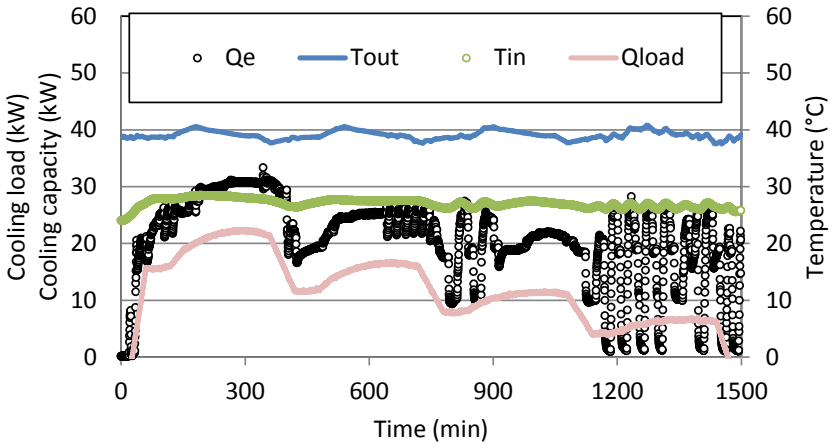

Fig. 4.9 Experimental data (Rated capacity: 33.5 kW; West zone load; T_{out}: variable)

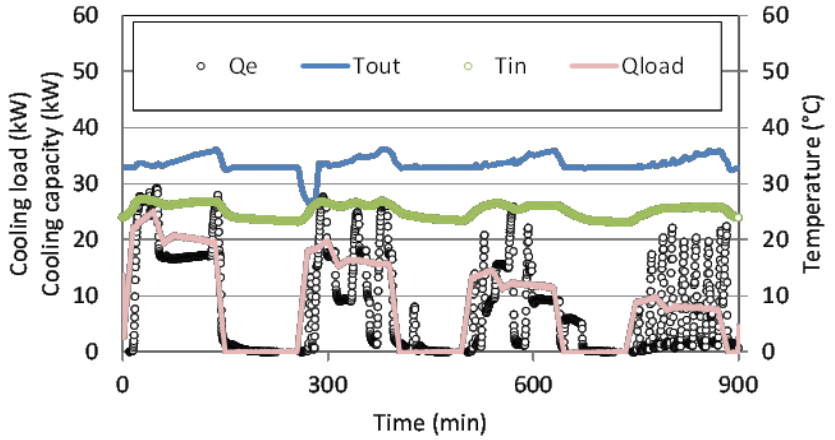

Fig. 4.10 Experimental data (Rated capacity: 33.5 kW; East zone load; T_{out}: variable)

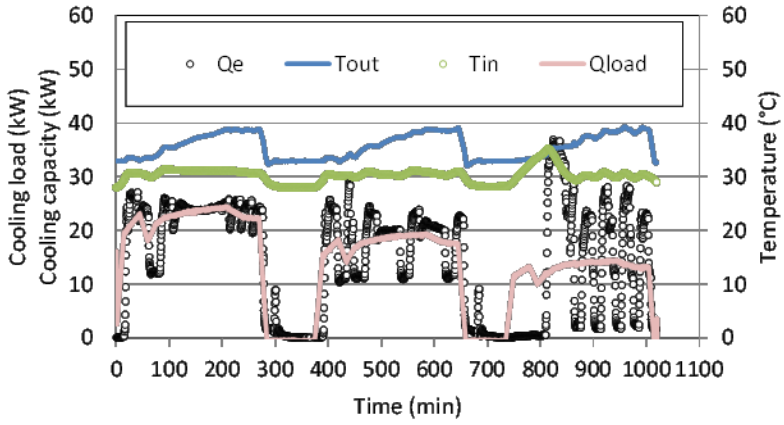

Fig. 4.11 Experimental data (Rated capacity: 33.5 kW; South zone load; T_{out}: variable)

Furthermore the experimental data with the VRF system of 28 kW are generated with different indoor and outdoor temperature settings. There are two scenarios of data variations with the same step load pattern. The data generated by this system are mainly used to examine the ANN model while predicting on different system. The list of experimental scenarios for VRF system of 28 kW can be seen in Table 4.3.

Table 4.3 Experimental scenarios for input and output data generation (VRF system 28 kW)

Case	Load pattern	$T_{in,set}$ (°C)	$T_{out,set}$ (°C)	No. data point
12	Step load (2h)	Constant 26	Constant 30	3688
13	Step load (2h)	Constant 28	Constant 40	3688

The representative experimental data characterized by the system of 28 kW are shown in Figs 4.12 and 4.13. It can be analyzed that the data fluctuations on the system of 28 kW are more stable compared to the ones presented in the system of 33.5 kW. It is highly affected by the control designed for each system is slightly different. According to the system of 33.5 kW, the intermittent operation mostly appears in low load operation. Meanwhile in system of 28 kW, the system works more smoothly for the whole load conditions. It indicates that the controllers of each system are not tuned with the same response performance, thus the dynamics characteristics are different.

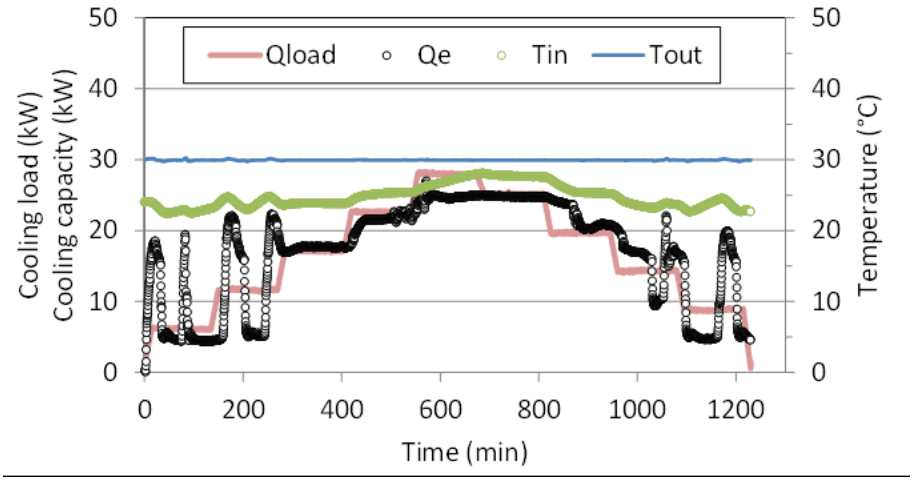

Fig. 4.12 Experimental data (Rated capacity: 28 kW; Step load; T_{out}: constant 30 °C)

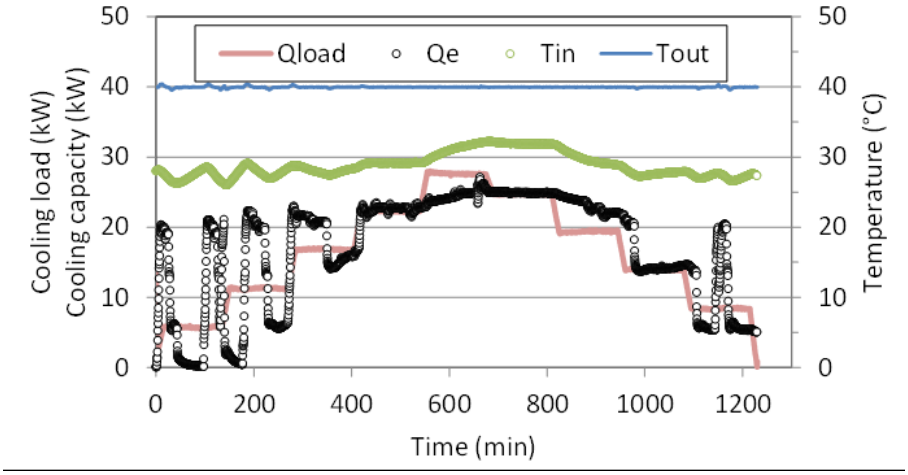

Fig. 4.13 Experimental data (Rated capacity: 28 kW; Step load; T_{out}: constant 40 °C)

4.3 Selection of measurement points for cycle representation

The pressures and temperatures representing the refrigeration cycle are measured from outdoor unit in seven points (denoted by red markers from point 1 to 7 in Fig. 4.14). Seven measurement locations are easily accessible for the installation of thermocouples. Each location on the refrigerant pipes represents a different location (i.e thermodynamic states, assuming that single values of the thermodynamic quantities can be associated to a given location) along the refrigerant cycle that governs the performance of the vapor compression system. The temperatures inputs for prediction should be carefully selected to properly represent the air conditioning cycle while avoiding locations affected by thermal noise or possibly large experimental uncertainties. Both the pressure and temperature sensors at corresponding measurement points are provided in the experimental facility.

In chapter 3, the refrigerant temperatures representing the corners of the system cycle has been proven to be applicable for performance prediction. In this section the selection of corresponding temperatures for representing the system cycle is presented. The steady state operation shown by the red mark in representative data (see Fig. 4.15) is selected as reference to plot in P-H diagram. As the expansion valve in a VRF system is located within the indoor unit (see Fig. 4.1), the temperatures and pressures at the evaporator inlet are not available. Thus point 8 at P-H diagram (see Fig. 4.16) follows the assumption of an isenthalpic process in expansion valve and no pressure drop during the evaporation process.

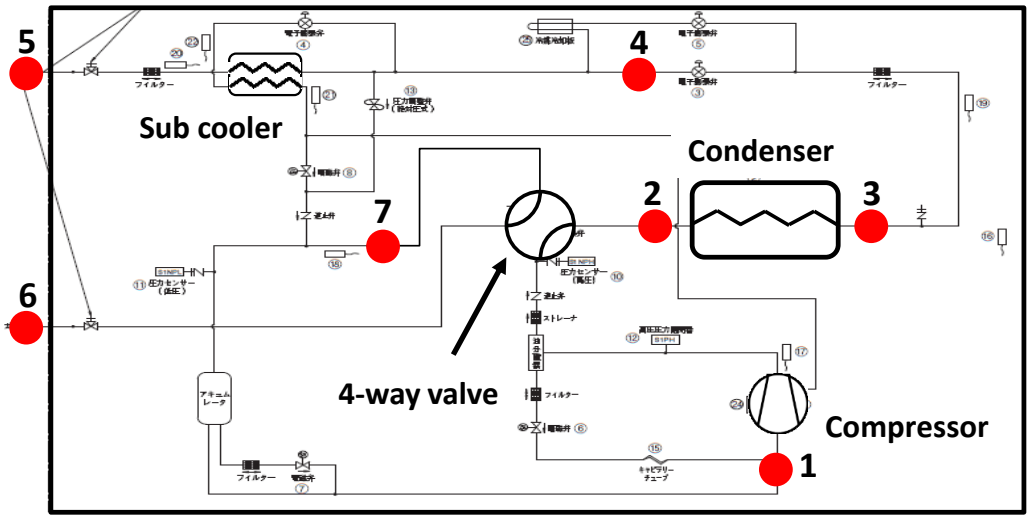

Fig. 4.14 Measurement point of refrigerant properties at outdoor units

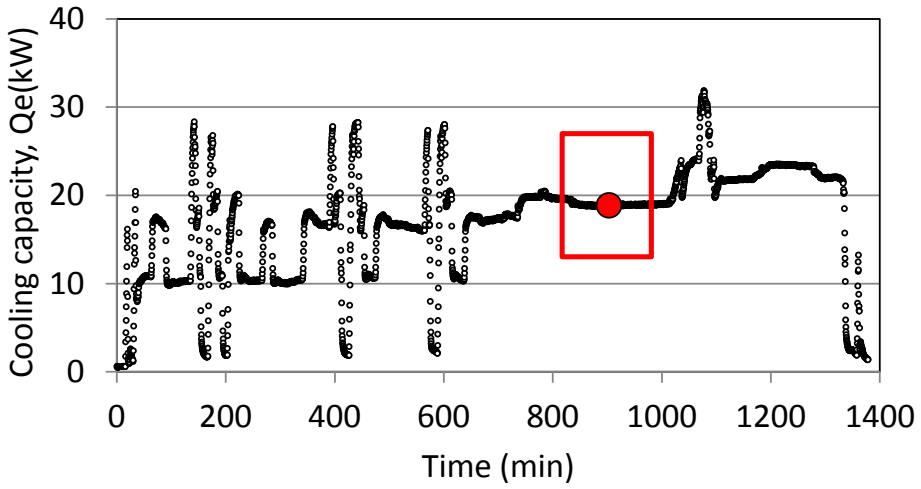

Fig. 4.15 Cooling capacity at steady condition for cycle representation

Figure 4.16 demonstrates the whole measured pressures and temperatures plotted on P-H diagram to represent the air conditioning cycle. The pressure and temperature at point 2 and 3 are representative of the refrigerant state at inlet and outlet of condenser. On the other hand, the sub cooling temperature (in this case at the corner of the refrigerant cycle) can be well represented by point 5, which provide information about the sub cooling degree obtained prior entering the expansion valve.

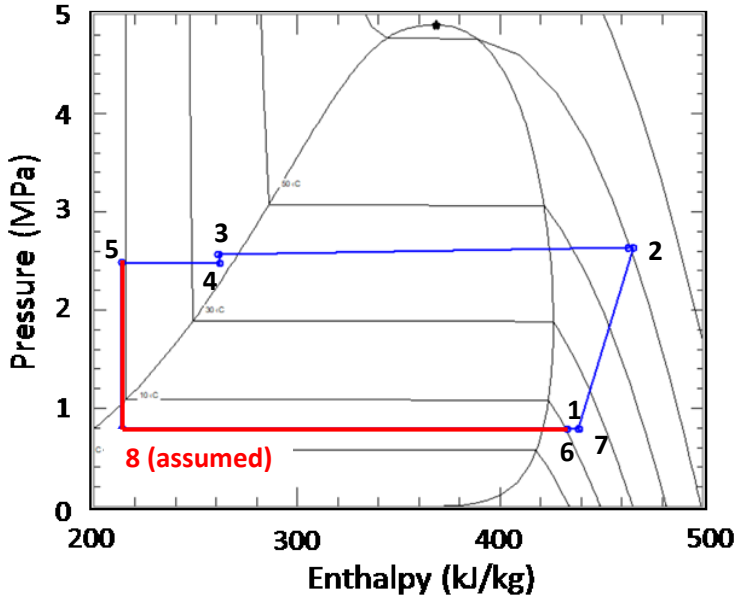

Fig. 4.16 Air conditioning cycle plot

Moreover, given the complexity of the system configuration (see Fig. 4.16), there are several options that can be selected to represent the state of the refrigerant at the evaporator outlet i.e. point 6, 1, and 7. As shown in Fig 4.17, these three points have the similar pressure and different temperature. The temperature at point 7 and 1 are higher than point 6 due to the heat transfer in the reversing valve. Additionally, the temperature at point 1 fluctuates with high amplitude as it is in close proximity to the compressor suction. Apparently, the temperatures at point 6 and 7 show the same pattern representing the dynamic performance behavior. However, the temperature at point 6 is preferred as it is located at the outlet of the indoor unit (not affected by heat transfer of the reversing valve). According to the above mentioned relationships between the measuring points and the physical characteristics of the P-H diagram of the system, the temperatures at point 2, 3, 5 and 6 are selected as the input to the ANN model for representing the air-conditioning cycle and for predicting the system performance.

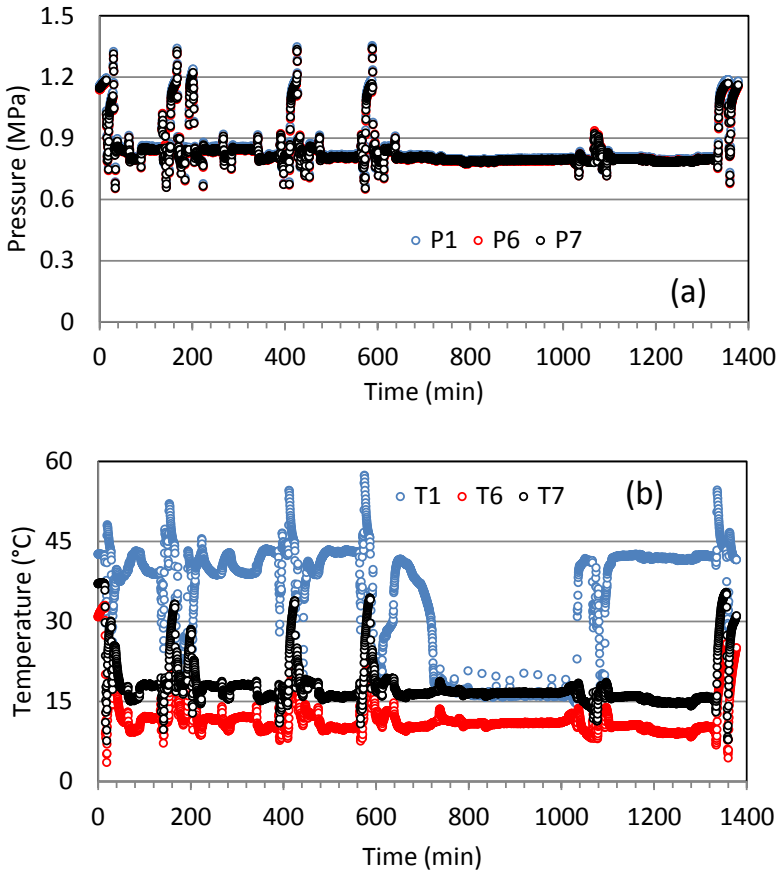

Fig. 4.17 Pressure and temperature fluctuation at measuring point 6, 1, and 7

4.4 Analysis of experimental data

Performance prediction involving simulation data is appropriate for analyzing and verifying the generalization capability of the ANN results in a broad spectrum of conditions. However, the experimental data obtained from operating systems may have different characteristics which are affected by different transient responses, noise, and ineffective control during on-off and hunting operation. Figures 4.18 to 4.20 show the representative experimental data with various load and operating temperature condition. Figure 4.18 shows fairly constant outdoor temperature T_{out} with increasing steps of cooling load, Fig. 4.19 has variable outdoor temperature T_{out} representing the daily variation along with continuous decline in cooling load, and Fig. 4.20 demonstrates the system behavior with fairly constant outdoor temperature T_{out} and variable rate of cooling load.

According to those three figures, it can be observed that the change of four temperatures have relationship with cooling capacity modulation. Specifically, the inlet temperature of condenser seems to have high sensitivity to cooling capacity due to the effect of compressor operation. Meanwhile, the outlet temperature of condenser shows similar trend with outdoor temperatures. Even though it has less sensitivity to cooling capacity, this temperature can capture the system performance related to effect of outdoor temperature.

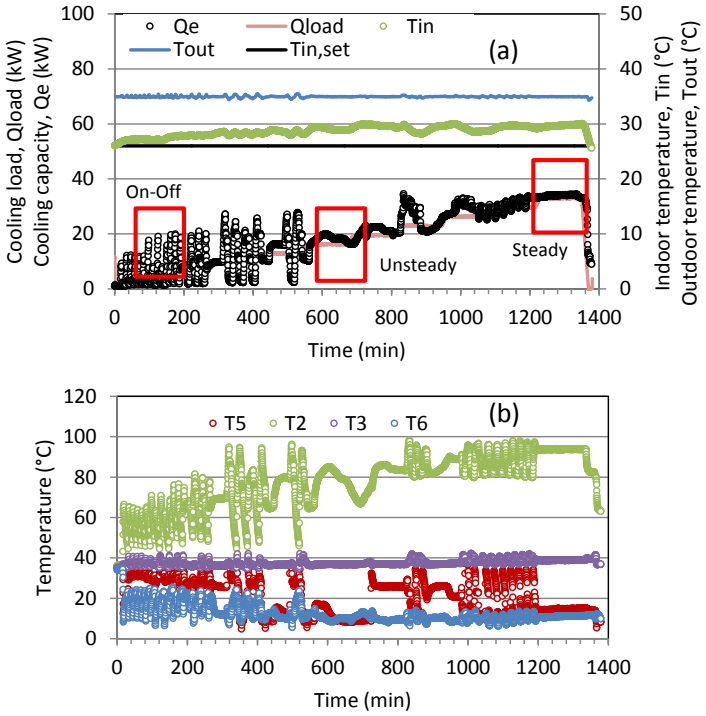

Fig. 4.18 Representative input and output data with constant T_{out} and step load

In Fig. 4.18, the typical system dynamic operation including on/off, unsteady and, steady characteristics are highlighted. Cooling capacity and four selected temperature have large amplitude variations at low cooling load, especially below 30% of the nominal cooling capacity. This dynamic operation illustrates the intermittent (on–off) system operation in the modulation of its capacity. Moreover it can be observed that the package controller shows limited ability in maintaining the indoor temperature T_{in} under these cooling load and outdoor temperature variations. The actual indoor temperature in all figures deviates from its set point temperature $T_{in,set}$. Furthermore the experimental data also indicate that the actual system operation responds with unsteady characteristics even when interfaced with steady heat loads and outdoor temperature. These operative conditions and the consequent system response are associated with the time evolution of the measured refrigerant temperatures, which are used as the quantities to identify the operative performance of the system in relation to the internal cycle.

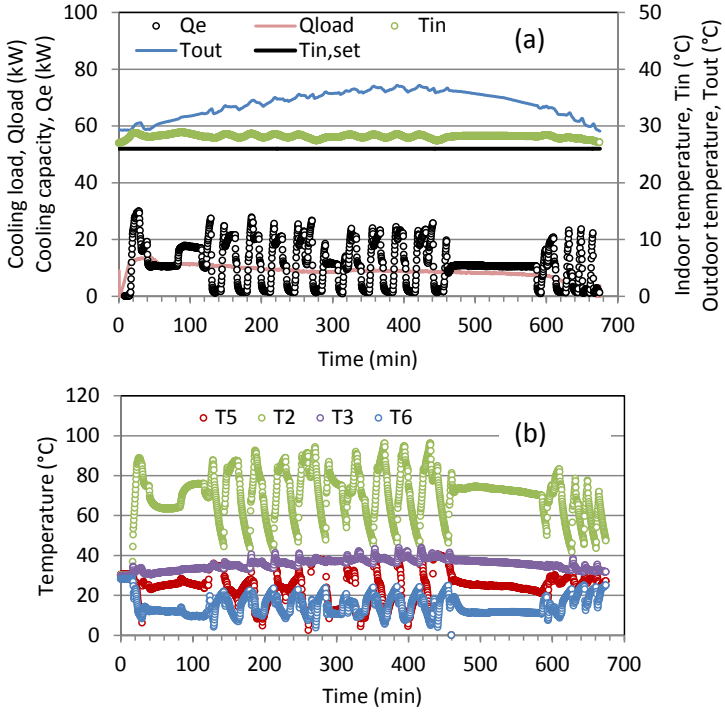

Fig. 4.19 Representative input and output data with variable T_{out} and continuous decline load

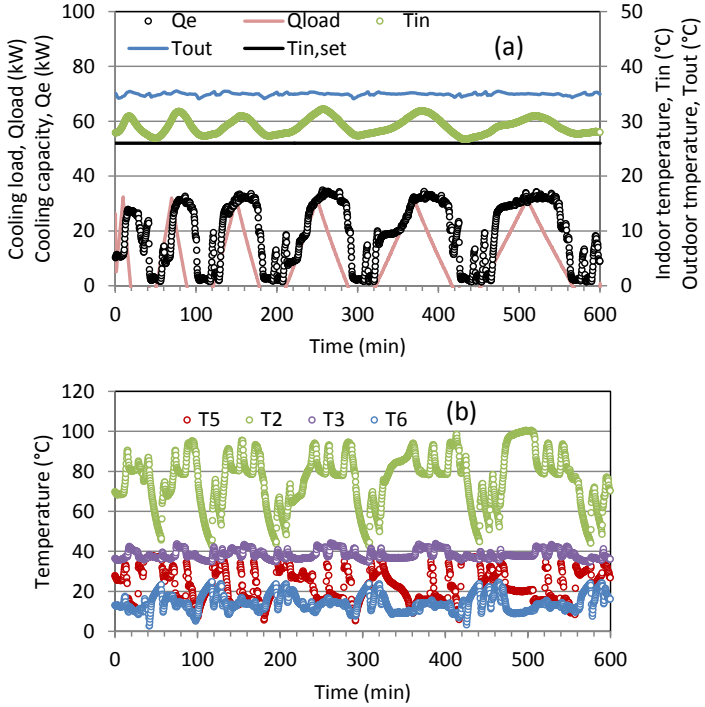

Fig. 4.20 Representative input and output data with constant T_{out} and variable rate load

From the experimental data depicted in Figs. 4.18- 4.20, it obviously shows that the data characteristics are mostly dominated by unsteady operation. Representative steady and unsteady data features from Fig. 4.18 are analyzed and presented in Fig. 4.21- 4.23 to show in detail the difference of both data characteristics in relation to the selected ANN modeling.

During steady operation (see Fig. 4.23), the recorded cooling capacity is associated with unique and steady values of the four input temperatures. This suggests the possibility of a strong relationship, which would ensure a direct dependency between the input and output parameters for the training of the ANN model. During unsteady and on–off operation (see Figs. 4.21 and 4.22), the measured temperatures and cooling capacity are highly related to the previous behavior, hence suggesting the necessity of including time characteristics for representing these operative conditions, such as temperature rate and rate of change, besides the magnitude of the measured temperature. In this regard, the inclusion of a certain number of the values of the inputs from previous time steps is thus investigated to develop an ANN model with sufficient input information for approximating such unsteady characteristics of real operation. Along with the time characteristics of the measured data, the effects of external disturbances, such as indoor and outdoor temperatures and cooling load pattern, are investigated to effectively define a reliable prediction method.

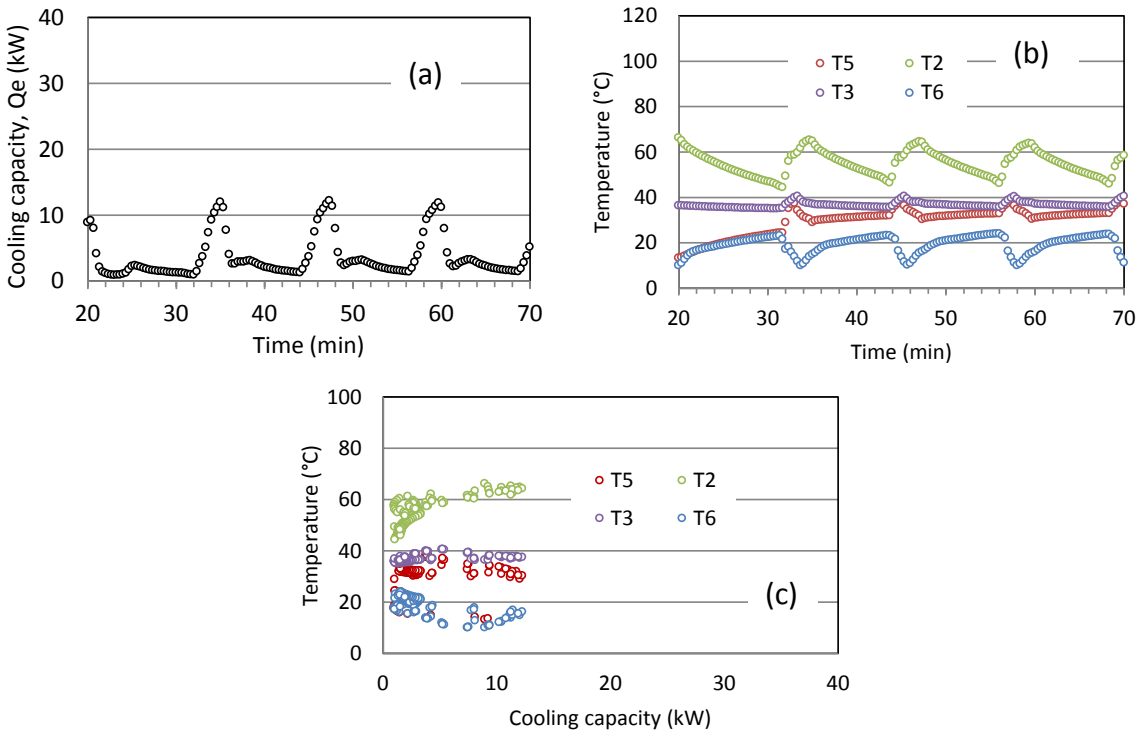

Fig. 4.21 Data characteristic of intermittent (on/off) operation

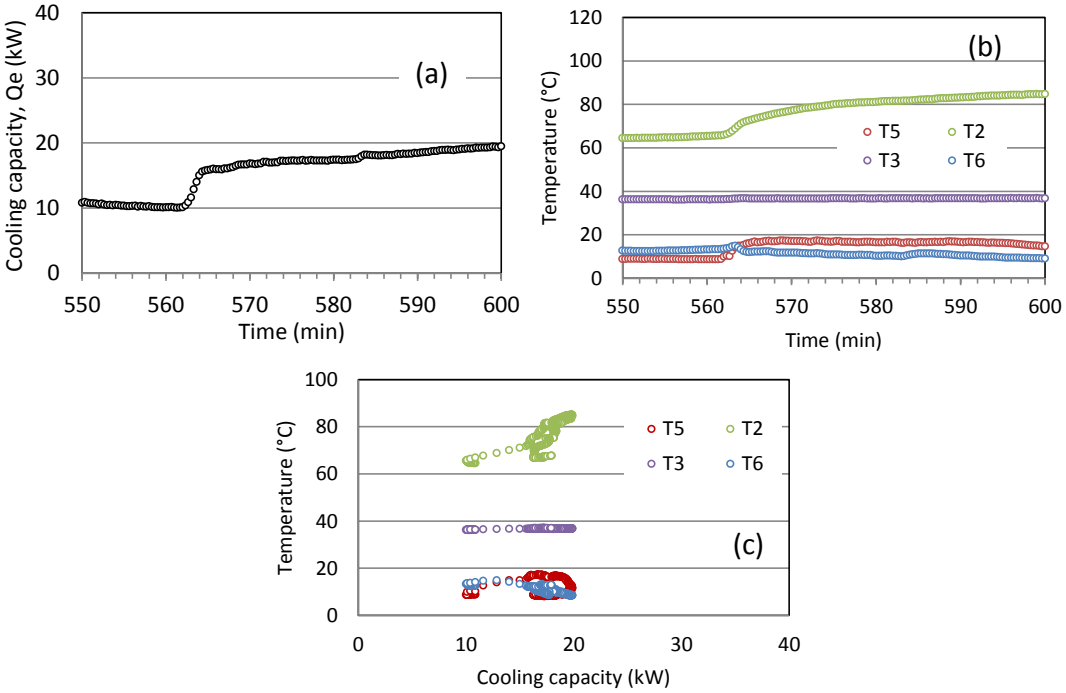

Fig. 4.22 Data characteristic of unsteady operation

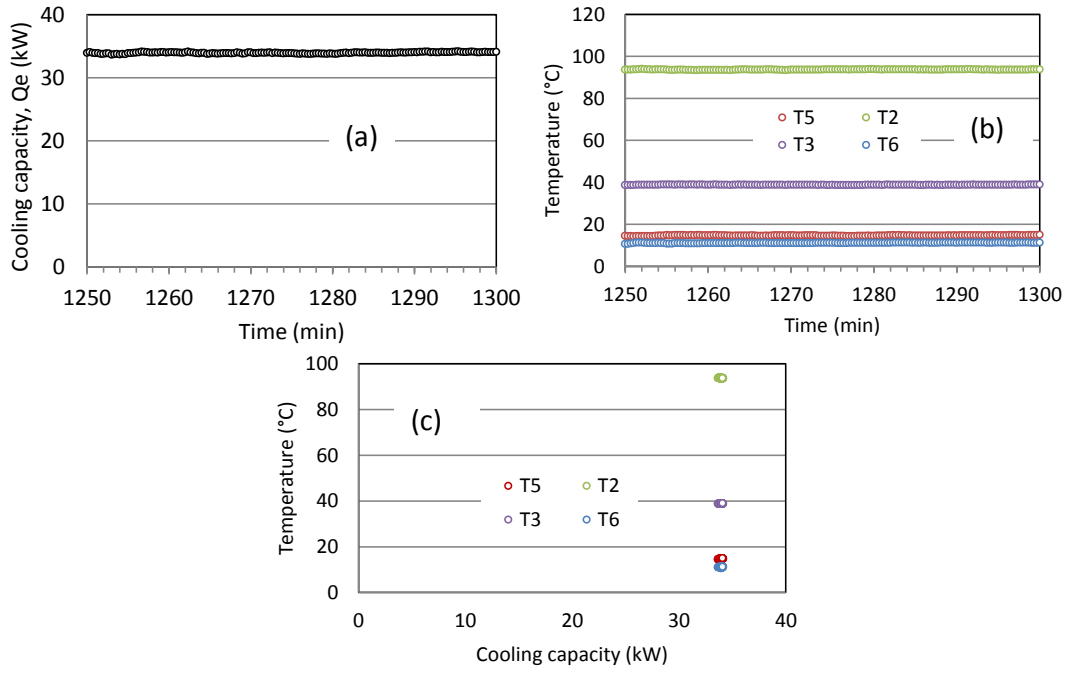

Fig. 4.23 Data characteristic of steady operation

4.5 Dynamic input characteristics

During steady state operation, the current cooling capacity can be approximated using the instantaneous value of the selected input temperature. However, this kind of univocal relationship is not encountered during dynamic operation. As a simplified interpretation of the calibration of such mathematical relationship within the ANN model, Fourier analysis offers an approximated representation of the relationship between input and output. A generic function can be approximated with Taylor series as expressed in Eqs. (4.2 - 4.4). In the case of a dynamic response of the system, the experimental data recorded have shown that the accurate representation of the performance of the AC system (in this case, $Q_e(t)$) may not be sufficiently accurate when only the instantaneous value of the input temperatures are used as expressed in Eq. (4.5). The inclusion of several inputs in previous time steps may be necessary for capturing the dynamic modulations of the system capacity through the rate of temperature variation ($\dot{T}(t)$) and the rate of change of temperature variations ($\ddot{T}(t)$). This technique has been applied in Taylor series method to get a precise approximation in data fitting of transient operation[84]. Figure 4.24 indicates that the higher the degree of the Taylor polynomial approximation, the more accurate the representation of the function is. It suggests the importance of previous time step inputs in the time distribution of the approximation.

$$f(x) = f(x_0) + \frac{f\prime(x_0)(x-x_0)}{1!} + \frac{f\prime\prime(x_0)(x-x_0)^2}{2!} + \cdots + \frac{f^{(n)}(x_0)(x-x_0)^n}{n!} + o(n+1) \tag{4.2}$$

$$f'(x_i) = \frac{f(x_i)-f(x_{i-1})}{\Delta x} + o(h) \tag{4.3}$$

$$f''(x_i) = \frac{f(x_i)-2f(x_{i-1})+f(x_{i-2})}{(\Delta x)^2} + o(h^2) \tag{4.4}$$

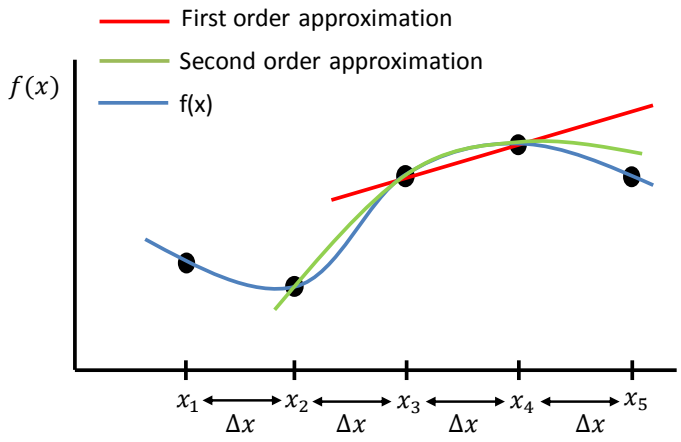

Fig. 4.24 Taylor series representation

The dynamic ANN model can be developed to predict the cooling capacity at current time $Q_e(t)$ using the temperature at current and previous time steps as written in Eqs. (4.6). As the actual system operation is mostly dominated by transient behavior, the inclusion of previous time step inputs data is required for capturing the dynamic operation with an advanced ANN training procedure.

$$Q_e(t) \equiv f\big(T(t)\big) \qquad T(t) = \langle T_{E,I}(t), T_{E,O}(t), T_{C,I}(t), T_{C,O}(t)\rangle \tag{4.5}$$

$$Q_e(t) \equiv f(t, T(t), \dot{T}(t), \ddot{T}(t), \dots) \qquad \dot{T}(t) = \langle \frac{\partial T_{E,I}(t)}{\partial t}, \frac{\partial T_{E,O}(t)}{\partial t}, \frac{\partial T_{C,I}(t)}{\partial t}, \frac{\partial T_{C,O}(t)}{\partial t}\rangle \tag{4.6}$$

$$\ddot{T}(t) = \langle \frac{\partial \dot{T}_{E,I}(t)}{\partial t}, \frac{\partial \dot{T}_{E,O}(t)}{\partial t}, \frac{\partial \dot{T}_{C,I}(t)}{\partial t}, \frac{\partial \dot{T}_{C,O}(t)}{\partial t}\rangle \tag{4.7}$$

4.6 Cycle prediction

According to the selection of measurement points in the outdoor unit as discussed in section 4.3, the selected pressure and temperature at point 2, 3, 5, and 6 are the most representative variables to identify the refrigerant cycle (see Fig. 4.16). In this section the cycle prediction is conducted by using three temperatures at point 6, 2, and 5. By approximating the process within the expansion valve as an isenthalpic process and by neglecting the pressure drop at evaporator, the experimental air conditioning cycle can be plotted only using three measuring points as shown in Fig. 4.26.

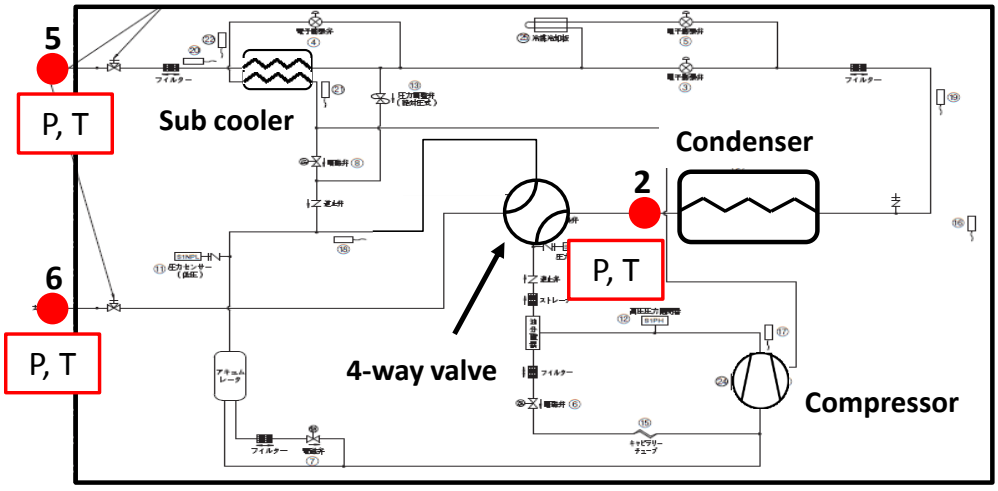

Fig. 4.25 Measurement point on outdoor unit for cycle prediction

The air conditioning cycles are predicted using experimental data generated by the system with 33.5 kW nominal cooling capacity. The training and testing data are obtained with constant

outdoor temperature of 35 °C. The training data are selected to be able to cover the range of testing data characteristics. The ANN model is developed with three temperature inputs (*T2, T5, T6*) and three pressure outputs (*P2, P5, P6*).

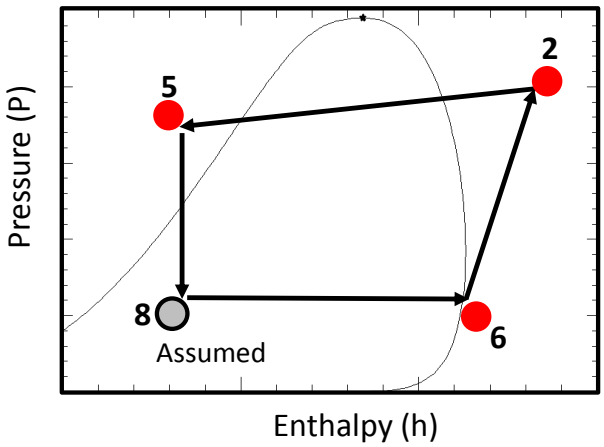

Fig. 4.26 Cycle representation by three measuring points

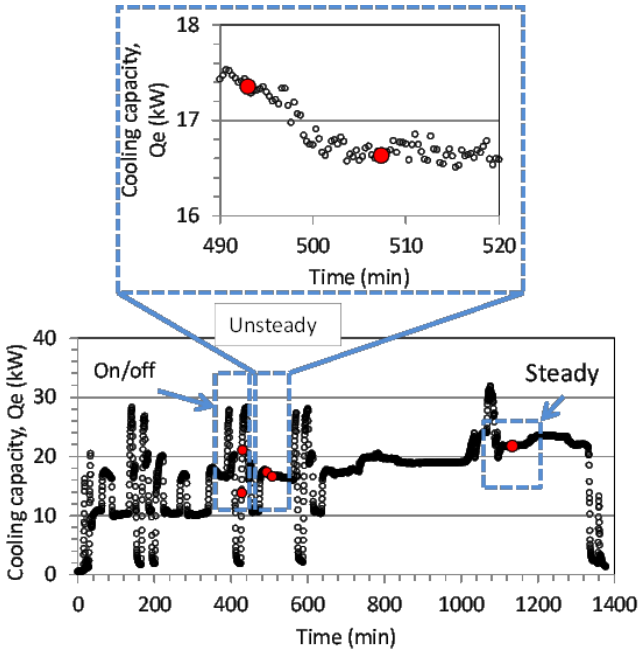

Fig. 4.27 Selected operating condition for on/off, unsteady and steady condition

The prediction accuracy on cycle performance is quantified by comparing the coefficient of performance (COP) between predicted and corresponding data. The COP is calculated as the ratio of the output cooling capacity to the energy input as expressed in Eq. (4.8). The specific enthalpy

denoted by h is a function of pressure and temperature (P, T). The fluctuation of the refrigerant flow rate within the cycle during unsteady and on/off operation is assumed to be less significant.

$$\mathrm{COP} = \frac{(h_6 - h_8)}{(h_2 - h_6)} \tag{4.8}$$

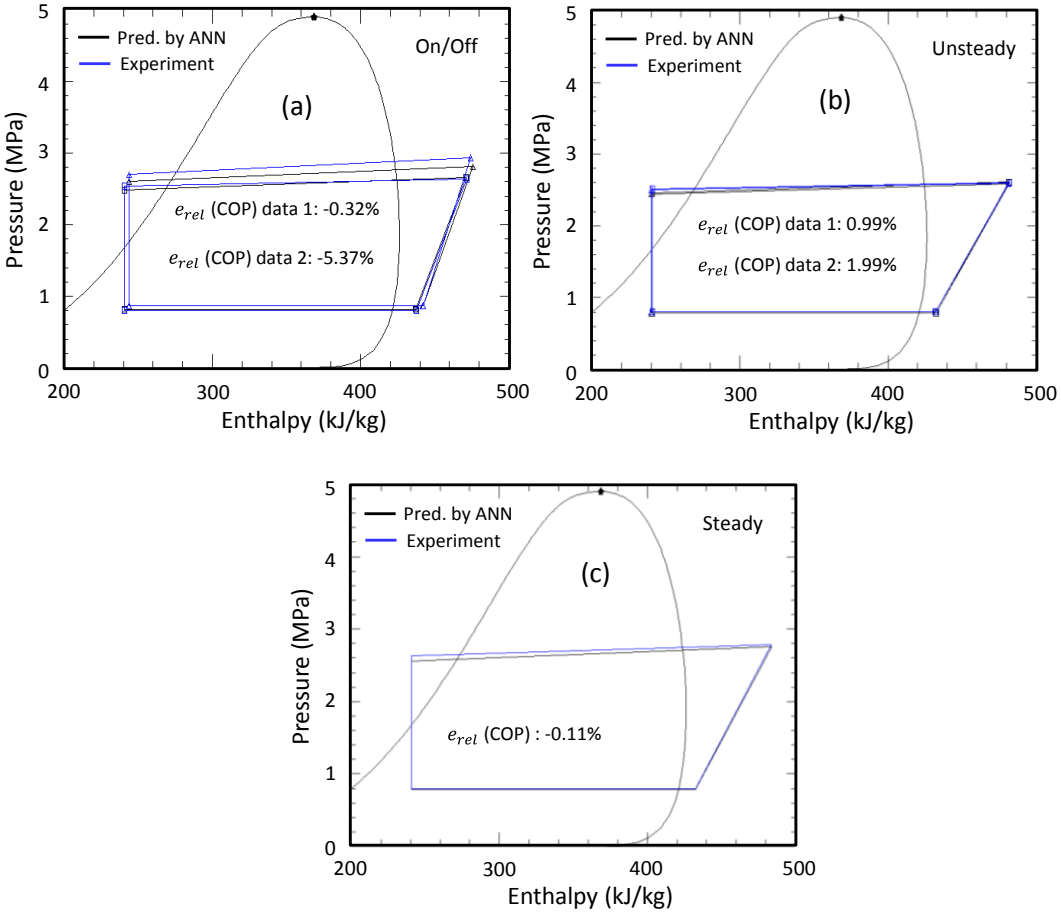

Fig. 4.28 Prediction of cycle performance (a) on/off ;(b) unsteady; (c) steady

The prediction results are mainly evaluated in three selected operating condition as shown in Fig. 4.27, where data characteristics for on/off, unsteady and steady behavior are demonstrated. Few representative conditions of the results of cycle prediction are presented in Fig. 4.28. For on/off and unsteady condition, two data points are selected to demonstrate the cycle change during dynamic operation. The results show a high accuracy of the cycle predictions for all the selected operating conditions with a relative error mostly below 5%. This result indicates that the selected temperatures have successfully captured the modulation of corresponding pressure during on/off, unsteady, and steady operation. Therefore, the changes of system cycle are precisely predicted.

5. Performance prediction on actual systems

In chapter 3, the proposed ANN model for AC systems performance prediction, using four refrigerant temperatures that represent the system cycle as input parameters, has shown satisfying results when applied to system with different rated capacities. Training and testing data were generated by a simulator. In this section, the performance prediction of actual AC systems, represented by the experimental data collected in the previously presented experimental campaign, is attempted by relying on simulation and experimental platform with different rated capacities for generating the training scenario.

Training data are generated through the simulation of a VRF system of 50 kW rated capacity, while the testing data are obtained from actual AC systems characterized in experimental facility (VRF system 33.5 kW and 28 kW). This investigation aims to verify the generalization capability of the fundamental hypothesis underlying this method for actual implementation. The hypothesis guiding this research effort is that, although AC systems have different configuration and size, and the specific data characteristics of simulation and experiments differ in the specific response determined by the control package, the training data obtained via a reliable simulator still provide a fundamental representation of the refrigerant cycle realized in actual systems. If such hypothesis is proved true and the simulator could reliably approximate the data behavior of actual AC systems, the ANN model can learn the system cycle from simulation data with a much broader variability of conditions, configurations and climates, which could be impossible (in terms of time, cost, and measuring method) to collect experimentally. This will reduce the time, cost, and complexity of data generation. Additionally, the simulator can be flexible and could provide the data that are difficult to generate in experimental facility.

Table 5.1 Scenario for performance prediction
(Training using simulation and testing on experimental data based)

System	$T_{in,set}$ (°C)	$T_{out,set}$ (°C)	Training	Testing
Simulation VRF 50 kW	Constant 27, 29	Constant 35	●	
	Constant 27, 29	Constant 40	●	
Experiment VRF 33.5 kW	Constant 28	Constant 35		●
Experiment VRF 28 kW	Constant 28	Constant 40		●

The simulator has been designed with including a PI controller acting on standard controllable parameters to have the realistic performance behavior. The investigation procedure follows the data division presented in Table 5.1. The training data are simulated under different operating scenarios, covering a broad range of operating conditions. The cooling capacities are

varied from 30% to 100% of rated capacity with step pattern. The input output training data characteristics generated by simulating the VRF system, with 50 kW nominal capacity, are shown in Figs. 5.1 and 5.2.

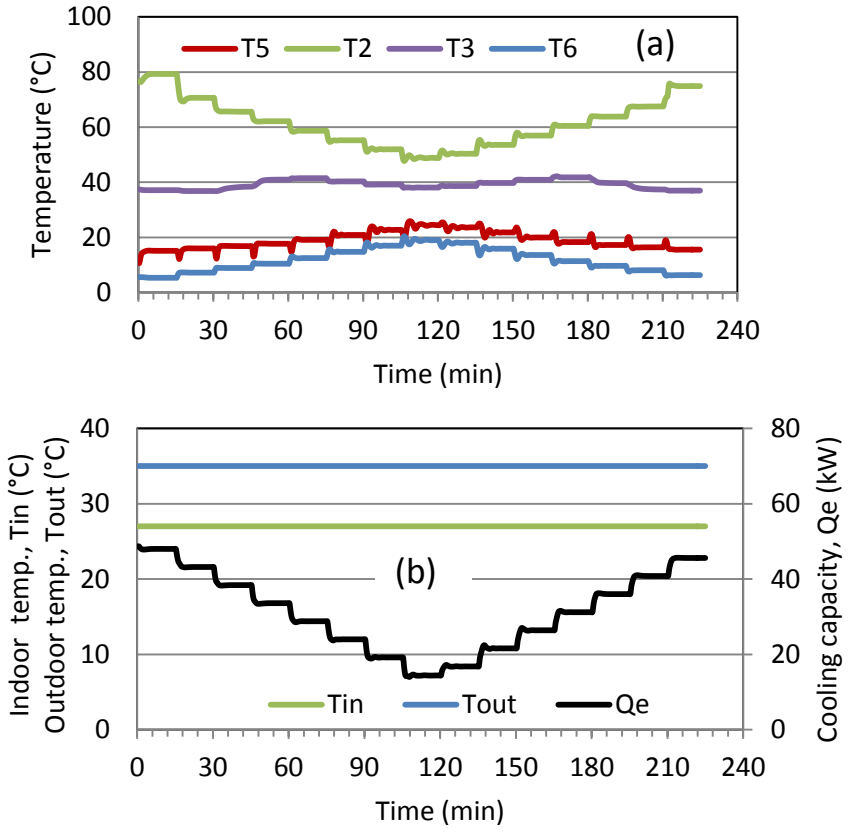

Fig. 5.1 Characteristics of input output of training data (a) refrigerant temperatures (b) cooling capacity (T_{in}: 27 °C; T_{out}: 35 °C; Q_{load}: 30-100%)

The performance prediction is conducted using the selected four temperatures that represent the corners of the refrigerant cycle of the system. The temperature selection in VRF system configuration has been discussed in previous chapter (section 4.3). The cooling capacity Q_e is predicted using the sub cooling temperature (T5), indoor unit outlet temperature (T6), and inlet and outlet of condenser temperature represented by (T2) and (T3). The data characteristic for testing are taken from the previous experimental campaign. The layout of temperature points selected in outdoor unit for prediction inputs are illustrated in Figs. 5.3 and 5.4 for simulation and experiment, respectively. It should be noted that the temperatures at T2 and T3 show the inlet and outlet of condenser. While the temperatures at T5 and T6 represent the inlet and outlet of outdoor unit.

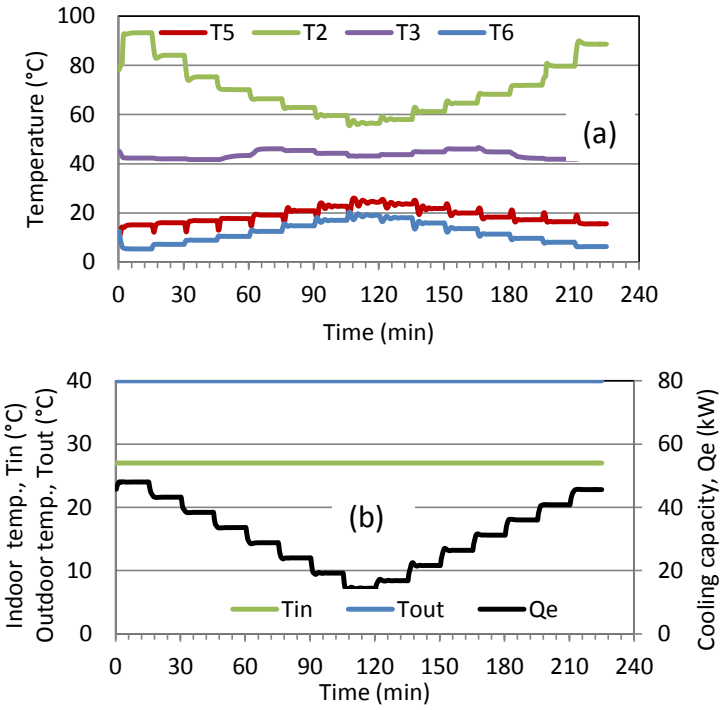

Fig. 5.2 Characteristics of input output training data (a) refrigerant temperatures (b) cooling capacity (T_{in}: 27 °C; T_{out}: 40 °C; Q_{load}: 30-100%)

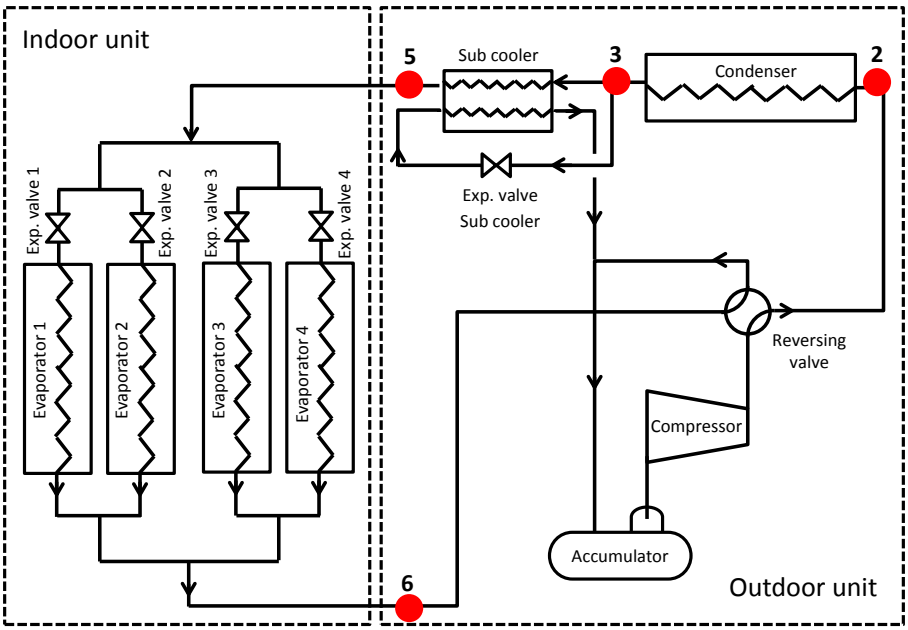

Fig. 5.3 Layout of four temperature inputs on outdoor unit (Simulation based)

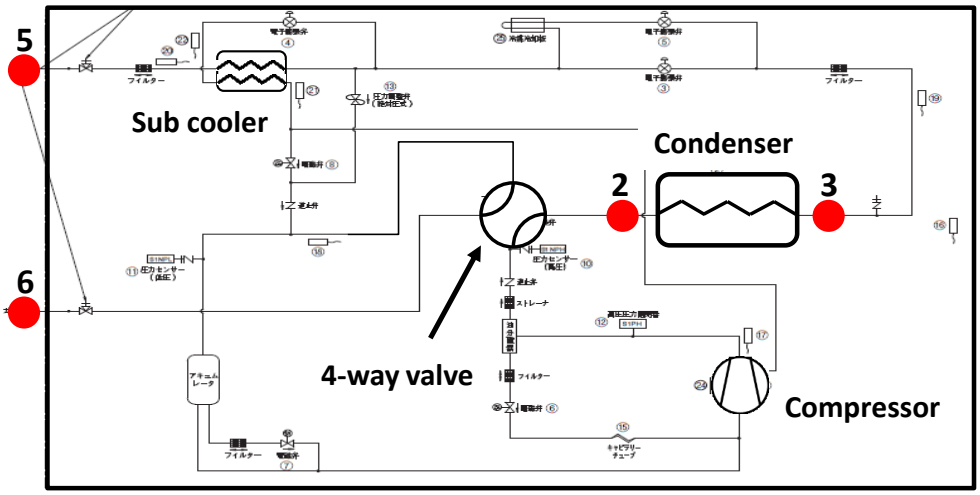

Fig. 5.4 Layout of four temperature inputs on outdoor unit (Experimental based)

The prediction on different systems relies on the normalization procedure for input and output data, as presented in Chapter 3, Eq. (3.14). The data are normalized with reference to the minimum and maximum values presented in Table 5.2. The lower and upper bound of temperatures are taken with the assumption that all those temperatures fluctuate on the corresponding range while operating from the minimum and maximum load. Cooling capacity is normalized ranging from 0 to maximum nominal cooling capacity of each systems, which is provided in the product catalogue.

Table 5.2 Lower and upper bound of data normalization

Variable	Minimum	Maximum
Temperature, T6 (°C)	0	30
Temperature, T2 (°C)	40	100
Temperature, T3 (°C)	20	50
Temperature, T5 (°C)	0	30
Cooling capacity, Qe (VRF 50 kW)	0	50
Cooling capacity, Qe (VRF 33.5 kW)	0	33.5
Cooling capacity, Qe (VRF 28 kW)	0	28

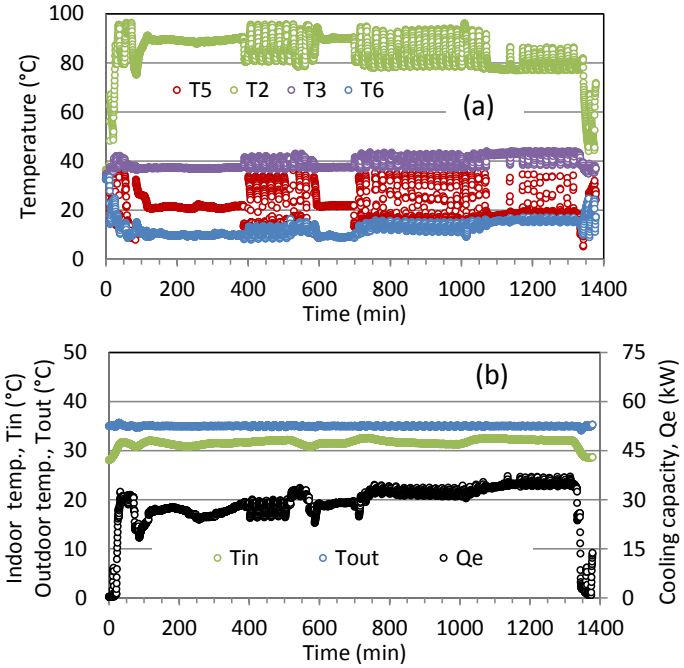

Fig. 5.5 Characteristics of input output of testing data (a) refrigerant temperatures (b) cooling capacity (experiment 33.5 kW; $T_{in,set}$: 28 °C; T_{out}: 35 °C; Q_e: 0-100%)

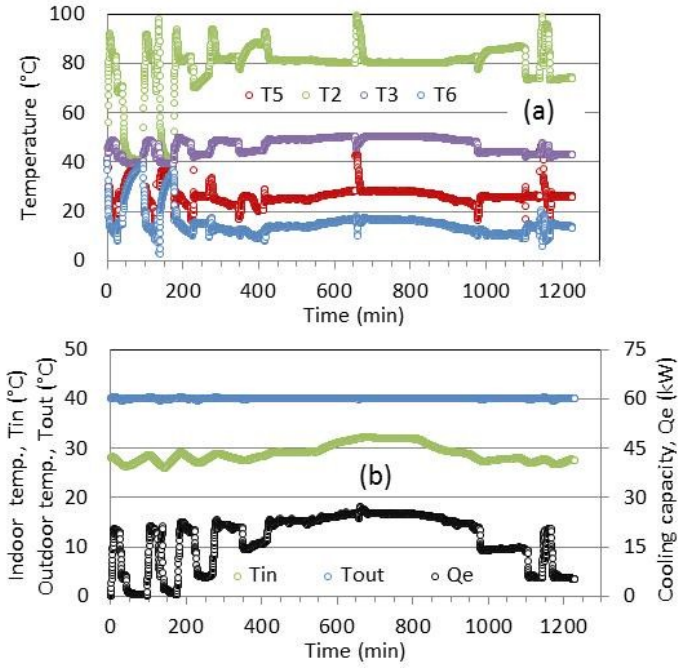

Fig. 5.6 Characteristics of input output of testing data (a) refrigerant temperatures (b) cooling capacity (experiment 28 kW; $T_{in,set}$: 28 °C; T_{out}: 40 °C; Q_e: 0-100%)

The characteristics of testing data generated by the actual machine are presented in Figs. 5.5 and 5.6 for the system with nominal capacity of 33.5 and 28 kW, respectively. According to those two figures, it can be observed that the dynamic behavior of both systems seems to be slightly different. The data shown in the system of 33.5 kW have more intermittent operation. While the data fluctuation on the system of 28 kW are slightly more stable. It implies that the controller design for both systems is different which results in different dynamic data characteristics. Moreover the simulated data used for ANN training are mostly dominated by smooth data with very small noise in some conditions only. In this section the capability of ANN model to predict the system performance relying on the different data characteristics is investigated. Two ANN models are trained with different outdoor temperatures, namely 35 and 40 °C. It ensures that the training and testing data are in the same range of operating condition. Then the trained ANN model with outdoor temperature 35 °C is applied for testing on the system 33.5 kW, while the other pre-trained ANN model with outdoor temperature 40 °C is used for testing on the system 28 kW.

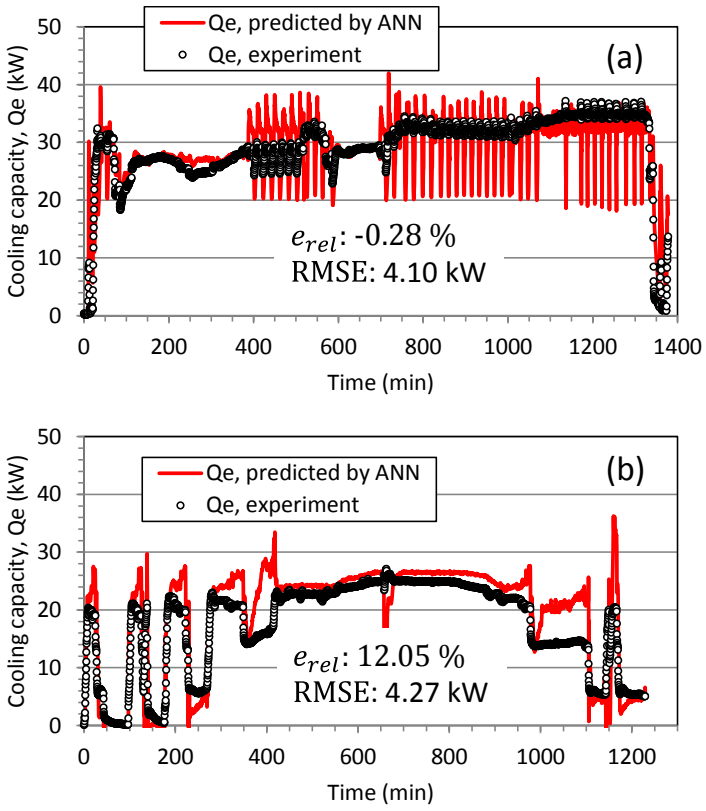

Fig. 5.7 Prediction results on experimental VRF system (ANN trained with simulation data 50 kW) (a) 33.5 kW (T_{out}: 35 °C) ; (b) 28 kW (T_{out}: 40 °C)

Figure 5.7 shows the prediction results on the system with 33.5 kW and 28 kW. The results demonstrate that the predicted cooling capacity has good agreement with the corresponding value for both systems in some operation conditions. It indicates that the air conditioning cycle of the actual system can be identified by simulation data. Therefore, the ANN model trained with simulation data could successfully capture the actual system performances.

The error analysis for the prediction results are specifically demonstrated in Figs. 5.8 and 5.9 for the system of 33.5 and 28 kW, respectively. According to Fig. 5.8, the highest deviations mostly occur when the system runs in intermittent (on-off) operation, specifically highlighted in between 800-1000 min. Meanwhile, the testing results demonstrated in 100- 300 min are closer to the target values as the data are not fluctuating very much. The unstable control acting on system 33.5 kW produces high-frequency oscillation data which are not accurately represented in the simulation data; hence the ANN model has no sufficient information to capture such intermittent operation and other characteristics with a quick dynamic response.

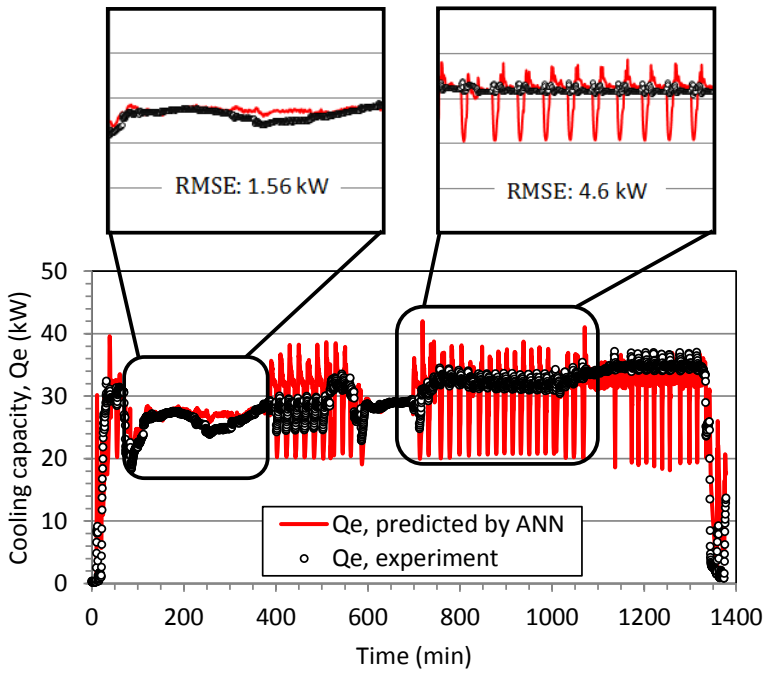

Fig. 5.8 Enlarged results of small and high error data on VRF system 33.5 kW

Furthermore the results presented in Fig. 5.9 shows that cooling capacity in 400-900 min can be precisely predicted with high accuracy. However it has poor accuracy in some condition such as 1000-1100 min due to insufficient training data. The different control design greatly affects the system dynamic characteristics. Consequently, the ANN model trained by the simulation data with the most ideal control cannot well recognize the transient behavior of testing data generated

from experimental facility. The PI controller of AC simulator has been properly tuned to provide good response with considering overshoot and settling time. Thus, the system works very smoothly while reaching various cooling capacity from 30%-100%. In experimental facility, the actual system includes many disturbances such as noise, unstable control, and others during the operation. This condition causes the gap between simulation and experimental data. Since the training data generated by simulation include only few unsteady state and intermittent behavior, the dynamic data characteristics are not well recognized by the ANN model.

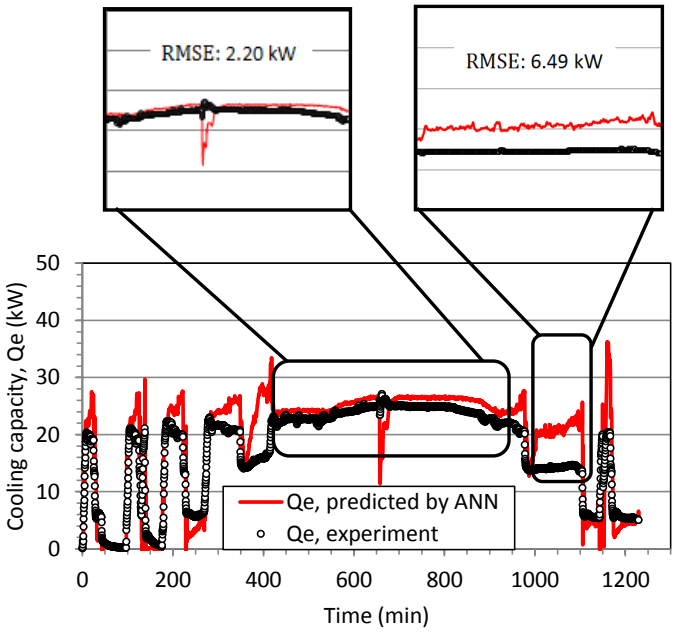

Fig. 5.9 Enlarged results of small and high error data on VRF system 28 kW

The investigation presented in this section has proven that the ANN model can be trained using the representative data generated from simulation equipped with reliable control to predict the system performance on a system produced by a different manufacturer and featuring a different rated capacity. The results also reveal that the AC simulator can be used to characterize the dynamic system behavior to provide training data for ANN to establish intelligent method for performance prediction. In order to provide reliable data during intermittent and quick response operation, the controller and the model of the AC simulator should be adjusted to meet an advanced precision in the representation of the dynamic behavior of the actual system.

6. Advanced cooling capacity prediction

Effective cooling capacity prediction is fully conducted using experimental data presented in Table 4.2 and 4.3 provided in Chapter 4. Thus the experimental data scenarios used for the prediction in this section refer to those tables. The effect of dynamic inputs, sampling time, data variability, and indoor and outdoor temperature are investigated. The ability of ANN model on cooling capacity prediction in various operating condition is investigated with the system of 33.5 kW. Moreover the performance prediction on different system is proposed with training and testing data are obtained from the system of 33.5 and 28 kW, respectively.

6.1 Effect of previous time inputs, sampling time, and indoor temperature

In practice, the occupants may frequently change the indoor temperature setting according to their different thermal comfort standards and sensations. The effect of the number of time steps considered for the input parameters and sampling time variation is investigated with reference to the prediction ability over different load patterns and indoor set temperature values. The data scenario for prediction is referred to Table 6.1. Three different data sets with various indoor temperatures are included for training and testing data. It aims to investigate the effect of indoor temperature on system performance prediction with ANN. The ANN model is trained using the data with $T_{in,set}$: 26 °C (case 2a) and tested on the other data with $T_{in,set}$: 28 °C (case 2b) and $T_{in,set}$: 24 °C (case 2c). The outdoor temperature is set as constant at 35 °C and the cooling loads are varied with step modulation until 100% for all three cases.

Table 6.1 Prediction data for indoor temperature analysis (adopted from Table 4.2)

Case	Load pattern	$T_{in,set}$ (°C)	$T_{out,set}$ (°C)	No. data points
2a	Step load 0 - 100% (2h)	26	35	4140
2b	Step load 0 - 100% (5h)	28	35	8280
2c	Step load 0 - 100% (5h)	24	35	9000

In Chapter 3, it has been clarified that the sampling time in the range of 0.1τ to τ could provide the proper combination between steady and transient responses of the system without overloading the training with redundant data, especially those related to prolonged phases of steady operation. Nonetheless the prediction relying on simulation data does not represent the actual data behavior, where the data oscillation was not appeared. As the PI controller is well designed in simulation system, the prediction data do not include the intermittent operation as existed in actual system. The effect of sampling time for prediction with experimental data based is investigated. The sampling time is varied as 20, 60, 120, 300, and 600 s. The dynamic ANN model is developed with including previous time step inputs (see section 4.5). The number of previous time step inputs is incrementally changed from 0 to 3. The case with zero-previous time steps indicates that the

training and testing are conducted by the input values at the current time step only. The difference between static and dynamic ANN configuration is explained in Chapter 3 (Fig. 3.6).

The prediction results for training and testing are presented in Table 6.2. The accuracy varies according to the sampling time and number of time steps to be considered for the input values. The ANN model trained with sampling time of 20 s shows good accuracy, with a maximum RMSE on testing data below 1.80 kW (cooling capacity range is 0 – 37 kW). Then, the errors tend to increase slightly as the sampling time increases. The accurate prediction indicates that the input output of testing data characteristics are similar to those used during the training phase. As presented in Fig. 6.1, it can be observed that the variation of indoor temperature settings have less significant impact on training and testing data behavior. Accordingly the ANN model could successfully predict the corresponding data with high accuracy as they are inside the range of training data.

Theoretically, at the same cooling capacity and outdoor temperatures, different indoor temperatures are achieved by controlling the evaporating temperature. However, the temperature inputs collected from outdoor unit in this study, under different indoor temperature set points demonstrate a minor influence, which could be related to the limited precision of the control package (see experimental data characteristics in section 4.4). This suggests the necessity of expanding the training data considering indoor temperature set point variation to improve the reliability of the proposed method.

Table 6.2 Prediction results under various sampling times, previous time step inputs, and indoor temperatures

Sampling time	RMSE of cooling capacity (kW)											
	Training $T_{in,set}$: 26 °C Number of previous time inputs				Testing $T_{in,set}$: 28 °C Number of previous time inputs				Testing $T_{in,set}$: 24 °C Number of previous time inputs			
	0	1	2	3	0	1	2	3	0	1	2	3
20 s	1.18	1.07	0.99	1.02	1.79	1.77	1.59	1.65	1.58	1.45	1.46	1.42
60 s	1.13	1.01	1.10	0.86	1.82	1.69	1.66	1.71	1.59	1.47	1.50	1.39
120 s	1.24	1.05	0.94	0.63	1.87	1.77	1.69	1.60	1.71	1.48	1.51	1.41
300 s	1.07	1.71	2.03	1.94	2.18	2.09	1.91	1.99	2.05	1.90	2.07	2.07
600 s	1.36	2.32	2.25	2.18	2.30	2.14	2.09	2.01	1.97	2.23	2.32	2.35

According to Table 6.2, it can be seen that if the sampling time stays within the order of the time constant of the system, approximately 20 – 40 s[85]. It is generally demonstrated that the inclusion of inputs from previous time steps provides more information and improves the accuracy of the testing results provided that the sampling time enables a sufficient resolution for capturing dynamic phenomena. When the network is trained without input values from previous time steps, the model recognizes only the relationships between current time temperatures $T(t)$ and cooling capacity $Q_e(t)$ and neglects the transient phenomena, such as those represented in Fig. 6.2(a). The reduced error by one additional input from the previous time step (for each temperature) is related to the gained ability of the network to relate the current time temperature to the slope of temperature in time $\frac{dT}{dt}$. The lower error (although with generally lower improvement) obtained with two additional inputs from the previous time steps is associated with the ability of approximating the slope $\frac{dT}{dt}$ and acceleration of temperature in time $\frac{d^2T}{dt^2}$, besides the current time input temperature. The effect of previous time step inputs on prediction during dynamic operation can be seen in Fig. 6.2(a).

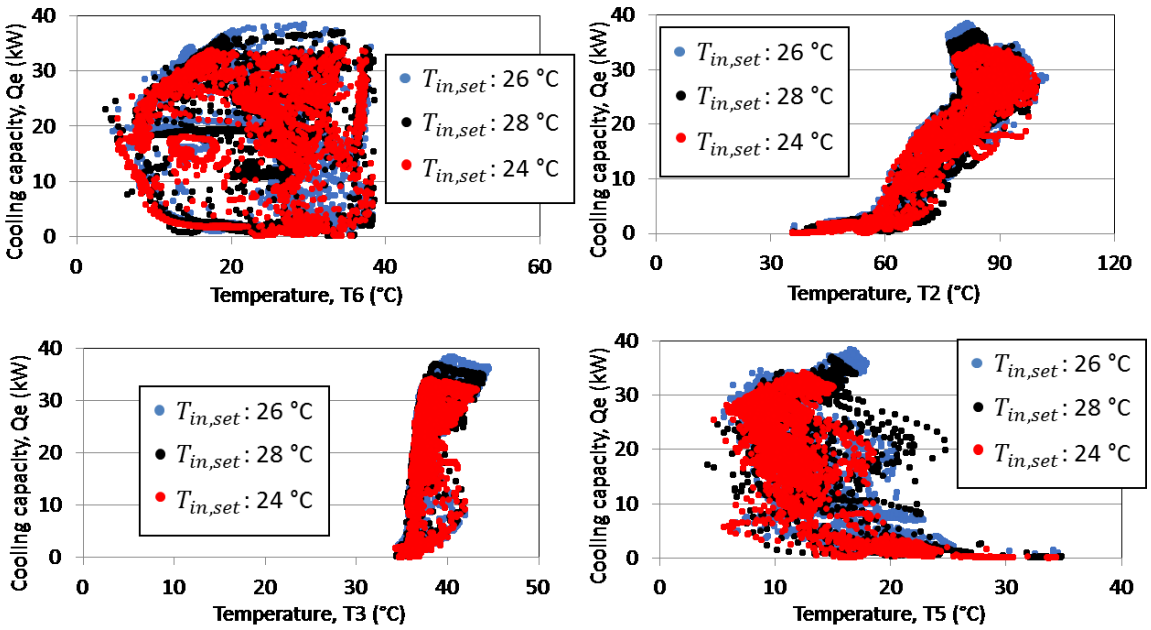

Fig. 6.1 Relationship between individual input and output at the same outdoor temperature and different indoor temperature setting

The degree of accuracy in the approximation of these dynamic features is related to the sampling time. Specifically, if the sampling time is too long, the approximation by a larger number of sparse data of the input values from previous time steps will actually lead to higher error. Additionally, it has been reported in literature[75] that the input values from three or more additional previous time steps generally do not bring a significant improvement to the prediction accuracy and,

contrarily, often tend to cause over-fitting in the testing phase due to data redundancy with respect to phenomena and characteristics not strongly related to the operation history.

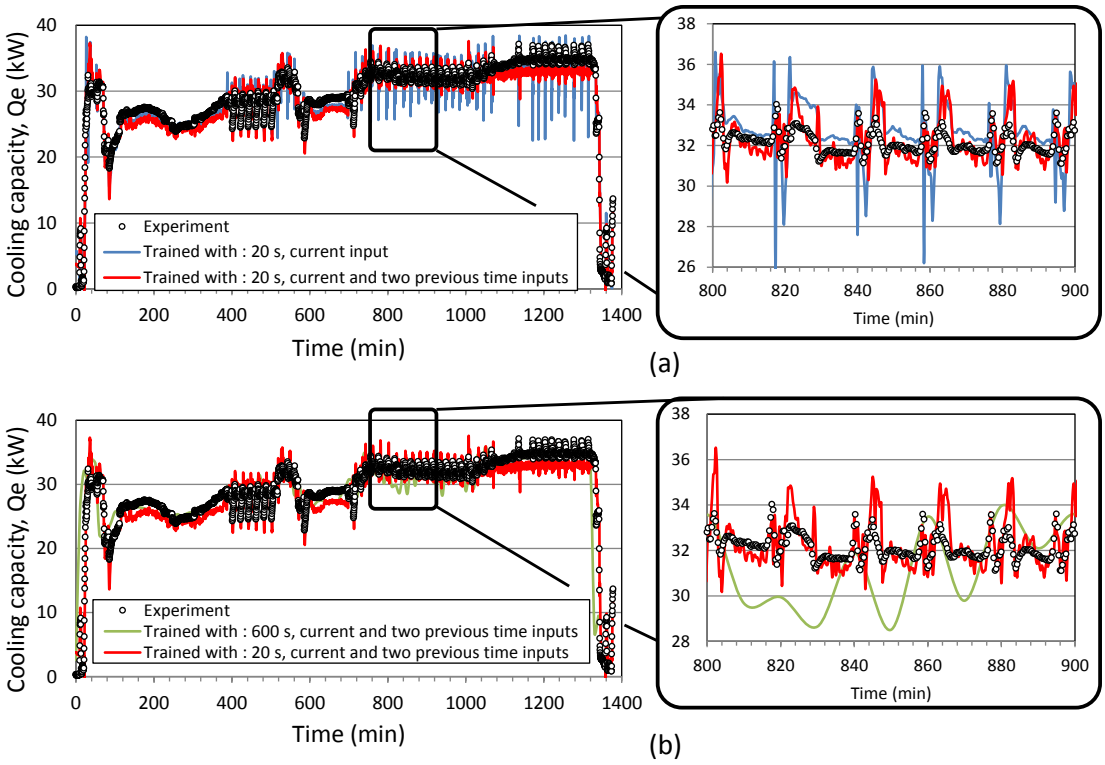

Fig. 6.2 Effect of (a) previous time step inputs and (b) sampling time on prediction accuracy

The effect of sampling time on prediction results can be clearly distinguished in Fig. 6.2(b). It is shown that the predicted cooling capacity by sampling time of 600 s deviates from the true values. In general, as a larger sampling time results in loss of resolution towards unsteady characteristics, the higher the sampling time is, the higher the error becomes. The differences in data characteristics among various sampling time are statistically observed via student's t-test[86] with confidence level of 95%, as demonstrated in Fig. 6.3. The P-values show how significant the difference in characteristic between 20 s sampling time data (population data) and 60 s, 120 s, 300 s, and 600 s sampling time data (sample data). As P-values are higher than 0.05, it indicates no substantial difference is recorded. However, as P-values tend to decrease when sampling time increases, the discrepancy on data characteristic relatively increases as sampling time gets higher.

Besides sampling time, the importance of the number of time delays considered for the input parameters also depends on the magnitude of temperature variations and the rate of variation. As the data are mostly unsteady, the effect of the input of temperatures from previous time steps is significant to capture the dynamic behavior of the cooling capacity, especially in transient condition. According to this investigation, an ANN structure with the current time input and two previous time

step inputs, along with sampling time of 20 s, is suggested for the prediction in the present work and is applied in the following feature analysis.

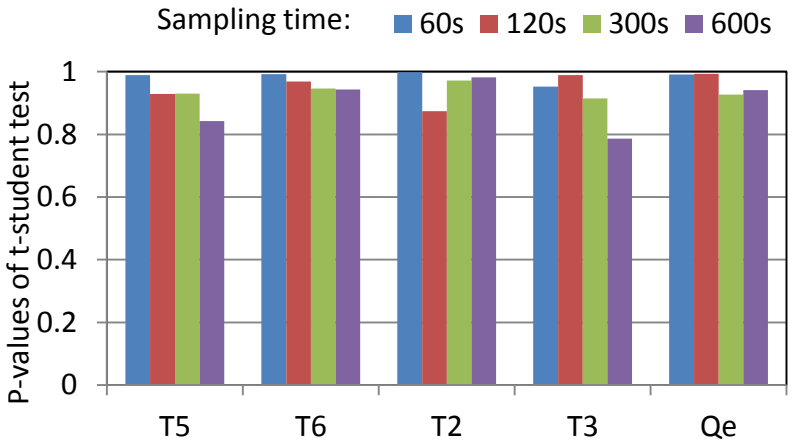

Fig. 6.3 P- values of student t-test under different sampling time (confidence level 95%)

6.2 Effect of number of training data

In actual operation, the cooling load varies according to the occupant behavior, operating devices, and weather conditions. As the data characteristics during the operation are mostly unsteady, the number of training data affects its variability and the generalization capability of the ANN model. The effect of number of training data is investigated by training the ANN model using data with a step load pattern (case 2) and testing the pre-trained ANN model on the data with a variable rate (case 1) and continuous decline (case 5) load pattern. The outdoor temperature is set at 35 °C for all conditions. The prediction data scenarios are provided in Table 6.3. The number of training data sets is varied as one set (case 2a), two sets (case 2a and 2b), and five sets (cases 2a, 2b, 2c, 2d, and 2e) to demonstrate the effect of data variability.

Table 6.3 Prediction data for number of training data analysis (adopted from Table 4.2)

Case	Load pattern	$T_{in,set}$ (°C)	$T_{out,set}$ (°C)	No. data points
1	Variable rate 0- 100%	26	35	1800
2a	Step load 0 - 100% (2h)	26	35	4140
2b	Step load 0 - 100% (1h)	26	35	2970
2c	Step load 0 - 70% (5h)	26	35	8280
2d	Step load 0 - 100% (5h)	24	35	9000
2e	Step load 0 - 100% (5h)	28	35	8280
5	Continuous decline	26	35	4500

The prediction results for training and testing are presented in Table 6.4. The errors for both testing cases decrease as more training data are included. It indicates that the additional data provide more variability to the training scenario and successfully increase the testing accuracy. The significant improvement is shown by the error discrepancy between the ANN model trained with one set (4140 data points) and five sets (32670 data points) of training data. The additional four-data sets used in training can reduce the RMSE by approximately 44.27% and 43.36% for the variable rate and continuous decline load patterns, respectively.

The prediction gap among various scenarios with different number of training data is depicted in Fig. 6.4, exemplifying that larger training data representations bring the testing prediction closer to the measured values. As the experimental scenarios are multiform and cover a wide range operation in the recorded characteristics, the additional training data improve the variability and are beneficial to increase the accuracy over the range of testing, without the occurrence of over-fitting. The results reveal that any cooling load patterns can be used to perform an effective training able to represent any variable operating condition as long as a wide range operation is covered with high variability.

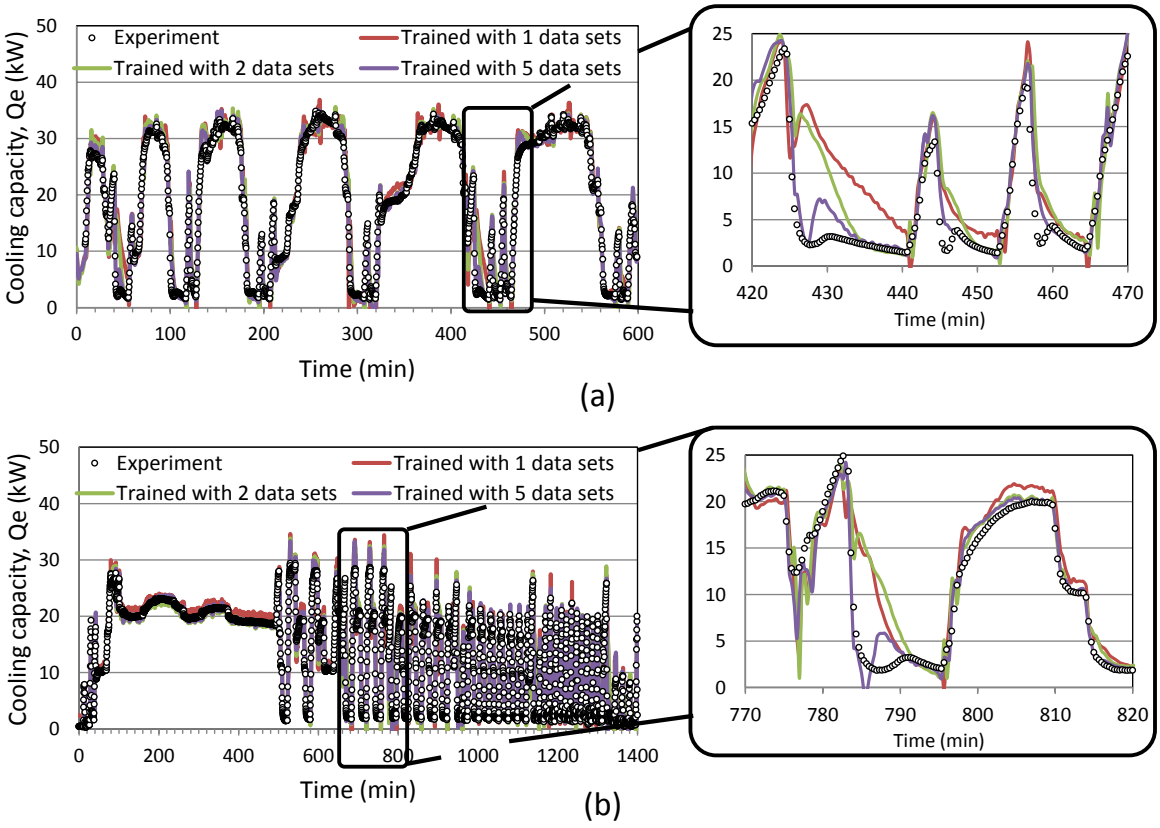

Fig. 6.4 Effect of number of training data on prediction accuracy: (a) variable rate (b) continuous decline load patterns

Table 6.4 Prediction results under different number of training data

Number of training data sets	RMSE of cooling capacity (kW)		
	(Training) Step load	(Testing) Variable rate load	(Testing) Continuous decline load
1	0.62	2.43	2.20
2	0.70	2.12	2.15
5	0.70	1.33	1.19

6.3 Effect of outdoor temperature

The effect of outdoor temperature in the generation of a proper training scenario for effective predictions is investigated by comparing different training data obtained under diverse outdoor temperature patterns. Four datasets with different patterns of outdoor temperature are considered (Table 6.4). The first three cases include data with constant outdoor temperature, at approximately 30 °C (case 7), 35 °C (case 2), and 40 °C (case 3); the fourth scenario features variable outdoor temperature (case 8), representing a daily variation during summer ranging from 30 to 40 °C. The indoor temperature is set at 26 °C and the cooling load is varied up to 100% for all corresponding cases. The training and testing accuracy of three different ANN models with various training data compositions is shown in Fig. 6.5. The empty markers show the training accuracy, while the full markers represent the testing accuracy.

Table 6.4 Prediction data for outdoor temperature analysis (adopted from Table 4.2)

Case	Load pattern	$T_{in,set}$ (℃)	$T_{out,set}$ (℃)	No. data points
7	Step load 0 - 100% (5h)	26	30	9000
2	Step load 0 - 70% (5h)	26	35	8280
3	Step load 0 - 100% (5h)	26	40	9000
8	West load 0 - 100%	26	30-40	21420

The first training scenario refers to a single data set with constant 30 °C outdoor temperature (case 7) for training and the other data are considered for testing. The results show large errors for testing accuracy with RMSE always higher than 5 kW for all testing data. The error increases as the difference in outdoor temperature between the training and testing data is higher. It indicates that the variation in outdoor temperature leads to the significant difference in data characteristics. According to Fig. 6.6, it can be observed that the change of outdoor temperature is highly associated with the outlet temperature of condenser. From a more detailed perspective, at the same capacity and indoor temperature a higher outdoor temperature leads to higher condensing

temperature, which, in turn, affects the heat transfer on the condenser side in terms of inlet pressure and the degree of sub cooling at the condenser outlet. As the training data are limited to one constant outdoor temperature, the error becomes higher when applied on the other outdoor temperature conditions.

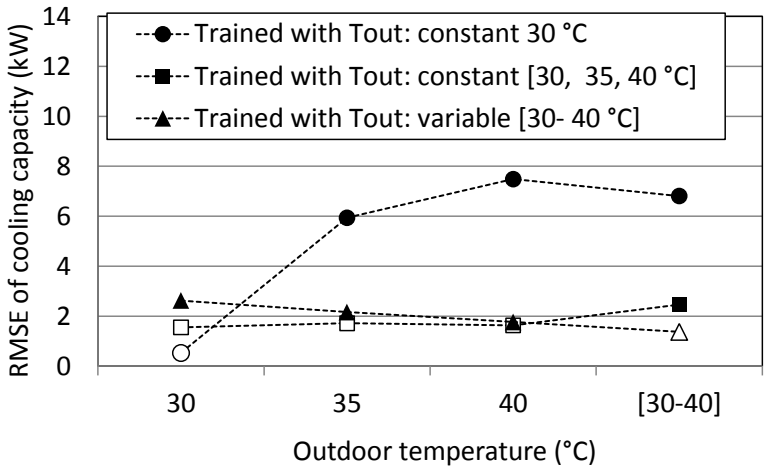

Fig. 6.5 Prediction results under various outdoor temperatures in relation to different sets of training data (empty and full markers show training and testing accuracy, respectively).

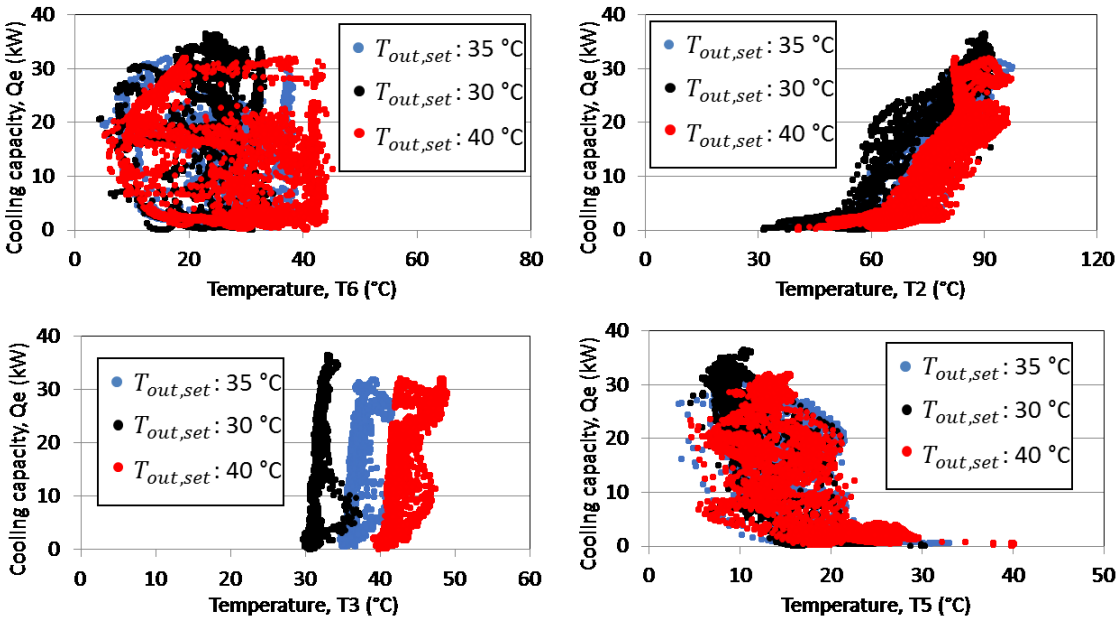

Fig. 6.6 Relationship between individual input and output at the same indoor temperature and different outdoor temperature

A second training scenario includes all three data sets with constant outdoor temperature (case 7, 2, and 3). The testing is applied only to data with variable temperature (case 8). The additional training data aims to extend the data coverage in a wider range. The results show that the error on testing data becomes lower, dropping drastically by approximately 62.87%, as more data that cover outdoor temperatures of 35 and 40 °C are included for training. This indicates that wider outdoor temperature ranges in the training data are significant to improve the prediction accuracy.

The last training scenario investigates the effect of a variable outdoor temperature pattern on the training data sets. The data generated with variable outdoor temperature (case 8) are used for training and the other three data sets with constant outdoor temperatures (case 7, 2, and 3) are used for testing. Even though the ambient temperature patterns in the training and testing data have fundamentally different patterns (constant and variable), the ANN model can successfully predict the cooling capacity owing to the sufficient data coverage and higher variability. Accordingly, it is confirmed that such training data with high variability over a wide range are beneficial for effective training.

6.4 Prediction on various cases using variable outdoor temperature and extended training scenario

As demonstrated in the previous section, the outdoor temperature variation significantly affects the data characteristics. Moreover, the number of data is very influential on data variability owing to the unsteady operation. The variation of indoor temperature between 24, 26, and 28 °C shows limited effect on the four input refrigerant temperatures as the controller has poor accuracy, consequently the indoor temperature fluctuation on various set points are identical. Therefore, a large number of data with variable outdoor temperature become a necessity for an effective training.

In this section, a large number of data with high variability, which include constant and variable outdoor temperature adopted from Table 4.2, are used for prediction. The representative data obtained from all cases are selected for training (24% of all data) and the others are used for testing (76% of all data). It should be noted that the training and testing data are totally different. The training data are selected to provide the wide range of operating conditions considering indoor temperature, outdoor temperature, and cooling load variations. The ANN model is developed with current and two previous time step inputs and sampling time of 20 s.

The representative testing results in various operating conditions are demonstrated in Figs. 6.7 to 6.12. The predicted cooling capacities by ANN model seem to follow the actual values precisely with high accuracy. It shows that the ANN model could successfully predict the data while keeping relative error mostly below 5%. This verification proves that the ANN model with four selected temperature inputs can be applied to predict the actual dynamic cooling capacity in various operating condition. For the most cases in which the sufficient data are available, ANN model can predict the system performance accurately.

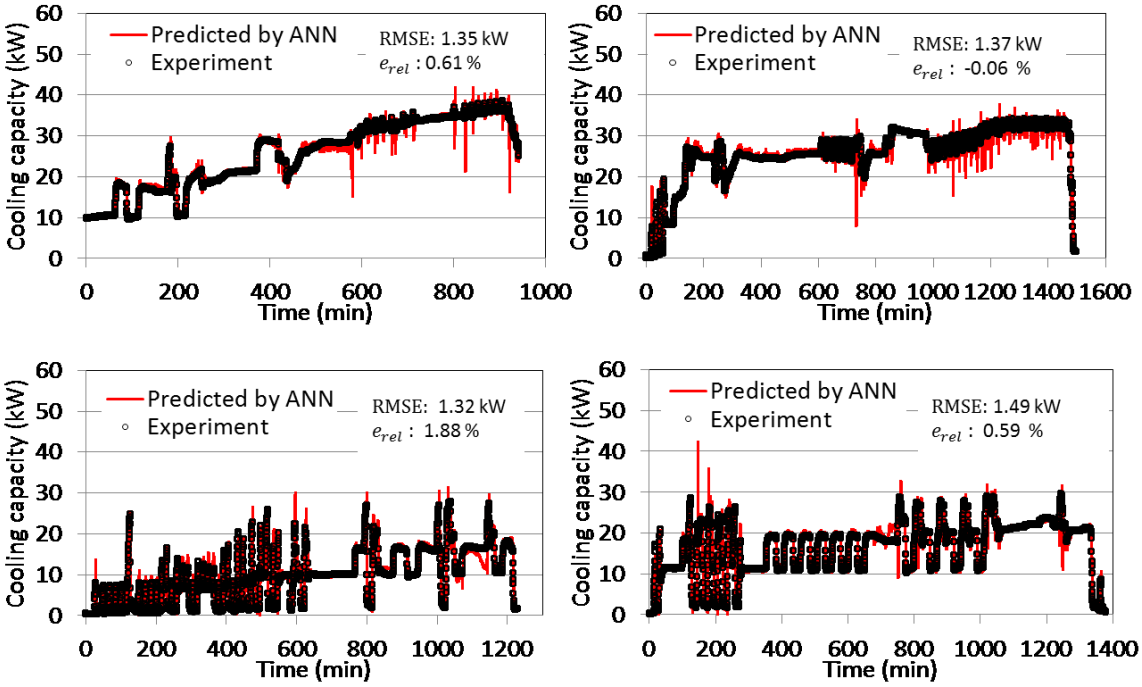

Fig. 6.7 Performance prediction with constant T_{out}: 35 °C (case 2, Table 4.2)

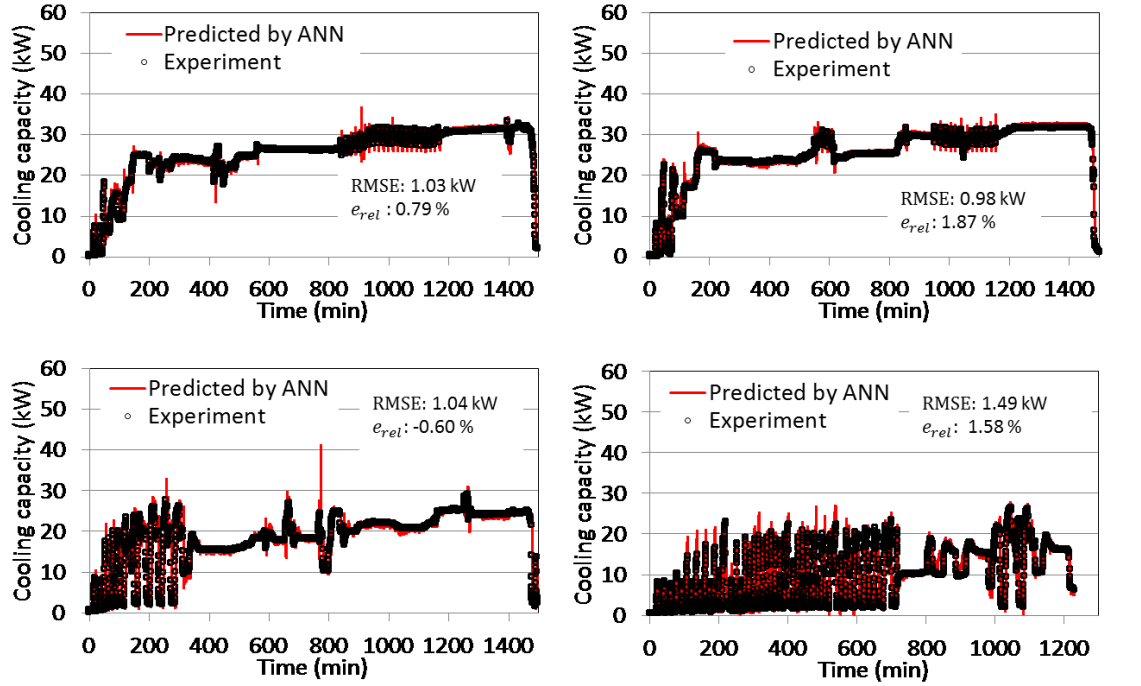

Fig. 6.8 Performance prediction with constant T_{out}: 40 °C (case 3, Table 4.2)

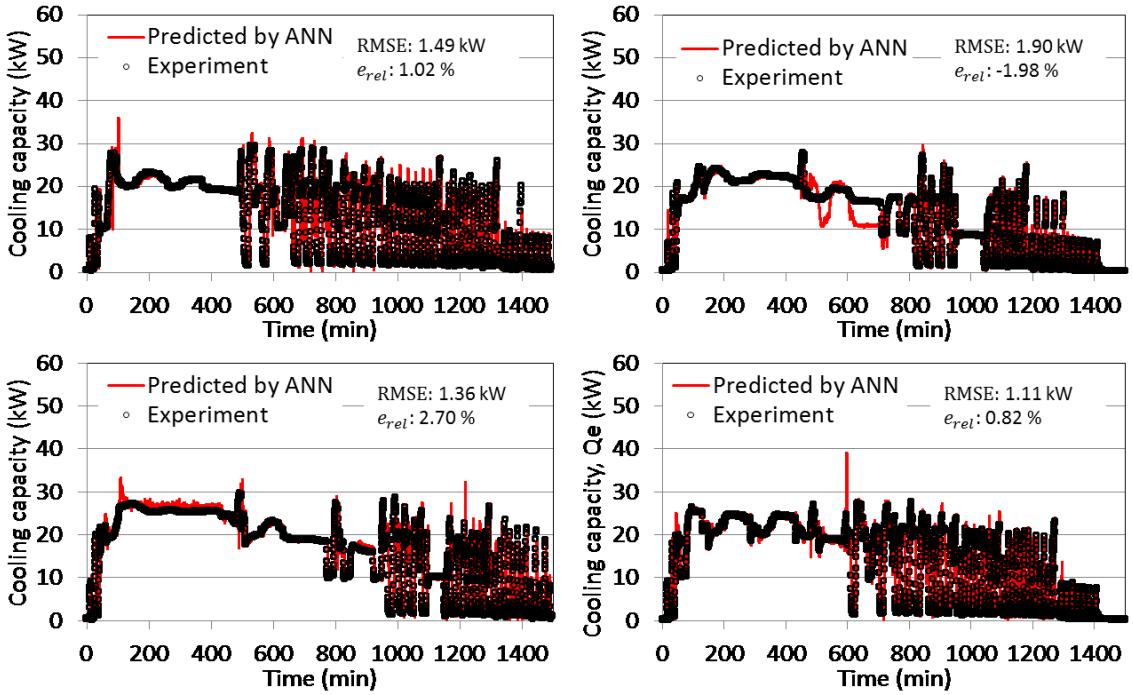

Fig. 6.9 Performance prediction with continuous decline load pattern (case 5, Table 4.2)

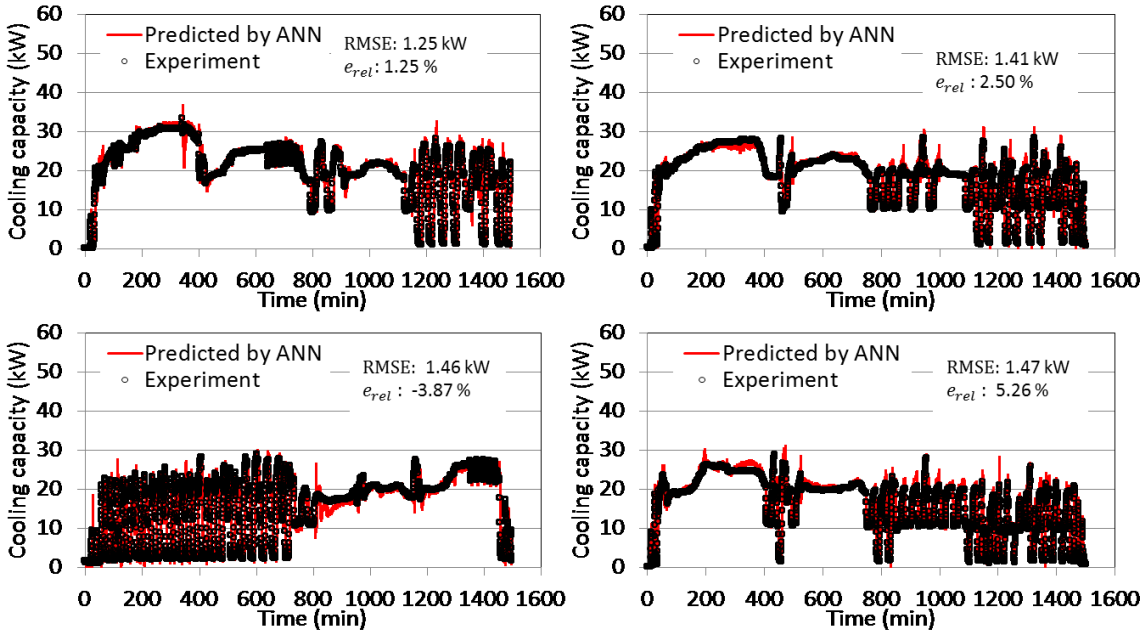

Fig. 6.10 Performance prediction with west load pattern (case 8, Table 4.2)

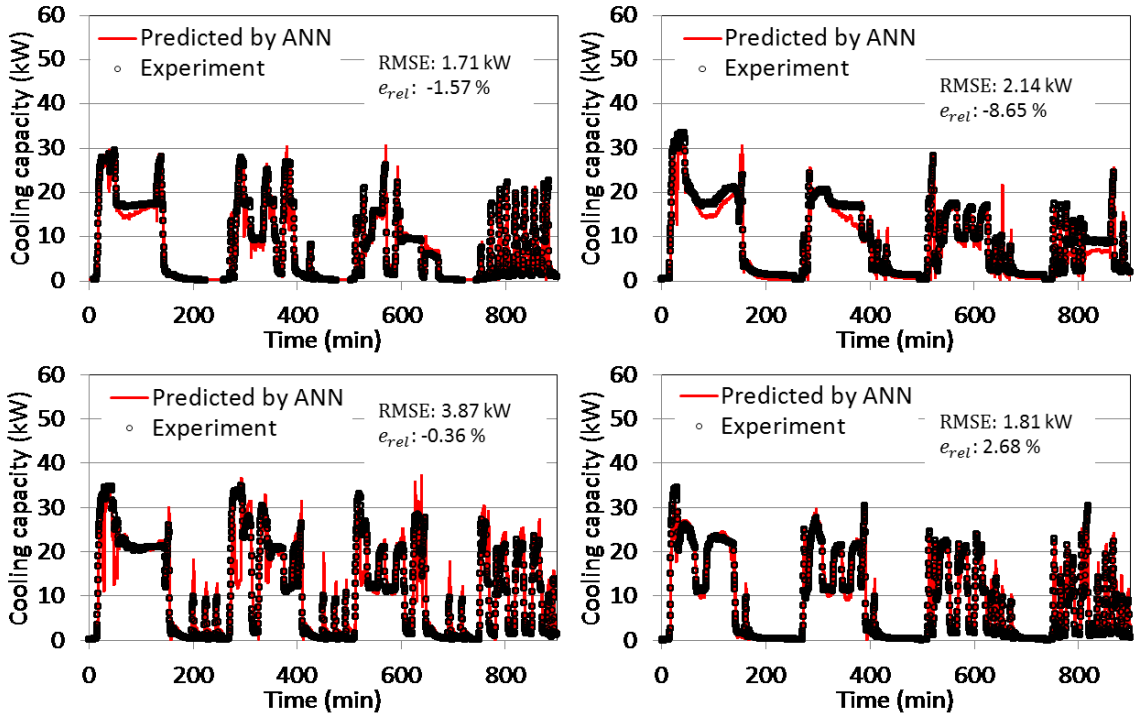

Fig. 6.11 Performance prediction with east load pattern (case 9, Table 4.2)

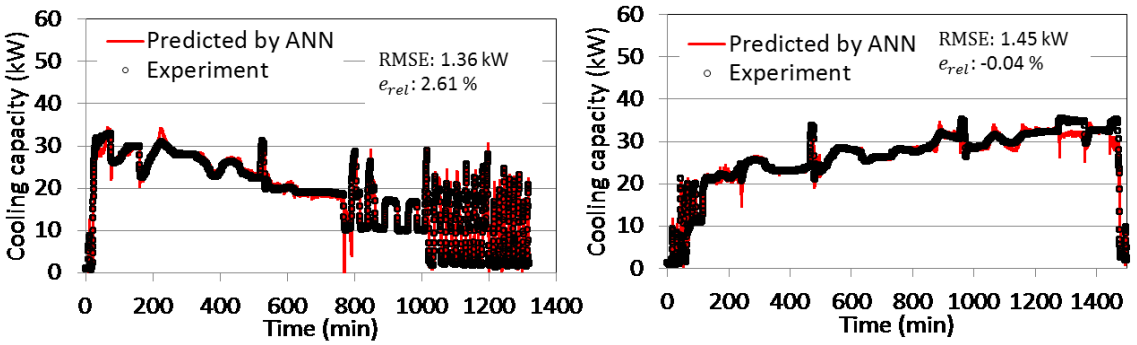

Fig. 6.12 Performance prediction with constant T_{out}: 30 °C (case 7, Table 4.2)

6.5 Advanced cooling capacity prediction on different system

In section 3.3, the performance prediction on different system has been carried out for input selection, which relies on the training and testing data obtained from simulations. It proved that the refrigerant temperatures are appropriate for use as input of performance prediction. Subsequently the prediction relying on the combined simulation and experimental data based has been established

in Chapter 5. The ANN model was trained using simulation data and applied for testing on experimental data. The results revealed that the ANN models have successfully predicted on smooth data characteristics. Nonetheless, it shows poor accuracy while applying on high fluctuation testing data characteristics since this kinds of data behavior are not available in present simulation training data.

According to the investigation presented in Chapter 5, the ANN model trained with simulation data only has lower accuracy when predicting on intermittent (on/off) or strongly dynamic experimental data. This is due to the lack of information provided by the simulation data during such circumstances. As previously demonstrated, such strongly unsteady experimental data have features that, at present, cannot be replicated by the numerical simulator developed. Accordingly, in order to demonstrate the possibility of higher accuracy prediction results by relying on the suggested method, the prediction of air conditioner performance on different systems is investigated by using experimental data for both training and testing.

Table 6.5 Prediction scenario for different system (experiment)

System	$T_{in,set}$ (°C)	$T_{out,set}$ (°C)	Training	Testing
Experiment VRF 33.5 kW	Constant 26, 28	Constant 30	●	
	Constant 24, 26, 28	Constant 40	●	
Experiment VRF 28 kW	Constant 24	Constant 30		●
	Constant 28	Constant 40		●

The prediction scenario is as listed in Table 6.5. The training and testing data are generated from experimental facility using the VRF system of 33.5 kW and 28 kW, respectively. The testing data are generated with constant indoor and outdoor temperature set in two different conditions namely, 24/30 °C and 28/40 °C. In order to provide the sufficient data for training, the system on 33.5 kW is run with more data variation with outdoor temperature set as the same with training. The cooling load pattern from 0 to 100% is introduced in both systems.

Two ANN models are trained with different outdoor temperature (30 and 40 °C). It aims to provide the training and testing data with the same operating conditions. The prediction results for both testing data are demonstrated in Figs. 6.13 and 6.14, respectively. The results yield good agreement between predicted and corresponding values with RMSE and e_{rel} of 2.10 kW and 2.36% for the data with T_{out}: 30 °C; and 2.75 kW and 9.73% for the data with T_{out}: 40 °C. The inclusion of intermittent data characteristics in the training improves the data variability and generalization ability of the ANN model. This result suggests that the ANN model could be applied to predict the performance of different systems using sufficient training data from a reference system.

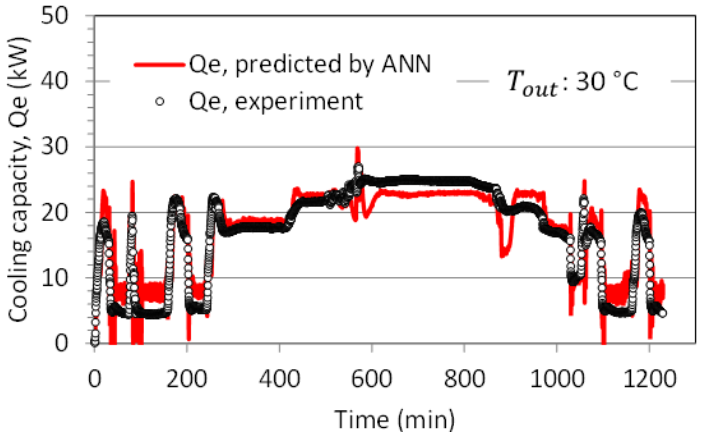

Fig. 6.13 Prediction results on different system at T_{out} : 30 °C
(Training with exp. 33.5 kW and Testing on 28 kW)

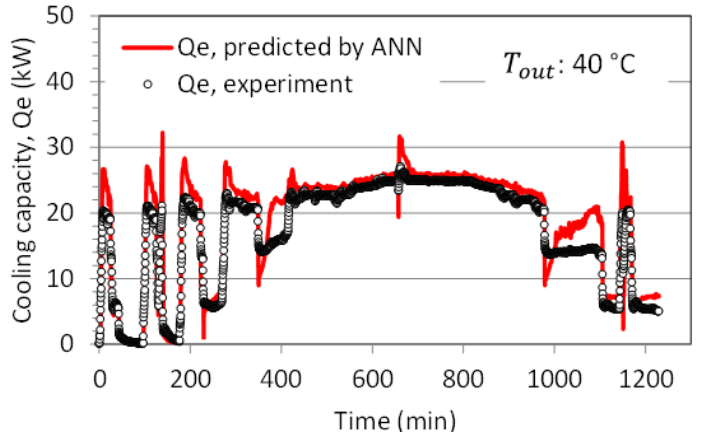

Fig. 6.14 Prediction results on different system at T_{out} : 40 °C
(Training with exp. 33.5 kW and Testing on 28 kW)

7. Conclusion and future prospects

Applicability of ANN model to predict the cooling capacity by employing four refrigerant temperatures representing air conditioning cycle measured on outdoor unit has been comprehensively investigated. This represents a performance prediction method relying on limited information, being non-intrusive and low-cost, and having high accuracy, which can be implemented in operative systems. The adoption of refrigerant-side properties is based on the hypothesis that the identification of the refrigerant cycle, rather than air-side properties or manipulated parameters (e.g., valve opening and compressor speed), could provide a generalizable representation, which could be expanded to other systems in addition to the one referenced during the ANN training.

7.1 Conclusions

The main conclusions of present work are summarized as follows:

- Input-output data for training and testing collected in experimental facility have extensively represented the performance of actual systems and provided useful information on actual data characteristics.

- Four corresponding refrigerant temperatures are the most representative inputs for performance prediction as they are inexpensive and non-intrusive to measure, scalable for different system application, and represent the system cycle.

- It has been demonstrated that, by adopting the suggested ANN modeling method, a generalizable ANN model for AC performance prediction can be developed. Additionally, by relying on a modular numerical simulator, the flexibility and generality of its fundamental physical model provides a nearly infinite range of possible training conditions and system configurations.

- From the analysis of the recorded data, during steady operation, the possibility of very close relationship between input refrigerant temperature and cooling capacity has been suggested. During unsteady and on–off operation, as the measured temperatures and cooling capacity has less strong relationship, the inclusion of time characteristics for representing these operative conditions, such as temperature rate and rate of change, besides the magnitude of cooling capacity, has been proposed. Specifically, the inclusion of a certain number of input values from previous time steps has been investigated.

- Additional data, which provide more variability to the training scenario especially during intermittent and unsteady operation, successfully increase the testing accuracy.

- It has been confirmed that training data with high outdoor temperature and cooling load variability over a wide range are beneficial for effective training.

- The results reveal that, if proper training scenarios are conceived, the ANN model can successfully predict the cooling capacity of an AC system during on–off, continuous unsteady, and steady operation, using four refrigerant temperature inputs, regardless of different manufacture and nominal rated capacity, while keeping the relative error mostly below 5%.

As the performance of ANN model is directly related to how representative the data used for the training are, a broader spectrum of training data, comprehensively covering actual dynamic system behavior and operating conditions (including outdoor temperature fluctuation, load variation, and indoor temperature change), would be beneficial for improving the reliability of the prediction.

7.2 Future prospects

Performance prediction of AC system presented in present work still remains several issues that should be solved for future study as follows:

- The inclusion of intermittent data characteristics for ANN training is necessary to capture the dynamic behavior of actual system. The reliable control on AC system simulator should be developed to provide the simulation data characteristics similar to the real operation condition especially on intermittent behavior.

- The ideal training data pattern that are able to cover all data characteristics generated by various control design need to observe.

- The prediction on different system should be expanded for many various operating conditions including variation of indoor temperature, outdoor temperature, and cooling load which represent the actual operation.

- System characterization for the new system with different nominal capacity and manufacture needs to be investigated and analyzed comprehensively to understand the gap between one and the other systems.

References

1. Electricity Final Cnsumption by Sector [https://www.iea.org/data-and-statistics?country=WORLD&fuel=Energy%20consumption&indicator=ElecConsBySector]
2. Chua KJ, Chou SK, Yang WM, Yan J: Achieving better energy-efficient air conditioning – A review of technologies and strategies. *Applied Energy* 2013, 104:87-104.
3. Pérez-Lombard L, Ortiz J, Pout C: A review on buildings energy consumption information. *Energy and Buildings* 2008, 40(3):394-398.
4. Ruparathna R, Hewage K, Sadiq R: Improving the energy efficiency of the existing building stock: A critical review of commercial and institutional buildings. *Renewable and Sustainable Energy Reviews* 2016, 53:1032-1045.
5. Klepeis NE, Nelson, W.C., Ott, W.R., Robinson, J.P., Tsang, A.M., Switzer, P., Behar, J.V., Hern, S.C., Engelmann, W.H.: The National Human Activity Pattern Survey (NHAPS): a resource for assessing exposure to environmental pollutants. *J Expo Anal Environ Epidemiol* 2001, 11(3):231-352.
6. Geng Y, Ji W, Lin B, Zhu Y: The impact of thermal environment on occupant IEQ perception and productivity. *Building and Environment* 2017, 121:158-167.
7. The Future of Cooling [https://www.iea.org/reports/the-future-of-cooling]
8. Ahn B-L, Yoo S, Kim J, Jeong H, Leigh S-B, Jang C-Y: Thermal management of LED lighting integrated with HVAC systems in office buildings. *Energy and Buildings* 2016, 127:1159-1170.
9. Scott MJ, Huang, Y.J., Annex, A.: Technical note: methods for estimating energy consumption in buildings in effects of climate change on energy production and use in the United States. In: *A Report by the US climate change science program and the subcommittee on global change research.* Washington (DC); 2007.
10. Lubis A, Jeong J, Saito K, Giannetti N, Yabase H, Idrus Alhamid M, Nasruddin: Solar-assisted single-double-effect absorption chiller for use in Asian tropical climates. *Renewable Energy* 2016, 99:825-835.
11. Xu S, Niu J, Cui Z, Ma G: Experimental research on vapor-injected heat pump using injection subcooling. *Applied Thermal Engineering* 2018, 136:674-681.
12. Tang R, Wang S, Shan K, Cheung H: Optimal control strategy of central air-conditioning systems of buildings at morning start period for enhanced energy efficiency and peak demand limiting. *Energy* 2018, 151:771-781.
13. Li N, Xia L, Shiming D, Xu X, Chan M-Y: Dynamic modeling and control of a direct expansion air conditioning system using artificial neural network. *Applied Energy* 2012, 91(1):290-300.
14. Duprez M-E, Dumont E, Frère M: Modeling of scroll compressors – Improvements. *International Journal of Refrigeration* 2010, 33(4):721-728.
15. Li Z, Aute V, Ling J: Tube-fin heat exchanger circuitry optimization using integer permutation based Genetic Algorithm. *International Journal of Refrigeration* 2019, 103:135-144.

16. Lazzarin R, Noro M: Experimental comparison of electronic and thermostatic expansion valves performances in an air conditioning plant. *International Journal of Refrigeration* 2008, 31(1):113-118.
17. Sholahudin, Ohno K, Giannetti N, Yamaguchi S, Saito K: Dynamic modeling of room temperature and thermodynamic efficiency for direct expansion air conditioning systems using Bayesian neural network. *Applied Thermal Engineering* 2019, 158:113809.
18. Nasruddin, Sholahudin S, Giannetti N, Arnas: Optimization of a cascade refrigeration system using refrigerant C3H8 in high temperature circuits (HTC) and a mixture of C2H6/CO2 in low temperature circuits (LTC). *Applied Thermal Engineering* 2016, 104:96-103.
19. Matsumoto K, Ohno K, Yamaguchi S, Saito K: Numerical analysis of control characteristics of variable refrigerant flow heat-pump systems focusing on the effect of expansion valve and indoor fan. *International Journal of Refrigeration* 2019, 99:440-452.
20. Park C, Lee H, Hwang Y, Radermacher R: Recent advances in vapor compression cycle technologies. *International Journal of Refrigeration* 2015, 60:118-134.
21. Nishijima D: Product lifetime, energy efficiency and climate change: A case study of air conditioners in Japan. *Journal of environmental management* 2016, 181:582-589.
22. Jain N, Alleyne A: Exergy-based optimal control of a vapor compression system. *Energy Conversion and Management* 2015, 92:353-365.
23. Miyaoka Y: Study on energy saving of air conditioning in the mass merchandising store. Mie University; 2017.
24. Qureshi BA, Zubair SM: Performance degradation of a vapor compression refrigeration system under fouled conditions. *International Journal of Refrigeration* 2011, 34(4):1016-1027.
25. Qureshi BA, Zubair SM: Predicting the impact of heat exchanger fouling in refrigeration systems. *International Journal of Refrigeration* 2014, 44:116-124.
26. Qureshi BA, Zubair SM: The impact of fouling on the condenser of a vapor compression refrigeration system: An experimental observation. *International Journal of Refrigeration* 2014, 38:260-266.
27. Yoo JW, Hong SB, Kim MS: Refrigerant leakage detection in an EEV installed residential air conditioner with limited sensor installations. *International Journal of Refrigeration* 2017, 78:157-165.
28. Kim W, Braun JE: Evaluation of the impacts of refrigerant charge on air conditioner and heat pump performance. *International Journal of Refrigeration* 2012, 35(7):1805-1814.
29. Fan C, Ding Y: Cooling load prediction and optimal operation of HVAC systems using a multiple nonlinear regression model. *Energy and Buildings* 2019, 197:7-17.
30. Kim J, Hong T, Jeong J, Lee M, Lee M, Jeong K, Koo C, Jeong J: Establishment of an optimal occupant behavior considering the energy consumption and indoor environmental quality by region. *Applied Energy* 2017, 204:1431-1443.

31. Gaetani I, Hoes P-J, Hensen JLM: Estimating the influence of occupant behavior on building heating and cooling energy in one simulation run. *Applied Energy* 2018, 223:159-171.
32. Hoes P, Hensen JLM, Loomans MGLC, de Vries B, Bourgeois D: User behavior in whole building simulation. *Energy and Buildings* 2009, 41(3):295-302.
33. Yau YH, Pean HL: The performance study of a split type air conditioning system in the tropics, as affected by weather. *Energy and Buildings* 2014, 72:1-7.
34. Yin X, Wang X, Li S, Cai W: Energy-efficiency-oriented cascade control for vapor compression refrigeration cycle systems. *Energy* 2016, 116:1006-1019.
35. Type of air conditioning plant [https://hmhub.me/types-of-air-conditioning-plants/]
36. Luo B, Zou P: Performance analysis of different single stage advanced vapor compression cycles and refrigerants for high temperature heat pumps. *International Journal of Refrigeration* 2019, 104:246-258.
37. Cecchinato L, Mancini F: An intrinsically mass conservative switched evaporator model adopting the moving-boundary method. *International Journal of Refrigeration* 2012, 35(2):349-364.
38. Zhou S, Gong L, Liu X, Shen S: Mathematical modeling and performance analysis for multi-effect evaporation/multi-effect evaporation with thermal vapor compression desalination system. *Applied Thermal Engineering* 2019, 159:113759.
39. Min Y, Chen Y, Yang H: A statistical modeling approach on the performance prediction of indirect evaporative cooling energy recovery systems. *Applied Energy* 2019, 255:113832.
40. Sholahudin, Giannetti N, Yamaguchi S, Saito K, Miyaoka Y, Tanaka K, Ogami H: Experimental implementation of artificial neural network for cost effective and non-intrusive performance estimation of air conditioning systems. *Applied Thermal Engineering* 2020, 181:115985.
41. Li B, Alleyne AG: A dynamic model of a vapor compression cycle with shut-down and start-up operations. *International Journal of Refrigeration* 2010, 33(3):538-552.
42. Kumar R, Aggarwal RK, Sharma JD: Energy analysis of a building using artificial neural network: A review. *Energy and Buildings* 2013, 65:352-358.
43. Mohanraj M, Jayaraj S, Muraleedharan C: Applications of artificial neural networks for refrigeration, air-conditioning and heat pump systems—A review. *Renewable and Sustainable Energy Reviews* 2012, 16(2):1340-1358.
44. Sholahudin S, Han H: Heating Load Predictions using The Static Neural Networks Method. *International Journal of Technology* 2015, 6(6):946.
45. Sholahudin S, Han H: Simplified dynamic neural network model to predict heating load of a building using Taguchi method. *Energy* 2016, 115:1672-1678.
46. Ding Y, Zhang Q, Yuan T, Yang F: Effect of input variables on cooling load prediction accuracy of an office building. *Applied Thermal Engineering* 2018, 128:225-234.

47. Nasruddin, Sholahudin, Idrus Alhamid M, Saito K: Hot water temperature prediction using a dynamic neural network for absorption chiller application in Indonesia. *Sustainable Energy Technologies and Assessments* 2018, 30:114-120.
48. Nasruddin, Aisyah N, Alhamid MI, Saha BB, Sholahudin S, Lubis A: Solar absorption chiller performance prediction based on the selection of principal component analysis. *Case Studies in Thermal Engineering* 2019, 13:100391.
49. Nasruddin, Sholahudin, Satrio P, Mahlia TMI, Giannetti N, Saito K: Optimization of HVAC system energy consumption in a building using artificial neural network and multi-objective genetic algorithm. *Sustainable Energy Technologies and Assessments* 2019, 35:48-57.
50. Kamar HM, Ahmad R, Kamsah NB, Mohamad Mustafa AF: Artificial neural networks for automotive air-conditioning systems performance prediction. *Applied Thermal Engineering* 2013, 50(1):63-70.
51. Tian Z, Qian C, Gu B, Yang L, Liu F: Electric vehicle air conditioning system performance prediction based on artificial neural network. *Applied Thermal Engineering* 2015, 89:101-114.
52. Atik K, Aktaş A, Deniz E: Performance parameters estimation of MAC by using artificial neural network. *Expert Systems with Applications* 2010, 37(7):5436-5442.
53. Wu J, Lu B, Liang Z: Performance Prediction of Room Air Conditioners and Optimization of Control Strategy for Energy Conservation. *Heat Transfer Engineering* 2017, 39(17-18):1616-1626.
54. Vinther K, Rasmussen H, Izadi-Zamanabadi R, Stoustrup J: Single temperature sensor superheat control using a novel maximum slope-seeking method. *International Journal of Refrigeration* 2013, 36(3):1118-1129.
55. Ohno K: Construction of General PurposeEnergy System Simulator and Global Simulation of Heat Pump. *Doctoral Thesis.* Waseda University: Waseda University; 2013.
56. Boeng J, Melo C: An innovative charge optimization process for capillary tube based cooling systems. *International Journal of Refrigeration* 2020, 118:202-209.
57. Eames IW, Milazzo A, Maidment GG: Modelling thermostatic expansion valves. *International Journal of Refrigeration* 2014, 38:189-197.
58. Knabben FT, Ronzoni AF, Hermes CJL: Application of electronic expansion valves in domestic refrigerators. *International Journal of Refrigeration* 2020, 119:227-237.
59. Knabben FT, Melo C, Hermes CJL: A study of flow characteristics of electronic expansion valves for household refrigeration applications. *International Journal of Refrigeration* 2020, 113:1-9.
60. Jackson B. Marcinichen JBM: Comparative Analysis Between a Capillary Tube and an Electronic Expansion Valve in a Household Refrigerator. In: *International Refrigeration and Air Conditioning Conference.* Purdue University: Purdue e-Pubs; 2006.

61. Sarfraz O, Bach CK, Bradshaw CR: Reduced order modeling for multi-circuit fin-and-tube heat exchangers with multiple identical circuit types. *International Journal of Refrigeration* 2019, 106:236-247.
62. Chisholm D: A theoretical basis for the Lockhart-Martinelli correlation for two-phase flow. *International Journal of Heat and Mass Transfer* 1967, 10:1767-1778.
63. JSME: JSME Text Series Heat Transfer Engineering. In. Edited by Engineers JSoM; 2005: 83.
64. JSME: Revised Gas-Liquid Two-Phase Flow Technology Handbook: Corona Publishing Co., Ltd; 2006.
65. Holman JP: Heat Transfer (10th edition). New York: McGraw-Hill; 2010.
66. Yoshida SN, K., Matsunaga, T., Nakata, H. : 冷媒の水平蒸発管内熱伝達に関する研究 "Study on Heat Transfer in Horizontal Evaporation Pipe of Refrigerant". *Refrigeration* 1983, 58(666):331-338.
67. Nozu S, Honda, H., Fuji., S.: 過熱蒸気の水平管内凝縮－熱伝達と圧力効果の式の提案 ― "Condensation of superheated steam in a horizontal tube-Proposal of formula for heat transfer and pressure effect". *Refrigeration* 1983, 58(669):659-668.
68. Fujii MaS, H: 低レイノルズ数域のプレートフィンチューブ熱交換器の性能(第 3 報, 性能の統一的整理) "Performance of Plate Fin Tube Heat Exchangers in the Low Reynolds Number Region (3rd Report, Unified Performance Arrangement)". In: *Proceedings of the Japan Society of Mechanical Engineers (B): 1987*; 1987: 1767-1772.
69. Ohno K, Saito, K., Yamaguchi, S., Kishimoto, T., Matsumoto, K.: Intermittent driving simulation of compression type heat pump- 1st report: Mathematical model and simulation of single-stage vapor compression type heat pump. *Transactions of the JASRAE* 2013, 30(2):107-122.
70. Ogata K: Modern Control Engineering: Prentice Hall; 2010.
71. Jani DB, Mishra M, Sahoo PK: Application of artificial neural network for predicting performance of solid desiccant cooling systems – A review. *Renewable and Sustainable Energy Reviews* 2017, 80:352-366.
72. Jiao J, Zhao M, Lin J, Liang K: A comprehensive review on convolutional neural network in machine fault diagnosis. *Neurocomputing* 2020, 417:36-63.
73. Mohanraj M, Jayaraj S, Muraleedharan C: Applications of artificial neural networks for thermal analysis of heat exchangers – A review. *International Journal of Thermal Sciences* 2015, 90:150-172.
74. Papantoniou S, Kolokotsa D-D: Prediction of outdoor air temperature using neural networks: Application in 4 European cities. *Energy and Buildings* 2016, 114:72-79.
75. Ng BC, Darus IZM, Jamaluddin H, Kamar HM: Application of adaptive neural predictive control for an automotive air conditioning system. *Applied Thermal Engineering* 2014, 73(1):1244-1254.
76. Martin T. Hagan HBD, Mark Hudson Beale, Orlando De Jesús: Neural Network Design 2nd Edition.

77. Heydecker BGaW, J.: Identification of Sites for Road Accident Remedial Work by Bayesian Statistical Methods: An Example of Uncertain Inference. *Advances in Engineering Software* 2001, 32:859-869.
78. Urresti A, Campos-Celador A, Sala JM: Dynamic neural networks to analyze the behavior of phase change materials embedded in building envelopes. *Applied Thermal Engineering* 2019, 158:113783.
79. Joudi KA, Al-Amir QR: Experimental Assessment of residential split type air-conditioning systems using alternative refrigerants to R-22 at high ambient temperatures. *Energy Conversion and Management* 2014, 86:496-506.
80. Hernandez AC, Fumo N: A review of variable refrigerant flow HVAC system components for residential application. *International Journal of Refrigeration* 2020, 110:47-57.
81. Norgaard M: Neural Networks for Modelling and Control of Dynamic Systems: Springer; 2001.
82. Jayalakshmi TaS, A.: Statistical Normalization and Back Propagation for Classification. *International Journal of Computer Theory and Engineering* 2011, 3(1):1793-8201.
83. Testing facility [http://www.jatl.or.jp/en/testing-facilities.html]
84. Li X, Deng Z: Identification of Dynamic Loads Based on Second-Order Taylor-Series Expansion Method. *Shock and Vibration* 2016, 2016:1-9.
85. Coster: A Guide to Understanding HVAC Components and Control Systems In.; 2020.
86. Feng Y-c, Huang Y-c, Ma X-m: The application of Student's t -test in internal quality control of clinical laboratory. *Frontiers in Laboratory Medicine* 2017, 1(3):125-128.

Appendix

A.1 Prediction results of ANN model trained with the same system of 33.5 kW (various operating conditions)

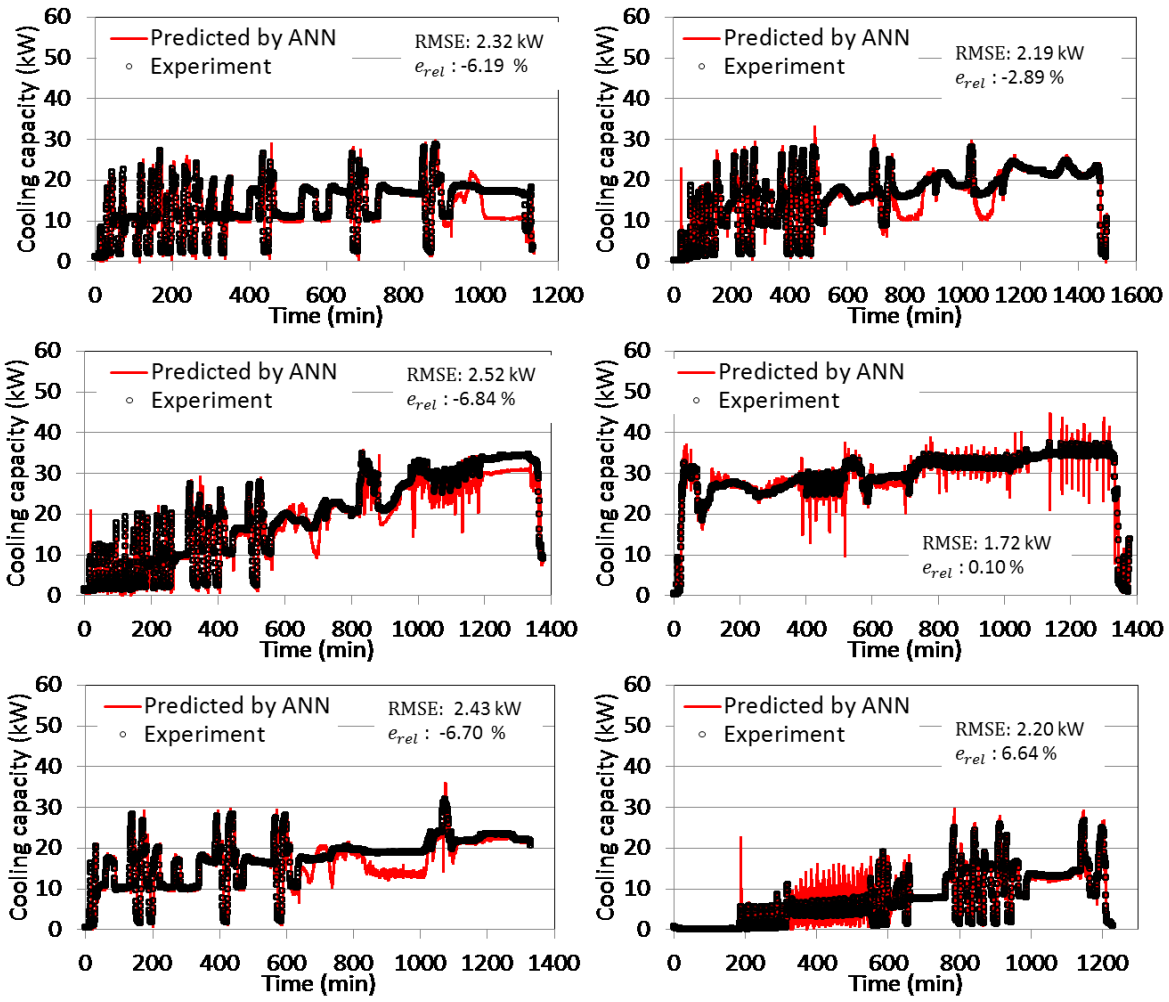

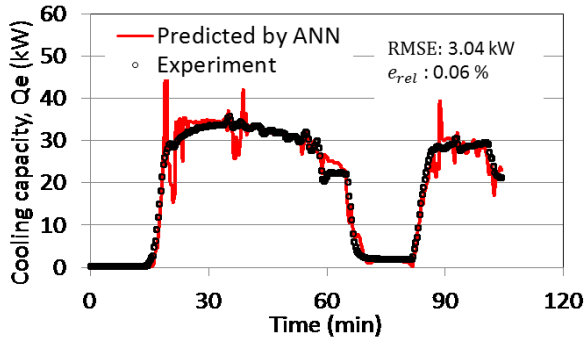
Predicted by ANN
Experiment
RMSE: 3.04 kW
e_{rel} : 0.06 %
Cooling capacity, Qe (kW)
Time (min)

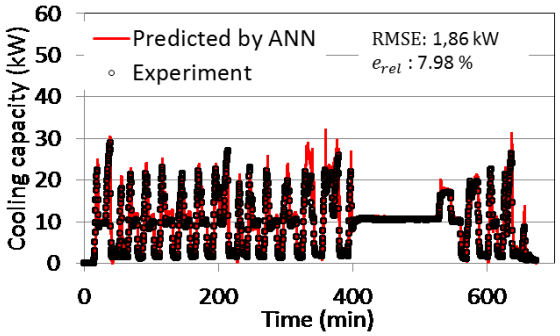
Predicted by ANN
Experiment
RMSE: 1,86 kW
e_{rel} : 7.98 %
Cooling capacity (kW)
Time (min)

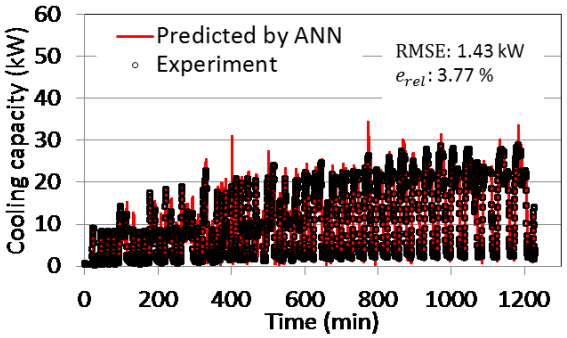
Predicted by ANN
Experiment
RMSE: 1.43 kW
e_{rel}: 3.77 %
Cooling capacity (kW)
Time (min)

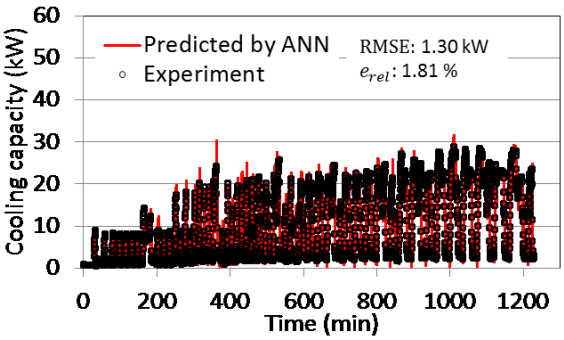
Predicted by ANN
Experiment
RMSE: 1.30 kW
e_{rel}: 1.81 %
Cooling capacity (kW)
Time (min)

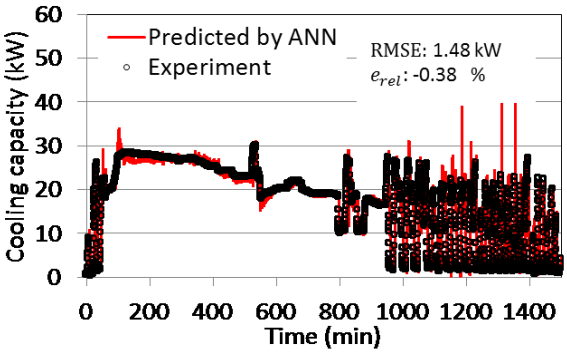
Predicted by ANN
Experiment
RMSE: 1.48 kW
e_{rel}: -0.38 %
Cooling capacity (kW)
Time (min)

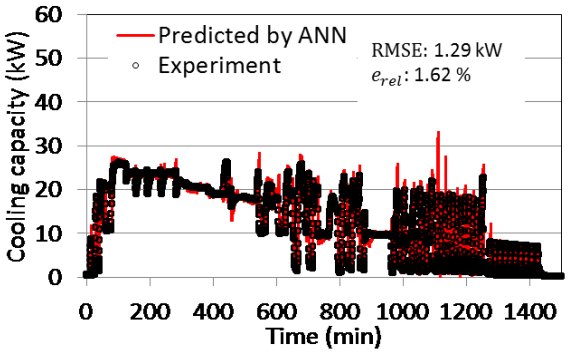
Predicted by ANN
Experiment
RMSE: 1.29 kW
e_{rel}: 1.62 %
Cooling capacity (kW)
Time (min)

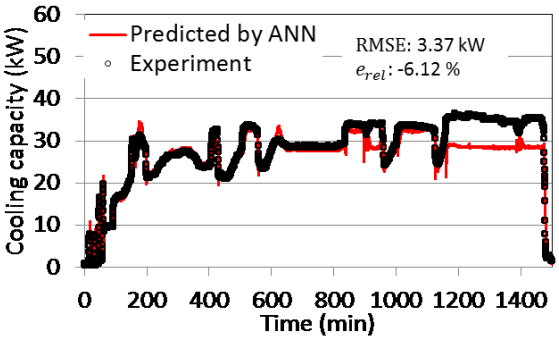
Predicted by ANN
Experiment
RMSE: 3.37 kW
e_{rel}: -6.12 %
Cooling capacity (kW)
Time (min)

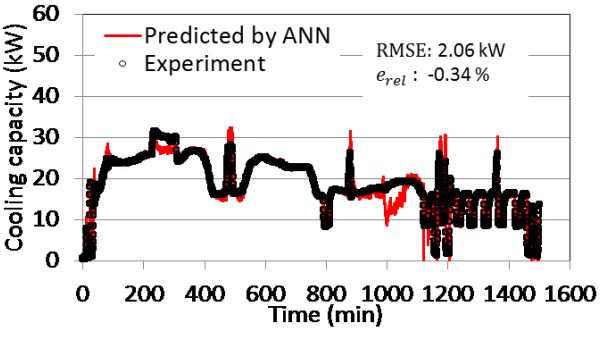
Predicted by ANN
Experiment
RMSE: 2.06 kW
e_{rel} : -0.34 %
Cooling capacity (kW)
Time (min)

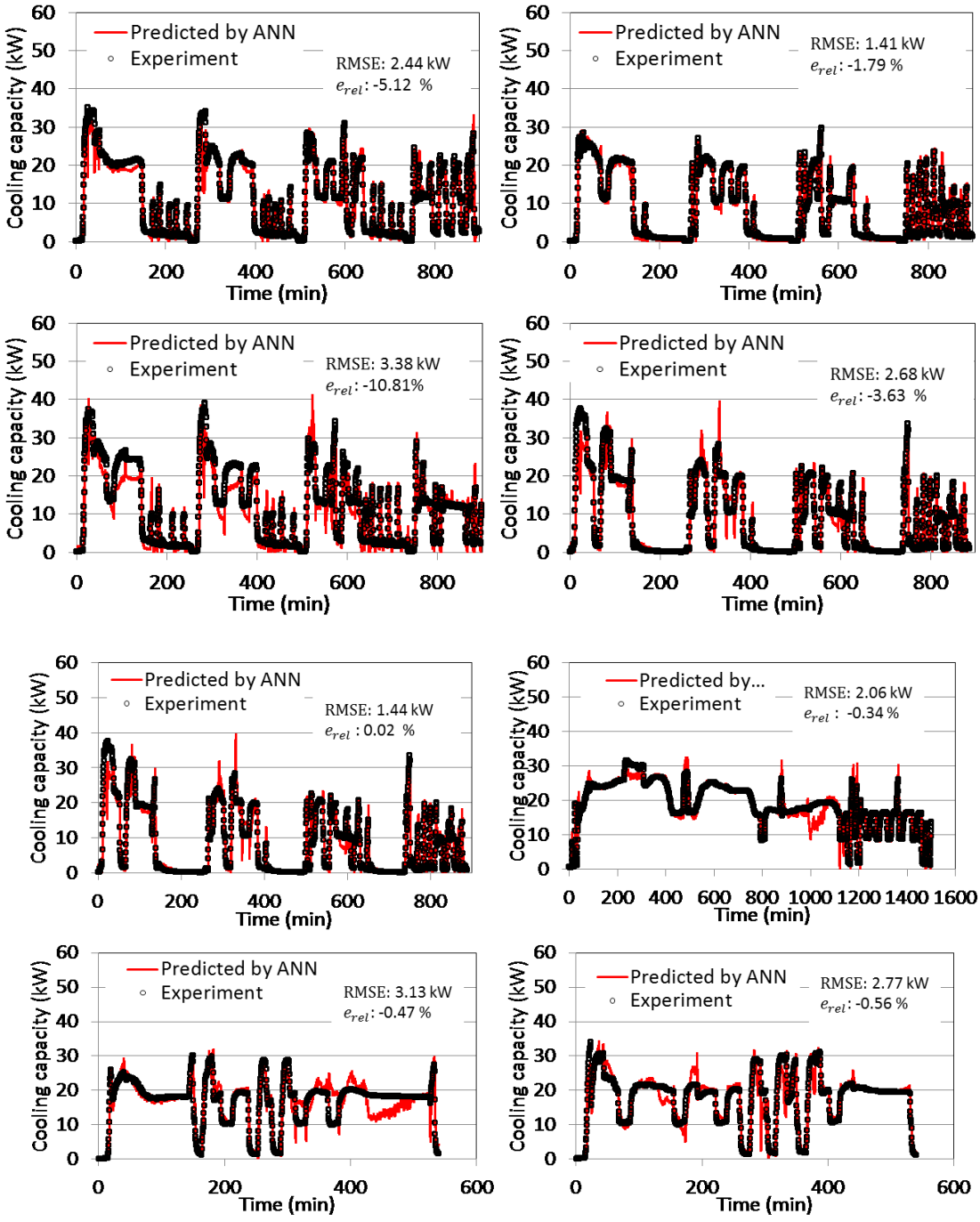
Predicted by ANN
Experiment
RMSE: 2.44 kW
e_{rel}: -5.12 %
RMSE: 1.41 kW
e_{rel}: -1.79 %
RMSE: 3.38 kW
e_{rel}: -10.81%
RMSE: 2.68 kW
e_{rel}: -3.63 %
RMSE: 1.44 kW
e_{rel} : 0.02 %
Predicted by...
RMSE: 2.06 kW
e_{rel} : -0.34 %
RMSE: 3.13 kW
e_{rel}: -0.47 %
RMSE: 2.77 kW
e_{rel}: -0.56 %
Cooling capacity (kW)
Time (min)

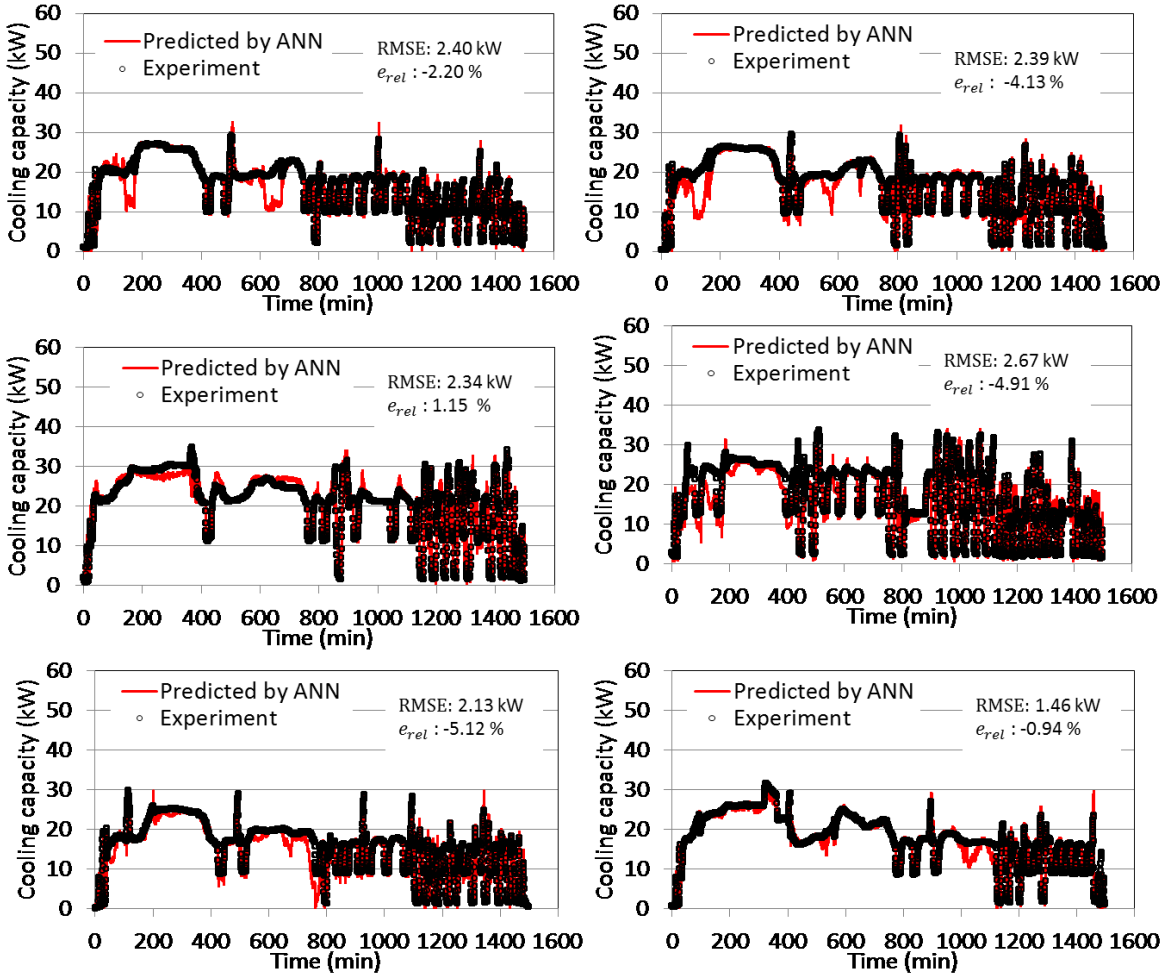
Predicted by ANN
Experiment
RMSE: 2.40 kW
e_{rel} : -2.20 %
RMSE: 2.39 kW
e_{rel} : -4.13 %
RMSE: 2.34 kW
e_{rel} : 1.15 %
RMSE: 2.67 kW
e_{rel} : -4.91 %
RMSE: 2.13 kW
e_{rel} : -5.12 %
RMSE: 1.46 kW
e_{rel} : -0.94 %
Cooling capacity (kW)
Time (min)
0 10 20 30 40 50 60
0 200 400 600 800 1000 1200 1400 1600

早稲田大学　博士（工学）　学位申請　研究業績書

(List of research achievements for application of doctorate (Dr. of Engineering), Waseda University)

氏名 Sholahudin　　印 (seal or signature　　)

（As of November, 2020）

種類別(By Type)	題名、　発表・発行掲載誌名、　発表・発行年月、　連名者（申請者含む） (theme, journal name, date & year of publication, name of authors inc. yourself)
Journal Paper	
1	A cost effective and non-intrusive method for performance prediction of air conditioners under fouling and leakage effect , Sustainable Energy Technology and Assessments, October 4 ,2020, **Sholahudin**, N. Giannetti, S. Yamaguchi, K. Saito, K. Tanaka, H. Ogami.
2	Experimental implementation of artificial neural network for cost effective and non-intrusive performance estimation of air conditioning systems, Applied Thermal Engineering, November 25, 2020, **Sholahudin**, N. Giannetti, S. Yamaguchi, K. Saito, Y. Miyaoka, K. Tanaka, H. Ogami.
3	Prediction of two-phase flow distribution in microchannel heat exchangers using artificial neural network, International Journal of Refrigeration, March 2020, N. Giannetti, M. A. Redo, **Sholahudin**, J. Jeong, S. Yamaguchi, K. Saito, H. Kim.
4	Optimization of HVAC system energy consumption in a building　neural network and multi-objective genetic algorithm, Sustainable Energy Technologies and Assessments, October 2019, Nasruddin, **Sholahudin**, P. Satrio, T. M. I. Mahlia, N. Giannetti, K. Saito.
5	Dynamic modeling of room temperature and thermodynamic efficiency for direct expansion air conditioning systems using Bayesian neural network, Applied Thermal Engineering, July 25, 2019, **Sholahudin**, K. Ohno, N. Giannetti, S. Yamaguchi, K. Saito
6	Solar absorption chiller performance prediction based on the selection of principal component analysis, Case Studies in Thermal Engineering, March 2019, Nasruddin, N. Aisyah, M. Idrus Alhamid, B. B. Saha, **S. Sholahudin**, A. Lubis
7	Hot water temperature prediction using a dynamic neural network for absorption chiller application in Indonesia, Sustainable Energy Technologies and Assessments, December 2018, Nasruddin, **Sholahudin**, M. Idrus Alhamid, T. M. I. Mahlia, K. Saito
8	Study of Solar Driven Adsorption Cooling Potential in Indonesia, Journal of Thermal Engineering, January 1, 2017, Nasruddin, Lemington, D. Budiman, M. Idrus Alhamid, **Sholahudin**
9	Simplified dynamic neural network model to predict heating load of a building using Taguchi method, Energy, November 15, 2016, **S. Sholahudin**, H. Han
10	Optimization of a cascade refrigeration system using refrigerant C3H8 in high temperature circuits (HTC) and a mixture of C2H6/CO2 in low temperature circuits (LTC), Applied Thermal Engineering, July 5, 2016, Nasruddin, **S. Sholahudin**, N. Giannetti, Arnas
11	Heating Load Predictions using The Static Neural Networks Method, International Journal of Technology, 2015, **S. Sholahudin**, H. Han

早稲田大学　博士（工学）　学位申請　研究業績書

(List of research achievements for application of doctorate (Dr. of Engineering), Waseda University)

種類別 By Type	題名、　発表・発行掲載誌名、　発表・発行年月、　連名者（申請者含む）(theme, journal name, date & year of publication, name of authors inc. yourself)
Proceeding	
12	Performance evaluation of radiant cooling system application on a university building in Indonesia, AIP Conference Proceedings, 2017, P. Satrio, **S. Sholahudin**, Nasruddin
13	Characteristics of evacuated tubular solar thermal collector as input energy for cooling system at Universitas Indonesia, AIP Conference Proceedings, 2017, M. Idrus Alhamid, Nasruddin, N. Aisyah, **Sholahudin**
14	Optimization Study of Hydrogen Gas Adsorption on Zig-zag Single-walled Carbon Nanotubes: The Artificial Neural Network Analysis." IOP Conf. Ser.: Mater. Sci. Eng, 2018, Nasruddin, M. Lestari, Supriyadi, **Sholahudin**
15	Multi-step ahead prediction of vapor compression air conditioning system behaviour using neural networks." IOP Conf. Ser.: Mater. Sci. Eng, 2019, **Sholahudin**, K. Ohno, N. Giannetti, S. Yamaguchi, K. Saito
Conference oral presentation	
16	Identification of vapor compression air conditioning system behavior using Bayesian regularization neural network, International Congress of Refrigeration (ICR), 2019, **Sholahudin**, K. Ohno, S. Yamaguchi, K. Saito
17	Dynamic behavior prediction of air conditioning system using Bayesian regularization neural network, Japan Society of Refrigeration and Air Conditioning Engineers Annual Conference, 2018, **Sholahudin**, K. Ohno, S. Yamaguchi, K. Saito
18	Multi-step ahead prediction of vapor compression air conditioning system behavior using neural networks. The International conference on Design, Energy, Materials, and Manufacture (ICDEMM), 2018, **Sholahudin**, K. Ohno, N. Giannetti, S. Yamaguchi, K. Saito
19	Direct inverse neural network to control cooling capacity of heat pump systems, International Conference on Cryogenics and Refrigeration (ICCR), 2018, **Sholahudin**, K. Ohno, S. Yamaguchi, K. Saito
20	Heating load prediction using neural network method, International Conference of Saving Energy in Refrigeration and Air-Conditioning (ICSERA), 2015, **Sholahudin**, H. Han
21	Prediction and analysis of building energy efficiency using artificial neural networks and design of experiments, International Meeting on Advances in Thermo fluids, (IMAT), 2014, **Sholahudin**, A. G. Alam, C. Baek, H. Han